Feasibility Study of CCS-Readiness in Guangdong Province, China (GDCCSR) Final Report: Part 2

Assessment of CO_2 Storage Potential for Guangdong Province, China

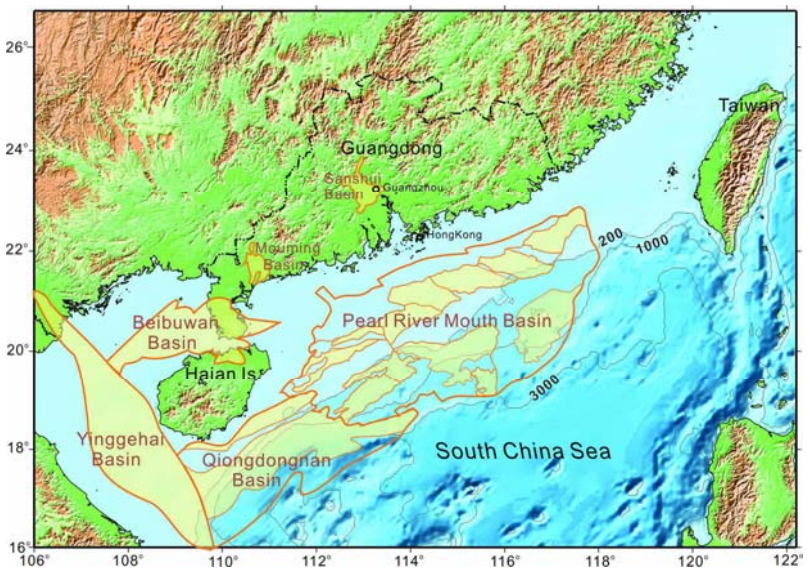

GDCCSR-SCSIO Team
March 2013

Authors (GDCCSR-SCSIO Team)

Di Zhou

Pengchun Li, Zhongxian Zhao, Jie Liao, Cuimei Zhang,

Yunfan Zhang, Hui Xie, Fucheng Li, Jialong Peng

(South China Sea Institute of Oceanology,

Chinese Academy of Sciences, Guangzhou, China)

For comments or queries please contact:

Prof. Di Zhou

zhoudiscs@scsio.ac.cn

Disclaimer

This is the second part of the final report of the project "Feasibility Study of CCS-Readiness in Guangdong (GDCCSR)", which is funded by the Strategic Programme Fund of the UK Foreign & Commonwealth Office joint with the Global CCS Institute.

The report is written based on published data mainly. The views in this report are the opinions of the authors and do not necessarily reflect those of the South China Sea Institute of Oceanology, nor of the funding organizations.

The full list of the GDCCSR project reports are as follows:

Part 1 Analysis of CO_2 emission in Guangdong Province, China.

Part 2 Assessment of CO_2 Storage Potential for Guangdong Province, China.

Part 3 CO_2 Mitigation Potential and Cost Analysis of CCS in Power Sector in Guangdong Province, China.

Part 4 Techno-economic and Commercial Opportunities for CCS-Ready Plants in Guangdong Province, China.

Part 5 CCS Capacity Building and Public Awareness in Guangdong Province, China

Part 6 CCUS Development Roadmap Study for Guangdong Province, China. .

Contents

Summary for Policy Makers

This report is the second part of the final reports of the project "The CCS Readiness Study for Guangdong Province" (GDCCSR). In this report, the effective storage capacity of CO_2 in sedimentary basins onshore Guangdong (the Sanshui Basin) and offshore (the Pearl River Mouth Basin, Beibuwan Basin, Qiongdongnan Basin, and Yinggehai Basin) are assessed based on available geological data. It is concluded that the CO_2 storage potential is limited inland Guangdong but abundant offshore. The offshore sedimentary basins in northern South China Sea, especially the Pearl River Mouth Basin, have sufficiently large and high-quality storage potential for storing the CO_2 from Guangdong province in over one hundred years. An early opportunity of full-chain CCS demonstration project is identified for feasibility studies.

- For CO_2 underground storage the geological conditions of Guangdong Province are representative to southeast China (including the provinces of Guangdong, Guangxi, Fujian, Zhejiang, Jiangxi, and Hainan) and quite different from other parts of China. These provinces reside in Paleozoic fold belt overlapped by Mesozoic volcanic arc. Sedimentary basins are small, scattered, and filled with continental sediments of poor reservoir quality. Taken into account of the dense population and heavy land use, there is essentially no CO_2 storage potential inland these provinces.

- However offshore Guangdong there are very large sedimentary basins developed in a Cenozoic passive margin. High-quality reservoirs and cap rocks in these basins are mainly in Miocene and Upper Oligocene formations at depths of 2000m-3000m below seafloor. According to our assessment, the effective storage capacity of CO_2, which is a subset of the theoretical (maximum) storage capacity obtained by multiplying a storage efficiency factor that reflects a range of geological and engineering limitations, in four sedimentary basins in northern South China Sea is 205 Gt[1] CO_2 at 85% probability level, among which 163 GtCO_2 in shallow water (<300m) areas. This capacity is sufficiently large for storing CO_2 emitted from large point sources in Guangdong and adjacent provinces for hundreds of years.

- Offshore CO_2 storage has many advantages over inland storage: There is less competition in land use, less risk to environment and groundwater, and thus easy to be accepted by public. The disadvantage of offshore CO_2 storage is its higher cost, several times of the cost of onshore storage. One way to offset the cost is to use existing infrastructure (platform, well, pipeline, etc.) of depleted oil/gas fields.

- The most favorable storage area is the northern Pearl River Mouth Basin (the Zhu-1 depression and the northern Dongsha Uplift). The area is the shallow water area proximal （mostly <200 km）to the large CO_2 point sources in the coastal Guangdong especially in the Pearl River Delta. The effective storage capacity of CO_2 in this area is 77 GtCO_2 at 85% probability level, more than 300 times of the

[1] In this report Gt is 10^9 tonnes, Mt is 10^6 tonnes, and Gm^3 is 10^9 m^3.

2010 total annual CO_2 emissions (252 Mt CO_2) from large point sources of thermal power, petrochemical and steel industries in Guangdong Province. Many oil fields have been found in this area and have been in production since 1990. The potential of CO_2-EOR is low because the oil fields are of high recovery rate with strong water drive. Several oil fields are near depletion, there is high possibility of using their infrastructures after depletion for CO_2 injection to offset partial cost of offshore CO_2 storage.

- An early opportunity for a full-chain CCUS demonstration project is identified. A planned oil refinery on the coast of the Huizhou city will emit 3.2 Mt/yr high-purity CO_2 from H_2 production. A small portion of these CO_2 will be utilized in industry, the majority of the CO_2 will enable a low-cost CO_2 capture because no or slight further purification of CO_2 is needed. An offshore oil field in the Pearl River Mouth basin 170 km south of the refinery is to be depleted soon, whose infrastructure may be used for CO_2 injection to offset the storage cost. These compose an ideal match for a cost-effective demonstration project, which is featured by the offshore CO_2 storage in the geological conditions of the northern South China Sea. A study on the technical and economical feasibility of the HZ project is needed urgently, because these have to be done before the start of the refinery construction and several years before the depletion of the oil field.

- Guangdong Province has the potential to lead in CCUS development in southeast China. because the province has strong economic background and is the only low-carbon pilot province in the region, also because the province has better CO_2 storage condition as being close to the oil-producing Pearl River Mouth Basin where the CO_2 storage capacity is large and the possibility of using existing infrastructure for CO_2 injection exists. If the offshore CO_2 storage in the northern Pearl River Mouth Basin has been demonstrated as feasible, a large-scaled CCUS employment would be foreseeable in the Guangdong Province, and this will have a significant impact to the low-carbon development in southeast China as well as in the world.

Chapter 1 Background and outline

Carbon dioxide Capture and Storage (CCS) technology is the technology for large-scaled greenhouse gas mitigation upon continued use of fossil fuels. It is the major "clean coal" technology and has received significant attention. By the end of January 2013, there are 72 large-scale integrated CCS projects[2] worldwide (GCCSI, 2013).

China's heavy reliance on coal means that CCS has the potential – once full commercial viability is achieved – to play a key role in the future development of China's stated goal of limiting emissions growth per unit of GDP. China is undertaking a range of technical research and development projects on CCS. These include the national 973 and 863 programs, projects for assessing the storage potential in the country, several demonstration projects in CO_2 capture, CO_2-EOR, and full-chain CCS, and international projects such as NZEC, GEOCAPACITY, COACH, STRACO2, CAGS, FutureGen, CACHETCO2, and MOVECBM, etc. In 2011 "The Technology Roadmap Study of Carbon Capture, Utilization, and Storage (CCUS) of China" was released (MOST and ACCA21, 2011), in which the need to utilize the captured CO_2 as a resource was emphasized.

However, there have been geographical gaps in the existing body of research and development of CCS in China. To date, all of the major CCS projects in China have focused on the regions north of the Yangtze River, with no substantial research having taken place in China's wealthy manufacturing provinces of the southeast. Other gaps are technical. Many coal-based power plants are being built without any consideration of CO_2 capture or capture readiness. Additionally, whilst there are a number of projects involve CO_2 storage, there have been none in offshore prior to this project. It is important that these issues are addressed in order to provide a comprehensive R&D basis to underpin any development of future CCS-related policy in China.

The research project "CCS readiness in Guangdong" (GDCCSR) is the first large-scaled CCS-related research project in Guangdong as well as on southeast China. Guangdong is China's largest provincial economy. In 2010 its GDP reached ~€530 billion with roughly 50% from industry. In 2010 Guangdong has been selected as one of the five low-carbon pilot provinces in China. However, the early draft of the roadmap of low-carbon economic development in Guangdong emphasizes the industrial reform, energy saving and efficiency, and renewable and nuclear energies, while CCS is not featured. The GDCCSR project aims to provide a comprehensive review on the need and feasibility of CCS in Guangdong.

This report presents the assessment of the CO_2 storage capacity and prospectivity onshore and offshore Guangdong, which is the essence for the feasibility of CCS in the province. Onshore Sanshui Basin and offshore Pearl River Mouth Basin, Beibuwan Basin, Yinggehai Basin, and Qiongdonghan Basin are examined based on available data (Fig. 1.1). Among these the Sanshui Basin and Pearl River Mouth Basin were assessed in a previous project PACOS-GD by the same authors and the estimation for the Pearl River Mouth Basin was published (Zhou et al., 2011). In the GDCCSR project the capacity estimates for the Sanshui and Pearl River Mouth basins have been checked and modified, and some additional analyses on the potential of CO_2-EOR and using

[2] By definition of GCCSI (2013), large-scale integrated CCS projects (LSIPs) are the projects involving the capture, transport and storage of carbon dioxide at a scale of: at least 0.8 Mt of CO_2 annually for a coal-based power plant, or at least 0,4 Mt of CO_2 annually for other emission intensive facilities. Projects that involve enhanced oil recovery (EOR) using anthropogenic CO_2 may also satisfy this definition

existing infrastructures have been added. Thus these two basins are included also in this report.

Our assessments show that the storage capacity is very limited onshore Guangdong Province but abundant offshore in northern South China Sea. Cost-effective early opportunity is identified for further investigation.

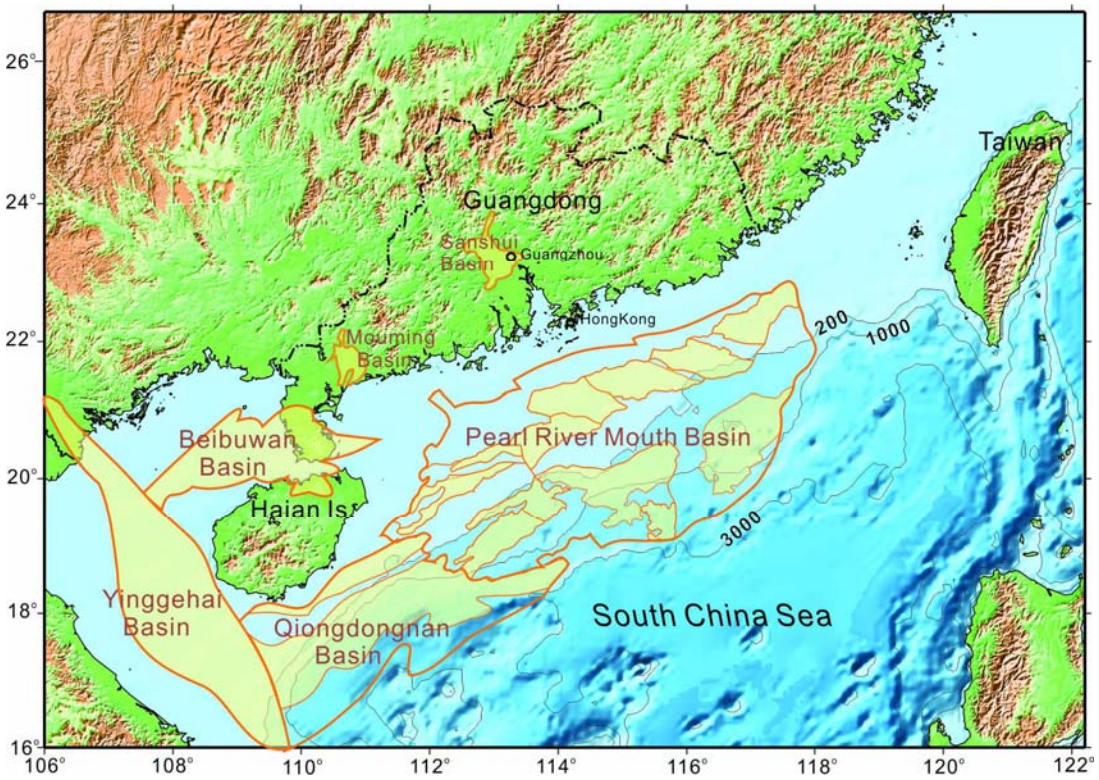

Figure 1.1 Map showing topography and the sedimentary basins being assessed for CO_2 storage capacity in this report.

Chapter 2 Methodology of CO_2 storage capacity assessment

2.1 Types and classification of storage capacity

Currently, there are two favorable types of geological storage options: oil and gas reservoirs, and deep saline formations. The largest capacity resides in deep saline formations, which are the porous rocks at depth below 800 m, where CO_2 would be stored in a critical state having higher density, and with formation water having total dissolved solids >10000 ppm so that the sources of fresh water are not contaminated (USDOE, 2008a).

The Techno-Economic Resource-Reserves Pyramid for CO_2 storage capacity proposed by CSLF (CSLF, 2007) indicated four classes of capacity (Fig. 2.1). From bottom to top in the pyramid, the estimated capacity is increasingly accurate by considering more physical, technical and general economic effects. The theoretical capacity is the maximum upper limit of storage potential. It assumes that the system's entire capacity to store CO_2 in pore space, or dissolved at maximum saturation in formation fluids, or adsorbed at 100% saturation in the entire coal mass. The effective capacity is a subset of the theoretical capacity with a number of geological and

engineering limitations applied. The practical capacity is a subset of the effective capacity gained by considering non-geological components (e.g. economics, regulation, legal infrastructure etc.). The matched capacity is a subset of the practical capacity obtained by matching sources to suitable sites (CSLF, 2008).

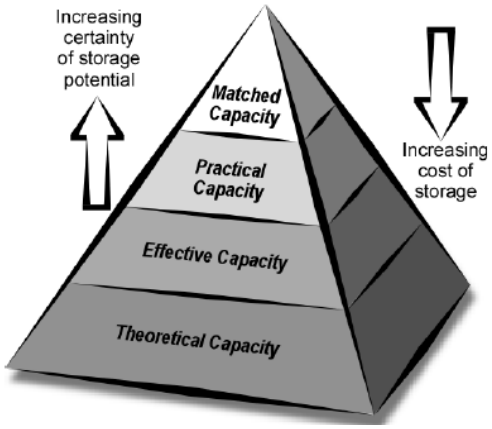

Figure 2.1 the pyramid schematic diagram of different CO_2 capacities

The effective capacity is the capacity that can be physically accessed and thus is suitable for being assessed for strategic purpose. In this project the effective storage capacities in saline formations and in oil and gas fields are estimated based on published data.

2.2 Capacity estimation for saline formations

For deep saline formations the methodology of assessment follows that of USDOE (2008a), where the effective storage capacity M_{CO2} is given by:

$$M_{CO2} = V \times R \times \varphi \times \rho_{CO2} \times E \quad (2.1)$$

where V is the volume of the saline formation, R and φ are respectively the net/gross ratio and the porosity of the formation, ρ_{CO2} is CO_2 density at formation depth, and E is the storage efficiency factor.

At first we compile formation isopach maps based on collected data. Then the formation volume V is estimated via GIS based on these isopach maps. Only the formations below the topmost regional seal are considered, and only their volumes at the depths from 800 m to 3500 m below ground surface or seafloor are calculated. This is because above 800 m the CO_2 is not in the super-critical state, and below 3500 m the formation may be too much compacted and thus not suitable for CO_2 storage. We also estimated the storage capacity in the shallow-water areas where the water depth is less than 300 m. The areas of deeper water are not favorable for CO_2 storage because of much higher engineering and operational costs.

The CO_2 density at depths varies with in situ pressure and temperature. We divide the basin into regions of relatively similar geothermal gradient and seafloor temperature, and then fit spline curves of CO_2 density versus depth for each region based on the data of Span and Wagner (1996). In final capacity calculation, the CO_2 density at any depth can be read from these curves.

The storage efficiency factor E is an important source of uncertainty for capacity assessment. The estimation of E is a topic that deserves specific researches and thus beyond the scope of this project. The USDOE (2008a) obtained through Monte Carlo simulations a statistical distribution

of E for deep saline aquifers at P15, P50, and P85 probability level as E = 0.01, 0.024, and 0.04 respectively (Bachu, 2008). Later thematic study (IEAGHG, 2009) suggests the overall mean value (P50) of E for all lithologies being 0.026 at the formation level. Combining these two results, we use E = 0.026 for mean and E = 0.01 and 0.04 for P15 and P85 probability levels, respectively for saline formations.

2.3 Capacity estimation for oil and gas fields

For oil or gas fields the effective storage capacity M_{CO2} is deduced from the original oil or gas in place (CSLF, 2007).

For oil fields,

$$M_{CO2} = \rho_{CO2} \times (R_f \times OOIP / B_f - V_{iw} + V_{pw}) \times C_e \quad (2.2)$$

where $OOIP$ is the volume of original oil in place, R_f and B_f are recovery and volume factors respectively, V_{iw} and V_{pw} are injected and produced waters, ρ_{CO2} is the CO_2 density, and C_e is the storage capacity factor. As there has been no water flooding in the basins of the northern SCS, V_{iw} and V_{pw} are zero and (2.2) becomes:

$$M_{CO2} = \rho_{CO2} \times (R_f \times OOIP / B_f \quad) \times C_e \quad (2.3)$$

For gas fields,

$$M_{CO2} = \rho_{CO2r} \times R_f \times (1 - F_{IG}) \times OGIP \times [(P_s \times Z_r \times T_r) / (P_r \times Z_s \times T_s)] \times C_e \quad (2.4)$$

where $OGIP$ is the volume of original gas in place, R_f is recovery factor; F_{IG} is the fraction of injected gas; P, T and Z denote pressure, temperature and the gas compressibility factor, respectively; The subscripts "r" and "s" denote reservoir and surface conditions, respectively. For the basins of the northern SCS, F_{IG} = 0 as there has been no gas flooding; R_f = 0.85 as the gas recovery factor is high. The term $(P_s \times Z_r \times T_r) / (P_r \times Z_s \times T_s)$ is the reservoir volume factor B_g. Then (2.4) becomes:

$$M_{CO2} = \rho_{CO2r} \times R_f \times OGIP \times B_g \times C_e \quad (2.5)$$

It should be pointed out that in China, hydrocarbon resources are assessed in the classes of perspective resource, geological resource, discovered reserve, and un-discovered resource. We use the value of "Geological Resources" in Chinese literature are as the values of $OOIP$ and $OGIP$.

The storage capacity factor C_e for oil/gas fields is equivalent to the E factor for saline formations in terms of defining a portion of the theoretical storage capacity as the effective storage capacity. There are very few studies on the C_e factor. According to Bachu and Shaw (2005), $C_e = C_{eff} \cdot C_{aq}$, where $C_{eff} < 1$ is the effective storage coefficient, representing the affects such as the CO_2 mobility and density with respect to oil and water and the heterogeneity of the reservoir, and C_{aq} represents the reduction in storage capacity as a result of aquifer effects such as the invaded aquifer water during the oil/gas production. Based on their study in western Canada, C_{eff} = 0.5 for oil fields and C_{eff} = 0.9 for gas fields; C_{aq} = 81% to 25% with average 50% for oil reservoirs, and C_{aq} = 1 to 52% with average 70% for gas reservoirs.

The oil/gas fields in the northern South China Sea are mostly associated with strong aquifers. Based on the study of Bachu and Shaw (2005), in this report we use the following C_e values:

For oil fields, $C_e = 0.5 \times 0.25 = 0.12$ for the low end, $C_e = 0.5 \times 0.81 = 0.4$ for the high end, and $C_e = 0.5 \times 0.5 = 0.25$ for the average.

For gas fields, $C_e = 0.9 \times 0.52 = 0.47$ for the low end, $C_e = 0.9 \times 1 = 0.9$ for the high end, and $C_e = 0.9 \times 0.7 = 0.6$ for the average.

Chapter 3 CO_2 Storage Capacity of inland Guangdong Province especially the Sanshui Basin

3.1 Geography and geology

Guangdong Province is located in subtropical zone of South China, with a land area of 180 000 km^2. Morphologically the province consists of the Pearl River Delta and coastal zones in the south, the E-W-running Nanling mountain range in the north, low mountains and terraces in the west, and upland and low mountains in the east. The middle and lower reaches of the Pearl River form a network through the province and enter the South China Sea at the river mouth near the city of Hong Kong (Fig. 1.1).

Tectonically the Guangdong province belongs to the Caledonian Fold Belt of the South China Block. The tightly folded basement consists of Proterozoic, Cambrian, Ordovician, and Silurian metamorphic rocks. The overlying platform cover consists of Devonian to Mid Triassic clastic and carbonate strata, which was folded and uplifted during the Indosinian Orogeny. Large-scaled granitic intrusions occurred during the Mesozoic Yanshannian Orogeny.

Sedimentary basins in Guangdong developed in Cretaceous to Tertiary. Although 108 basins has been named and occupy 17% area of the province, only 8 basins have the single basin area greater than 1000 km^2, namely the Sanshui, Maoming, Leiqiong, Dongguan, Xinhui, Kaiping, Nanxiong, and Dengta basins (Fig. 3.1.1) (Zhang, 1999). These are continental basins controlled by NE-striking large faults and NW and EW faults, and were filled with fluvial-lacustrine and volcanic clastic sediments. The sediment thickness is typically 1~4 km and seldom exceeds 6 km. Lignite, oil shale, gypsum, salts, fluorite, barite, copper and uranium deposits have been found in these sediments (Table 3.1.1).

Table 3.1.1 Major sedimentary basins in Guangdong Province

(Numbering follows that in Fig. 3.1.1)

	Name	Area(km^2)	Age	Volcanics	Resources
1	Sanshui	3300	K_1,K_2,E	Widely	Oil/gas, gypsum, CO_2
2	Dongguan	1400	K_1,K_2,E		
3	Xinhui	1100	K_1,K_2,E		
4	Kaiping	1000	K_1		
6	Dengta	1000	K_1,K_2		
8	Nanxiong	1240	K_2,E	No	Minor coal & uranium
12	Maoming	2000	K_1,K_2,E,N	K_2,E_1	Oil shale, lignite
15	Leiqiong	8400	K_1,K_2,E	Q basalt widely spread	Oil shown inland the Hainan Island

Basin geology and exploration activities

The Sanshui basin is chosen in this study because it is the second largest sedimentary basin in the Guangdong Province, it is the only sedimentary basin inland the province that contains oil fields, and it is the sedimentary basin most proximal to the industrialized area in the province. The basin reside in a area in 112°40′ to 113°24′ E and 22°50′ to 23°42′ N , straddling the Nanhai and Sanshui counties of the Foshan city, the northern Shunde City, and the western Guangzhou city, with a total area of about 3375 km^2 (Chen et al., 2008). The straight-line distance between the centers of Sanshui and Guangzhou is ~40 km, with railway, highway, and waterway connections.

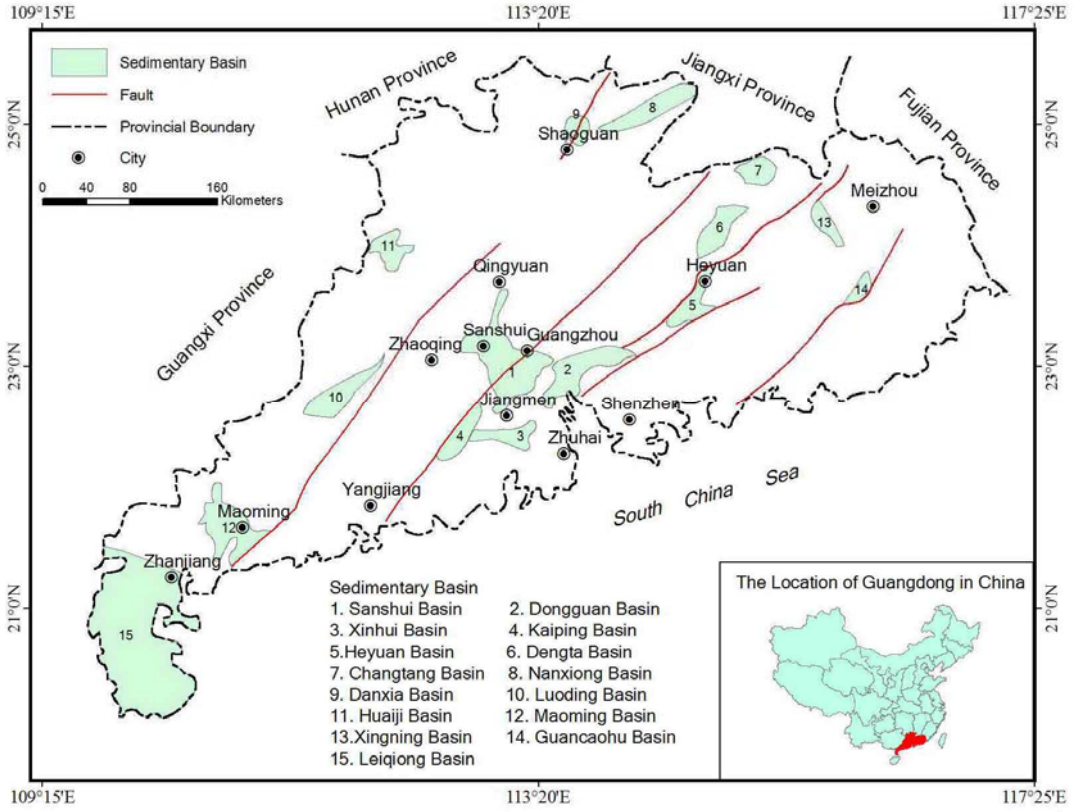

Figure 3.1.1 Simplified map showing the distribution of major Cretaceous-Tertiary sedimentary basins inland Guangdong Province. Simplified from Zhang (1999)**.**

The name of "Shanshui" means "three rivers" in Chinese, as the three tributaries of the Pearl River, the West, the North, and the Sui rivers, come close to intersect near the city. The Sanshui basin occupies the western portion of the Pearl River Delta, consists of flat plain with low hills in the north. The elevation is ~500 m in general with 100~300 m relief. The Pearl River and its tributary network incised the basin and flow into the South China Sea.

Geologically the Sanshui Basin lies in the mid-eastern portion of the South China Block. It is a Cretaceous-Paleogene complex syncline with a SN-elongated rhombic shape, gentle dipping (5~12°) center and steeply dipping (10~20°) flanks. It is bounded by NE-running Sanshui and Engping-Xinfeng faults and NW-running West-River and Xiqiaoshan faults, and cut by a EW-running Guangzhou-Sanshui fault (Figs. 3.1.2a and 3.1.3). The basin may be subdivided into 4 depressions, 2 uplifts, and 3 slopes (Fig. 3.1.2b) (Team735, 1975). Rift-related volcanic eruptions are found widely in the basin, composed of mainly basalt, rhyolite, trachyte, and related volcanic clasts. Episodic volcanic eruptions occurred in Late Cretaceous and Paleogene, with total thickness over 2600 m (Dong et al., 2006; Tang, 1994).

Geological surveying in the Sanshui Basin started in the 60's, and exploration for oil, gas, and gypsum was extensive during the 70's of the last century. So far 1:50 000 geological mapping, geophysical (seismic, gravity, and magnetic) survey have been conducted, more than 400 wells (including 187 deep wells) have been drilled in order to explore for oil/gas and gypsum (Hou et al., 2007a). 34 structural traps in sandstones have been found in the Sanjiang-Danzao Sag with the area of single trap mostly < 3 km^2. The Baoyue and Zhushangang oil fields in the northwest of the basin had the highest production rate of 139 m^3/d oil and 118 000 m^3/d gas. Commercial oil flow

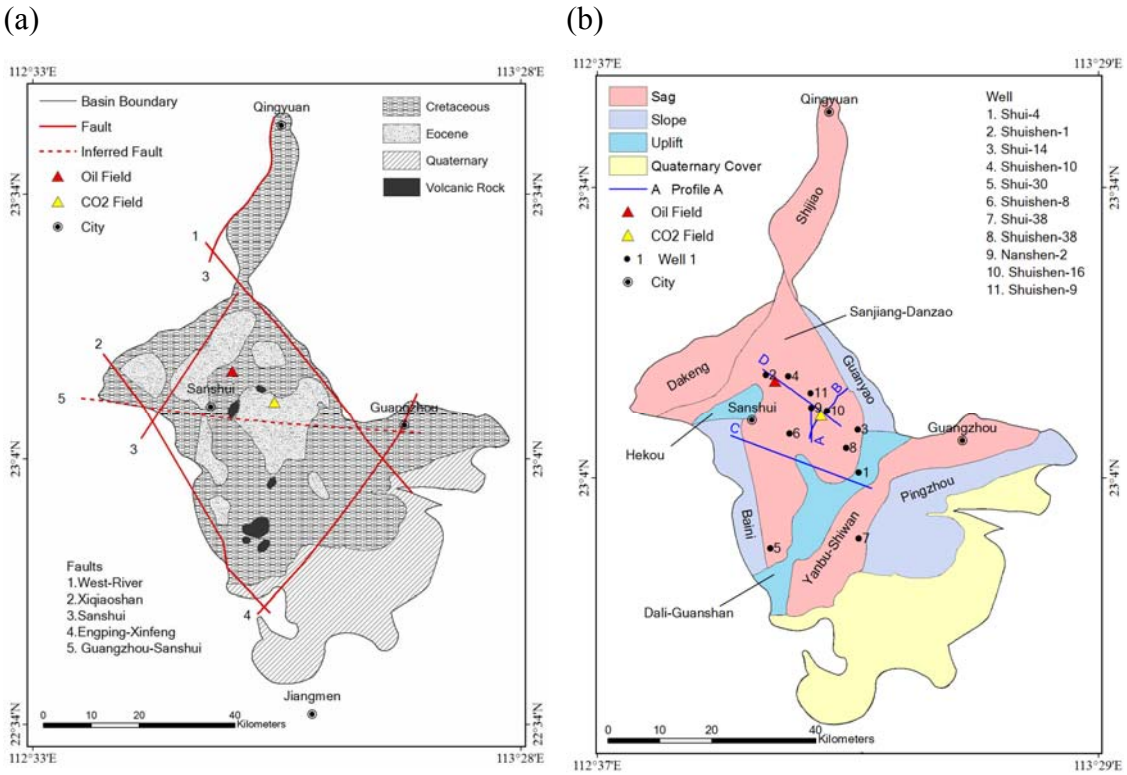

Figure 3.1.2 **(a) Simplified geological map of the Sanshui Basin** after Chen et al. (2008); and **(b) structure divisions** after (Team735, 1975).

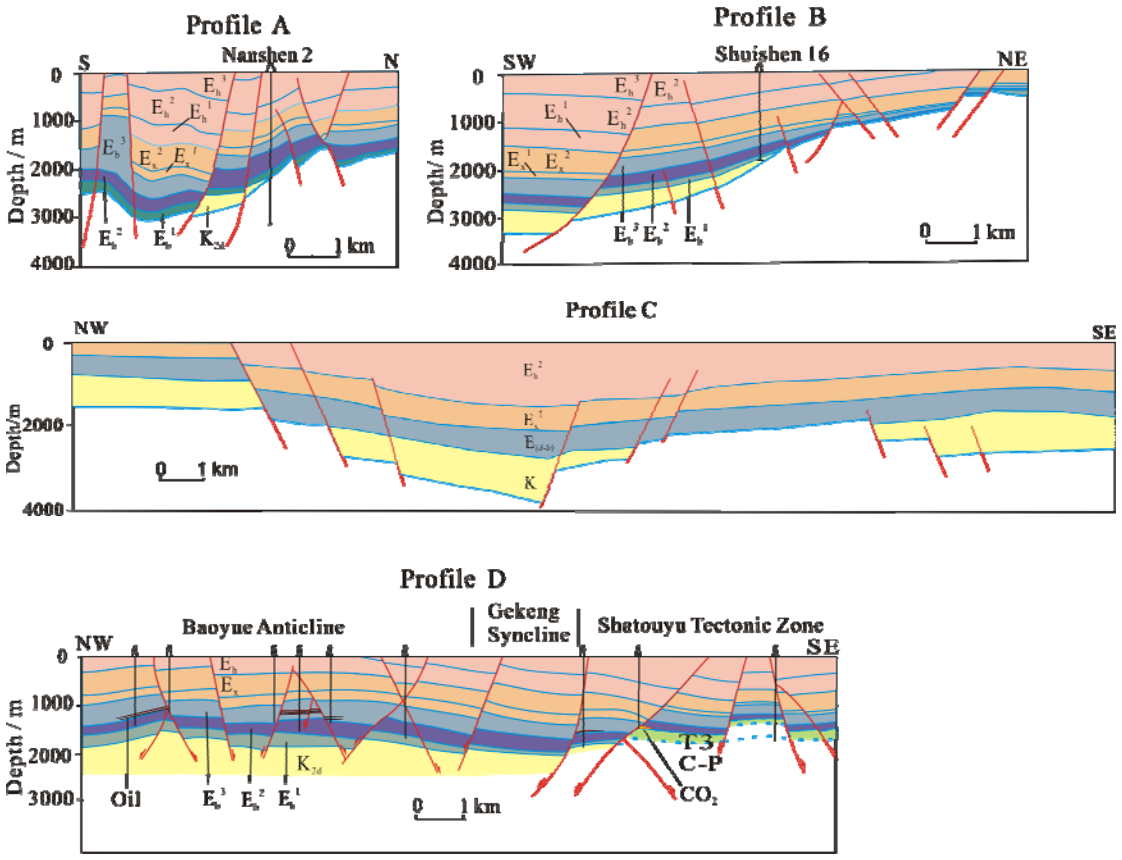

Figure 3.1.3 **Geological cross sections of the Sanshui Basin.**

Locations of the profiles are indicated in Fig. 3.1.2b.

was discovered also in carbonate reservoirs in the Yanbu Sag in the east of the basin (Team12, 1982; Team735, 1975). Small scale oil/gas and gypsum exploration is still ongoing to date. Informal source indicates that the proved oil/gas reserves in the basin is only 600 000 ton, and annual production is <6000 ton. According to the 2008 estimation, the geological resources in the Sanshui Basin are 12 Mt of oil and 1.7 Gm^3 of gas (MLRC et al., 2008).

In addition, pure (99.5%) CO_2 was produced from carbonate cavities of the Shuishen-9 well in the center of the Sanshui Basin. The rate of CO_2 flow was 0.5 million m^3/d, the highest single-well rate then in China, but dried out soon after the production began.

Stratigraphy and paleo-geography

The basement of the Sanshui Basin consists of Carboniferous-Permian carbonates and coal-bearing shales, Triassic-Jurassic clastic rocks, and Mesozoic granites.

The Sanshui Basin was filled with Cretaceous and Paleogene lacustrine sediments up to 5500 m in thickness. Several stratigraphic systems were proposed based on their lithology, lithofacies, cyclothem, and Paleontology (Team12, 1981; Team735, 1975; Zhang et al., 1993). In this report the naming of stratigraphic system follows that of the Team12, but the lithology, age, and thickness follow those of Zhang et al. (1993). See Table 3.1.2.

In general, the sedimentation in the Sanshui Basin started in Early Cretaceous with red-bed clastics (lower Baihedong Fm.), coarse in the lower portion and fining upwards, containing thin layers of gypsum, indicating lacustrine sedimentation in warm and dry climate. Earliest sedimentation occurred in a small lake in the east (the northern Yanbu Sag). In the middle Early Cretaceous the lake expanded and deepened, dark mudstone and marl deposited (middle and upper Baihedong Fm.). In Late Cretaceous another salty lake appeared in the NW of the basin (Sanjiang-Danzao Sag), separated from the Yanbu lake by a NE-striking fault-uplift, while the sedimentation was also red-bed clastics (the Sanshui and Dalangshan Fms). At the end of Cretaceous the basin was uplifted by the Himalayan Orogen, forming a regional unconformity (Hou et al., 2007a).

In the Paleocene the basin subsided again. The western basin became a large lake, and marshes developed in the eastern basin. During the Paleocene the climate kept dry and the sedimentation was coarse in the lower section and fining upwards, dominated by red beds (the lower Buxin Fm.). It is the major gypsum production layer in the basin. In Early Eocene the basin subsidence came to climax while the climate became warm and wet. Dark mud (with oil shale) and marl deposited in the deep lake in the west, which became the major oil/gas source rocks in the basin (middle and upper Buxin Fm.). In Middle Eocene the lake shrunk slightly and the climate became dry. The sediments were relatively fine and mainly of purple or dark grey color (Xibu Fm.). Late Eocene was the last stage of the basin development before the post-Eocene uplift. Sedimentation was restricted to the center of the basin, and volcanism was very active (Huachong Fm.) (Hou et al., 2007b).

Age	Forma-tion	Memb er	Thick ness /m	Lithology	Seal	Oil/ gas	CO_2 reservoir
Q.			48	Brownish red mud, sand and gravel			
Late Eocene	Huachong	E_h^{3-4}	323	Light grey and brownish grey sandstone & conglomerate, with gravel sandstone, red-brown muddy siltstone, and silty mudstone with dark grey calcareous mudstone			
		E_h^2	396	Greyly green tuff, trachyte, basalt, light-grey sandy conglomerate, brown silty-fine sandstone, dark or variegated mudstone with thin limestone and marl			
			263	Greyly green bracciated tuff, tuffaceous sandy conglomerate, rhyolitic porphyry, light grey sandy conglomerate, brown silty-fine sandstone with mudstone			
Middle Eocene		E_h^1	326	Interbedded purple grey and aubergine sandy mudstone, mudy silty-fine sandstone, light grey gravel sandstone, sandy conglomerate with variegated mudstone			
	Xibu	E_x^2	307	Interbedded Brown siltstone and fine-medium sandstone, with gravel sandstone and dark grey mudstone, silty-fine sandstone with cross bedding highly developed	●		
		E_x^1	193	Dark grey and brown calcareous mudstone with siltstone and fine sandstone	●		
Early Eocene	Buxin	E_b^3	143	Dark grey calcareous mudstone with brown siltstone, mudstone, salt, bottomed by tuff.	●		
			130	Dark grey gypsum-bearing calcareoud mudstone with silty-fine sandstone and salt.	●	●	●
			130	Interbedded grey medium-coarse sandstone			●
		E_b^2	266	Dark grey calcareous mudstone, marl, limestone, lean oil shale with siltstone and tuff	●	●	●
Paleocene		E_b^1	100	Dark brown and dark grey mudstone, marl, siltstone with gypsum	●		
			140	Brown red mudstone, siltstone with dark mudstone and gypsum	●		
			60	Sandy conglomerate with gravel sandstone			●
Upper Cretaceous	Dalang-shan	K_{2d}	176	Dark purple silty-fine sandstone with sandy conglomerate, dark grey calcareous mudstone, marl		○	○
			200	Dark sandy conglomerate, silty-fine sandstone with mudstone, marl, basalt			
	Sanshui	K_{2s}	314	Aubergine and brown red silty-fine sandstone, calcareous mudstone with sandy conglomerate, marl, and blocky gypsum			○
			260	Aubergine sandy conglomerate, gravel sandstone, silty-fine sandstone, with silty mudstone			
Lower Cretaceous	Baihedong	K_{1b}	207	Dark brown silty mudstone and muddy siltstone interbeds			
			572	Dark brown silty mudstone, muddy siltstone, with dark grey and green grey calcareous mudstone, with gypsum			
			243	Brown muddy siltstone, silty mudstone, light grey conglomerate, sandy conglomerate, and sandstone			

Table 3.1.2 General stratigraphy of the Sanshui Basin*

* Naming of stratigraphic system follows that of (Team12, 1982), but the lithology, age, and thickness follow those of (Zhang et al., 1993). Solid dots – most likely; open circles – possible.

Petroleum geology

Source rocks reside in the Lower Eocene Buxin Fm. Its E_b^2 member is the major source composed of dark mudstone intercalated with carbonate, which were deposited in the deep lake of the Sanjiang-Danzao Sag. This member occupies the area ~1000 km^2 and has the thickness >100 m and up to 350 m. The dark mudstone in the member may have continuous thickness >60 m (Team12, 1981). Secondary source rocks are in the E_b^3 member and the upper E_b^1 member of the Buxin Fm(Chen et al., 2008).

The reservoirs reside also mainly in the Lower Eocene Buxin Fm, sandstones in the west, and marl and limestone in the east. The area of single trap is mostly <3 km^2. Commercial oil/gas fields are found in turbidites and sandbars, generally thin with low permeability (Chen et al., 2008).

Several mudstone layers of dozens meters thick in Lower Eocene E_b^2 and E_b^3 of the Buxin Fm form excellent regional cap for hydrocarbon. The thickness of this cap layer is 50~1000 m. Secondary caps are the fine sandstone and mudstone interbeds in the Middle and Upper Eocene Xibu and Huachong Fms, whose thickness is 500~1000 m in general and may reach 1500 m in depo-centers (Chen et al., 2008). Two source-reservoir-seal assemblages exist in the basin. The best one in the Buxin Fm, and the secondary one in the lower member of the Xibu Fm.

Geological conditions for CO_2 storage

The Sanshui Basin has undergone extensive geological exploration, from which a significant amount of data has been accumulated. Here the geological conditions for CO_2 storage are analyzed based on published literatures and reports mainly.

From the CO_2 storage point of view the sediments in the basin may be summarized into three sequences: (1) the Lower Sequence of Cretaceous and Paleocene redbeds; (2) the Middle Sequence of the Early Eocene Buxin Fm and Middle Eocene Xibu Fm, consist of mainly mudstone and fine sandstone; (3) the Upper Sequence of the Late Eocene Huachong Fm, consists of coarse clastics with abundant volcanic materials. The Middle Sequence is a good regional seal, the Lower and Middle sequences may contain reservoirs, while the Upper Sequence has a minor contribution to capping the CO_2 storage.

The quality of seals in the Middle Sequence is “excellent” in terms of the classification on pore structures, especially in the western portion of the basin (Chen et al., 2008). The mudstones in the lower and middle members of the Buxin Fm have thickness of 300~400 m, and the dark mudstone layer in upper Buxin has thickness >100 m in the area of ~500 km^2 (Chen et al., 2008). The quality of the seal may decrease towards the basin margins due to the change of litho-facies to coarse clastics in paleo-lake margins.

Normal faulting was extensive in Late Eocene and cut down to the basement, but mostly small faults elongated in NE direction for a few km. These faults have vertical offset of dozens to over 100 m, and generally <300 m and less than the thickness of the Buxin Fm. Thus the faults tend to form fault traps and do not breeching the integrity of the capping layers (Yan and Jin, 1997). Eocene volcanism resulted in basaltic sheets, which may form local seals.

Earthquake activity is weak in the Pearl River Delta including the Sanshui Basin. No quake greater than M4 has occurred. There are 3 heatflow measurements in the basin area, giving the values in the range of 60~80 mW/m^2 (Wang, 1996). No hot spring has been found within the basin.

The quality of CO_2 reservoir is variable. According to Chen et al. (2008), in the sandstone reservoirs of middle and upper Buxin Fm the porosity is generally 10%~14% and permeability is 50~470 mD. But these numbers differ from those in the report of Team 735 (1976), which is listed in Table 3.2.2. The structural traps are small, usually 1 km^2 and up to 3~4 km^2, with single layer thickness of 1~2 m and up to 6 m. The total thickness of sandstone and siltstone is 2~57 m in lower Buxin, locally 20~42 m in middle Buxin, and in western basin 56~>200 m in upper Buxin. The coarse sediments in the Lower Sequence may be of some storage capacity and may be the future target for CO_2 storage. But relevant data are sparse, especially for the Lower Cretaceous Baihedong Fm. The effect of diagenesis in reducing reservoir porosity and permeability should be examined.

3.2 Capacity assessment for Saline formations

The GIS-based database was built for the stratigraphic formations in the Sanshui Basin, and capacity of CO_2 in deep formations (below 800 m and between 800m and 2500m from the surface,) of the Sanshui Basin is assessed under the following assumptions in addition to the general assumptions stated in Chapter 1:

(1) The middle and upper members of the Buxin Fm (E_b^{2-3}) and the lower member of the Xibu Fm (E_x^1) form regional seals;
(2) CO_2 reservoirs may reside in the sandstone and limestone interbeds in the Buxin Fm and in Cretaceous redbeds;
(3) The deepest Cretaceous Baihedong Fm is not considered in this study because lack of data;
(4) The groundwater chemistry is not considered, and all the formations are assumed saline. Thus the estimates should be considered as maximum.

Isopaches and isobaths of the formations

Isopach contours for individual formations were built after the maps of Team 12 (1982) (Figs. 3.2.1 and 3.2.3) except the Lower Cretaceous Baihedong Fm. The gross isopach of these formations is shown in Fig. 3.2.2a, and the gross isopach of the Sanshui, Buxin, and Xibu formations below 800 m from the surface is shown in Fig. 3.2.2b. The Huachong Fm is excluded in Fig. 3.2.2b because it lies above the regional seal. The volumes of individual formations below 800 m depth from the surface and in the depth range of 800~2500 m were calculated (Table 3.2.1). Isobaths contours for the tops of the formations are shown in Fig. 3.2.3.

Porosity and permeability

Limited and incomplete data on porosity, permeability, and net/gross ratio of the formations in the Sanshui Basin are taken from the early reports of the wells (Table 2-1, 3 and stratigraphic column of Team735 (1975)). Their ranges and calculated weighted averages are generally low (Table 3.2.2). The original tables do not include the data of sandy conglomerate and conglomerate, which are abundant in the lower members of the Cretaceous Sanshui and Dalangshan Fms, thus the porosity and permeability of these formations may be under-estimated. The missing data for the E_b^1 and K_{2d} are assumed equal to those of E_b^2 and K_{2s}, respectively. The parameters of the Buxin Fm are calculated by averaging weighted over thickness of the members.

Table 3.2.1 Areas and volumes of the formations in the Sanshui Basin

Formation	Member	Area (km^2)	Depth of top (m)	Thickness (m)	Volume (Gm3)		
					Gross	-800m	-800~ -2500m
Huachong	E_h	890		100-1540	37.0	4.6	4.6
Xibu	E_x	560	0~1500	50-900	27.2	11.8	11.8
Buxin	E_b	1000	350~2800	50-1000	42.2	25.7	25.1
Dalangshan	K_{2d}	460	>800	200-600	38.2	20.0	17.1
Sanshui	K_{2s}	490		100-600	27.1	18.5	14.1
Total					171.7	80.6	72.6

Capacity calculation

The effective capacity for CO_2 storage in the Buxin, Dalangshan, and Sanshui formations are calculated. Equation (2.1), $M_{CO2} = V \times R \times \varphi \times \rho_{CO2} \times E$, is used in the calculation with $E = 0.01$, 0.026, and 0.04 for a probability level of P15, P50, and P85, respectively. The CO_2 density at formation depths is simplified as a constant, for which the average value for the northern Pearl River Mouth Basin, 0.55 t m^{-3}, is used. Parameters and results are listed in Table 3.3.3. The estimated capacity of CO_2 in saline formations in the Sanshui Basin is 7.2 Mt to 27 Mt and in average 18 $MtCO_2$.

Table 3.2.2 Parameters of sandstones in the Sanshui Basin calculated from the data in Team 735 (1976). Numbers in parentheses are inferred from formation lithology or adjacent formations.

Formation	Member	Porosity (%)			Permeability(mD)			Sample number	Net/Gross (%)	
		Range	Ave.		Range	Ave.				
Buxin	E_b^3	0.4~21	7.3	5.3	<1~702	14.5	7.5	731	53.6	33.4
	E_b^2	0.3~17	4.6		<1~5700	2.8		86	17.4	
	E_b^1		2.5			(2.8)			25.4	
Dalangshan	K_{2d}		(5.2)			(1.2)			(50)	
Sanshui	K_{2s}	<5~16	5.2		<1~23	1.2		179	(50)	

Table 3.2.3 Parameters and capacity assessments for the saline formations in the Sanshui Basin

Parameter		Buxin	Dalangshan	Sanshui	Total
Volume below 800m V (m^3)		25.7×10^9	20.0×10^9	18.5×10^9	
Net:Gross ratio R		0.334	0.5	0.5	
Average porosity φ		0.053	0.05	0.05	
CO_2 density ρ_{CO2} (t m^{-3})		0.55	0.6	0.6	
Effective capacity (t) 800~2500 m	***E* = 0.01**	**2.5×10^6**	**2.6×10^6**	**2.1×10^6**	**7.2×10^6**
	***E* = 0.026**	**6.4×10^6**	**6.1×10^6**	**5.0×10^6**	**17.7×10^6**
	***E* = 0.04**	**9.9×10^6**	**9.4×10^6**	**7.8×10^6**	**27.1×10^6**

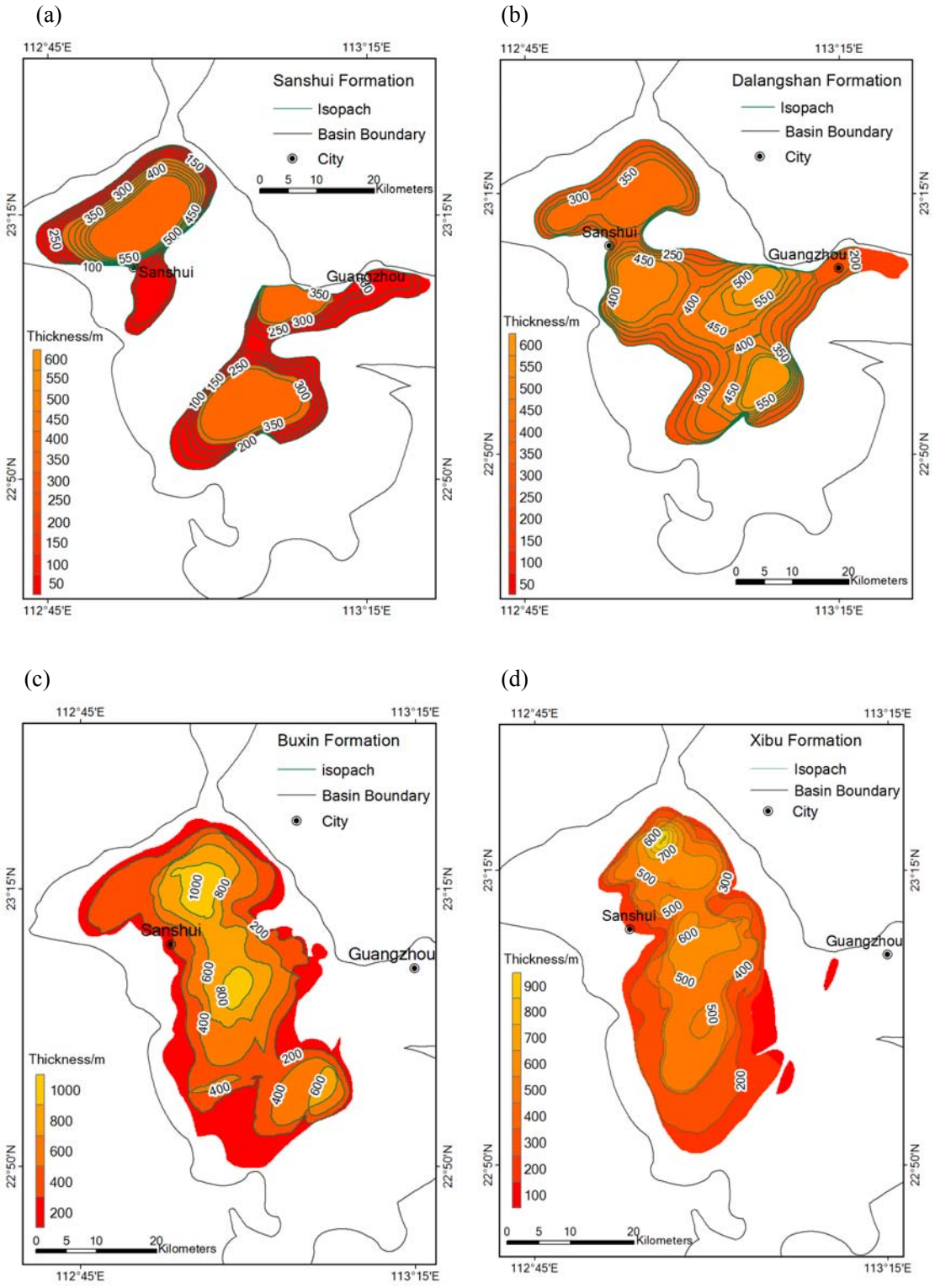

Figure 3.3.1 Isopach maps of the formations in the Sanshui Basin, Guangdong Province.

(a) Sanshui Formation, (b) Dalangshan Formation, (c) Buxin Formation, (d) Xibu Formation.

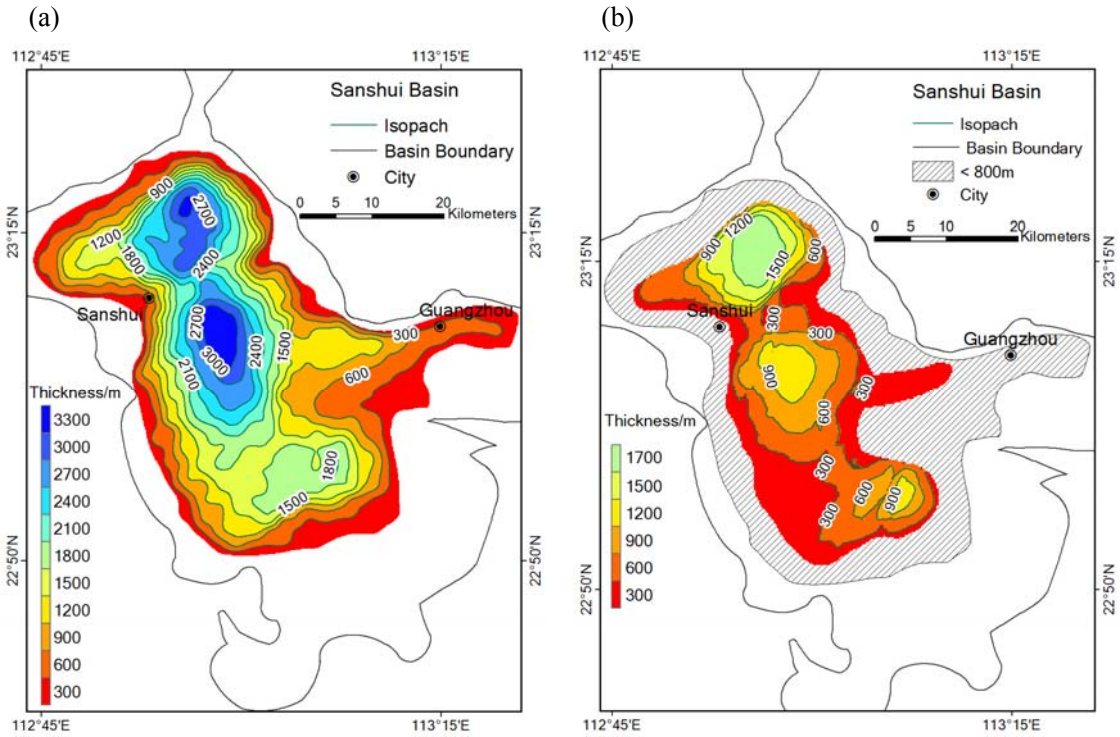

Figure 3.3.2 Maps of gross isopach in the Sanshui Basin, Guangdong Province.
(a) Gross isopach; (b) Gross isopach below 800m from the surface excluding the Huachong Fm.

3.3 Capacity assessment for oil/gas fields

The capacity of CO_2 in oil/gas fields of the Sanshui Basin is estimated using the formula (2.3) $M_{CO2} = \rho_{CO2} \times (R_f \times OOIP / B_f) \times C_e$ and formula (2.5) $M_{CO2} = \rho_{CO2r} \times R_f \times OGIP \times B_g \times C_e$. The parameters used are listed in Table 3.3.1. The estimated capacity of CO_2 in oil and gas fields of the Sanshui Basin is 2.3 Mt to 4.9 Mt and in average 3.23 MtCO_2.

Table 3.3.1 The capacity of CO_2 in oil fields of the Sanshui Basin

Parameter		Value	Data source
OOIP $V_{oil(STP)}$ (t)		12×10^6	MLRC et al. (2008)
Recovery rate R_f		0.4	Pearl River Mouth Basin
Volume factor B_f		1.03	Pearl River Mouth Basin
CO_2 density ρCO_2 (t/m^3)		0.55	Northern Pearl River Mouth Basin
Effective capacity M_{CO2} (Mt)	Ce = 0.12	0.31×10^6	
	Ce = 0.25	**0.64×10^6**	
	Ce = 0.40	1.02×10^6	

Table 3.3.2 The capacity of CO_2 in gas fields of the Sanshui Basin

Parameter		Value	Data source
OGIP $V_{oil(STP)}$ (m^3)		1700×10^6	MLRC et al. (2008)
Recovery rate R_f		0.55	Yinggehai Basin
Volume factor B_g		0.0084	Yinggehai Basin
CO_2 density ρCO_2 (t/m^3)		0.55	Northern Pearl River Mouth Basin
Effective capacity M_{CO2} (t)	Ce = 0.47	2.03×10^6	
	Ce = 0.6	**2.59×10^6**	
	Ce = 0.9	3.89×10^6	

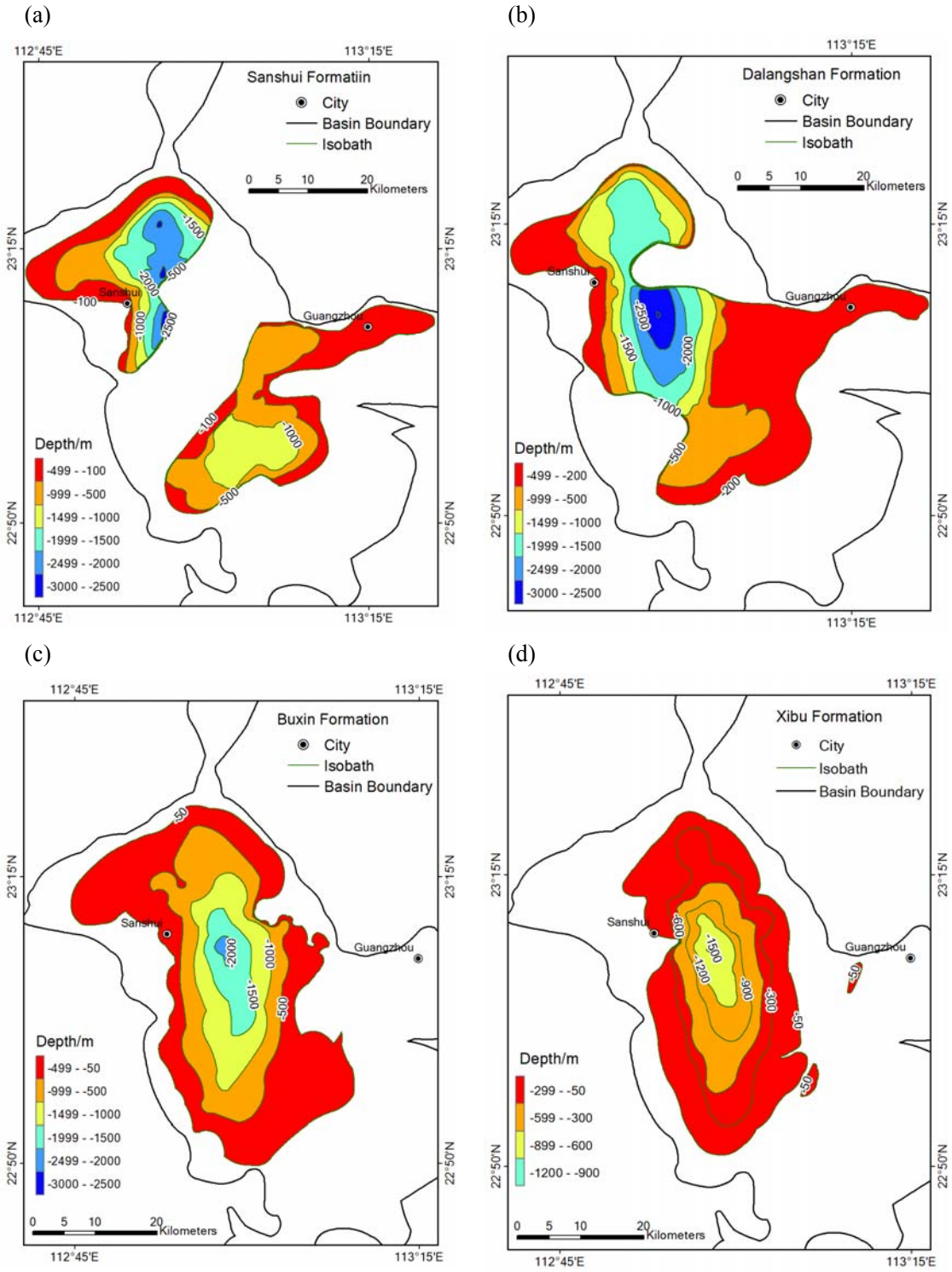

Figure 3.3.3 Isobath maps of the formation tops in the Sanshui Basin, Guangdong Province.

(a) top of Sanshui Fm,, (b) top of Dalangshan Fm., (c) top of Buxin Fm., (d) top of Xibu Fm.

3.4 Conclusions

In the Sanshui Basin, the estimated effective CO_2 storage capacity is only 20.4 MtCO_2 in average, include the storage capacity of 3.2 Mt in average in oil and gas fields. These estimates are of high uncertainty because they were obtained based on published incomplete data, and with the assumptions that all the formations are saline and all the pore space may be filled with injected CO_2. The capacity of the Lower Cretaceous Baihedong Formation at depth is not considered in the calculation because of the lack of data.

Compared with other sedimentary basins inland Guangdong, the Sanshui Basin is the most advantageous basin for CO_2 storage in the following aspects:

1) The 300~400 m thick mud-rich Early Eocene Buxin formation is excellent regional seal. It is faulted, but the faulting did not destroy its lateral continuity;
2) Very small oil/gas fields exist and may be transformed to CO_2 storage pilot or demonstration sites when they become depleted;
3) Extensive data and infrastructures are accumulated during a long period of exploration;
4) Proximal to major CO_2 point sources in the most industrialized Pearl River Delta.

However, the Sanshui Basin has the following disadvantages in terms of CO_2 storage:

1) The effective storage capacity is very small;
2) The reservoirs are of poor quality: their sizes and thickness are small, porosity and permeability are low, and heterogeneity is high;
3) The entire basin resides in a densely populated and economical developed region of the Pearl River Delta.

In summary, although the Sanshui Basin is proximal to the emission sources, the small storage capacity, poor reservoir property, and the heavy land use in the basin make it un-suitable for large-scaled CO_2 storage.

The Sanshui Basin is the only petroliferous basin inland Guangdong. The geological conditions of other inland basins in Guangdong are even less favorable for CO_2 storage in terms of even smaller size and poorer reservoir quality. Taking into account of the dense population and high economic development in the province, there are essentially no storage potential inland Guangdong.

Chapter 4 CO_2 Storage Capacity of the Pearl River Mouth Basin

4.1 Geography and geology

Geography

The Pearl River Mouth Basin (PRMB), 111°20′~118°0′E and 18°30′~23°00′N, is the largest sedimentary basin in the northern South China Sea offshore Guangdong Province. It is a NEE-elongated basin, 900 km long and 115-280 km wide, with total area of 170 000 km^2, or 147 000 km^2 if calculated with sediment thickness ≥1 km (Cai, 2005). The basin resides in the shelf (~68% in area) and the slope of the northern South China Sea, with water depth ranging from 50 m to over 2000 m (Fig. 4.1.1).

General geology

The PRMB has experienced extensive geological survey and oil/gas exploration since the 1970's of the last century. Numerous papers and books have been published on its geology and hydrocarbon resources (Chen et al., 2003; Gong and Li, 1997; Pang et al., 2007a).

Geologically the PRMB is an extensional basin in the passive continental margin of the northern South China Sea. It was formed by rifting of the South China Block in Paleogene and subsequent subsidence in Neogene. Geographically the basin was generally continental in Paleogene and marine in Neogene.

The basement of the PRMB is composed of Mesozoic granites and secondarily Paleozoic metamorphic rocks. Above the basement there are 4 depressions aligned in two NEE-running belts: The Zhu-3 and Zhu-1 depressions in the northern depression belt, and the Zhu-2 and Chaoshan depressions in the Southern depression belt (Fig. 4.1.1). The two belts are separated by a NEE-running belt of uplifts.

In vertical sections the structures are composed of the lower section of Paleogene rifts (half-grabens and grabens) and the upper section of Neogene post-rift downwarps (Fig. 4.1.1). Rifting occurred episodically since Late Cretaceous, reached the climax in Late Eocene, and ended in Early or Late Oligocene. NEE faults often controlled the orientation of the depressions, while NWW-EW faults controlled the distribution of sags and traps. NW-running large crustal or lithospheric faults cut the depression belts into blocks. In Neogene, long-wavelength subsidence occurred in wide areas by post-rifting lithosphere cooling and contraction.

Cenozoic volcanism occurred episodically from Early Eocene to Quaternary (Liang and Li, 1992). They are mostly acid and intermediate volcanic clasts, with mafic and intermediate lavas in Paleogene, and basaltic lavas in Neogene and Quaternary. Except the Quaternary basalts these appear usually in small sizes and in vicinity of large NW faults. Locally the volcanic rocks may have large total thickness, e.g., the BY7-1-1 well in the western Zhu-2 depression encountered Oligocene to Early Miocene tuff and basalts of ~400 m in thickness (Chen et al., 2003).

Earthquake activity has been sparse and weak in major portions of the PRMB (Fig. 4.1.2). The only M>6 earthquake occurred in the western central uplift belt (Sept. 1931, M6.75).

Stratigraphy and paleo-geography

The PRMB is filled with Cenozoic sediments with maximum thickness of >6 km in shelf areas and may be >14 km in slopes (Chen et al., 2003; Zhou et al., 2009), except in the Chaoshan depression where Paleogene is absent and the depression is filled with 1~2 km Neogene underlain by >7 km of Mesozoic un-metamorphosed sediments (Hao et al., 2009).

The stratigraphic column of the PRMB is shown in Fig. 4.1.3. During Paleogene the PRMB was inland on the South China Block, receiving fluvial and lacustrine sedimentation in rifted basins and incised valleys. The Paleogene to Early Eocene Shenhu Fm appears in restricted areas and consists of mudstone and sandstone interbeds. The Middle Eocene Wenchang Fm contains the major source rocks of the basin. Its middle section is composed of dark mudstone deposited in large and deep lakes, locally reaches a total thickness of 230 m and single layer thickness of >70 m. The dark-mudstone section is topped by the upper member of sandstone, siltstone with coal-bearing mudstone, and bottomed by gravel sandstones. The upper Eocene to Lower Oligocene Enping Fm is characterized by coal-bearing interbeds of clastic rocks and is another major source rock interval in the basin. The Late Oligocene Zhuhai Fm consists of three cycles of coarse-to-fine clastic rocks deposited in alternative continental-marine environments. It is relatively rich in sandstones (Cai, 2005).

After the breakup of the South China Sea in ~30 Ma, the PRMB subsided to a marine environment. The sealevel oscillated but in general trend of rising (Qin, 2002) (Fig. 4.1.3), opposite to the global trend of sealevel dropping during the Neogene period. Frequent fluctuation of sealevel has resulted in cyclic sedimentations throughout the period, forming multiple deltas in the north and sequences of marine strata in the south. The Lower Miocene Zhujiang Fm is characterized, in addition to clastic sediments, by the development of reefal limestone on local highs. The Middle Miocene Hanjiang Fm contains mainly sandstones in the lower section and mainly mudstone in its upper section. The Upper Miocene Yuehai Fm is composed of mudstone and sandstone. The Pliocene Wanshan Fm contains less compacted sandstone and mudstone. The Quaternary sediments are mainly silt and mud (Cai, 2005; Gong and Li, 1997).

Petroleum Geology

Major source rocks in the PRMB are the lacustrine dark mudstones of Middle Eocene Wenchang Fm and the coal-bearing sequences in Late Eocene to Early Oligocene Enping Fm. The dark mudstones in the Zhuhai and Zhujiang Fms are secondary source rocks (Cai, 2005).

There are three source-reservoir-seal assemblages in the PRMB: (1) the Paleocene-Eocene self-contained continental assemblage developed sparsely in northern PRMB; (2) the Paleogene-Eocene-Miocene assemblage with sources in continental Paleogene formations locally within sags, reservoirs in marine Zhuhai and Zhujiang Fms, and caprocks in upper Zhujiang Fm; (3) the Zhujiang-Yuehai marine assemblage with sources in Zhujiang Fm, reservoirs in Hanjiang Fm, and caprocks in upper Hanjiang Fm and in Yuehai Fm (Cai, 2005; Zhu et al., 2008) .

Structural traps in sandstone and the cavities in carbonate buildups are the principal reservoir types in the PRMB. Oil fields have been found mainly in the Zhu-1 depression along the edges between the northern Dongsha Uplift and the southern Huizhou Sag and southwestern Lufeng Sag, and in the southern Dongsha Uplift (Fig. 4.1.1). By the end of 2007, a total of 169.5 Mt oil has been produced from the northern South China Sea, the majority from the PRMB. Most oil fields

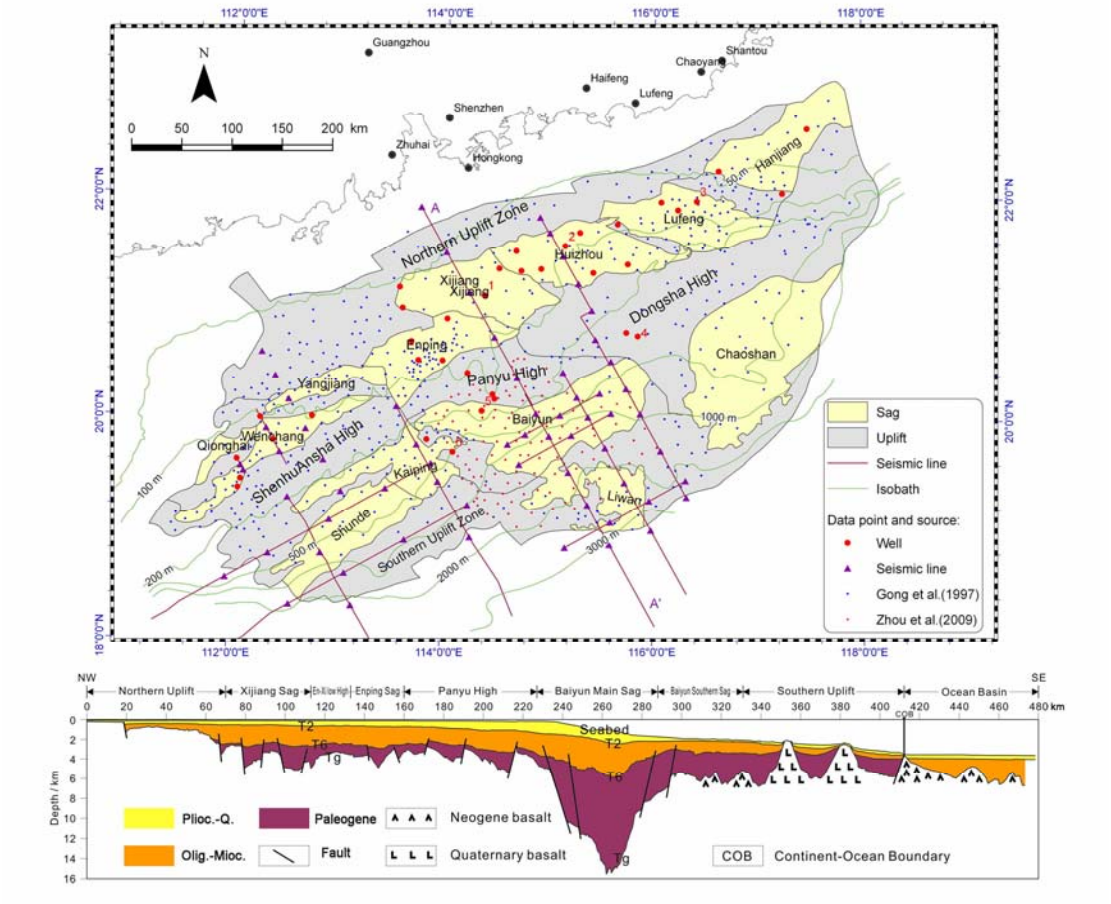

Figure 4.1.1 Simplified geological map and cross section AA' of the Pearl River Mouth Basin. Data points used in the assessment are superimposed.

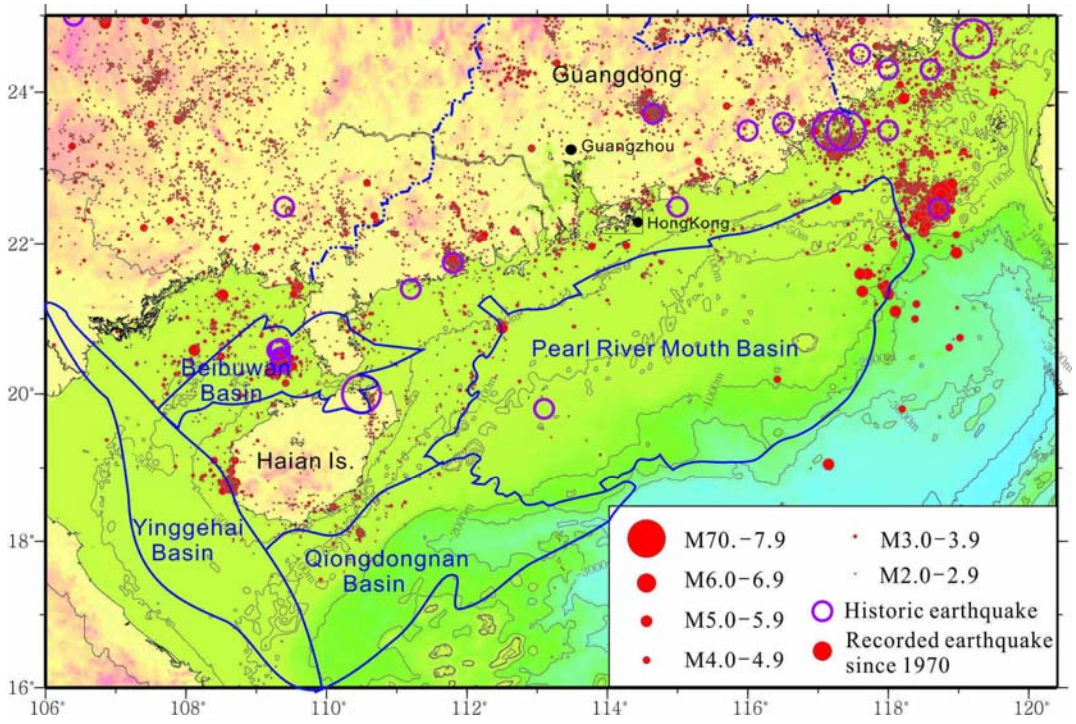

Figure 4.1.2 Seismic epicenters and magnitudes in Guangdong and northern South China Sea (courtesy of Jinglong Sun). Location of sedimentary basins is superimposed.

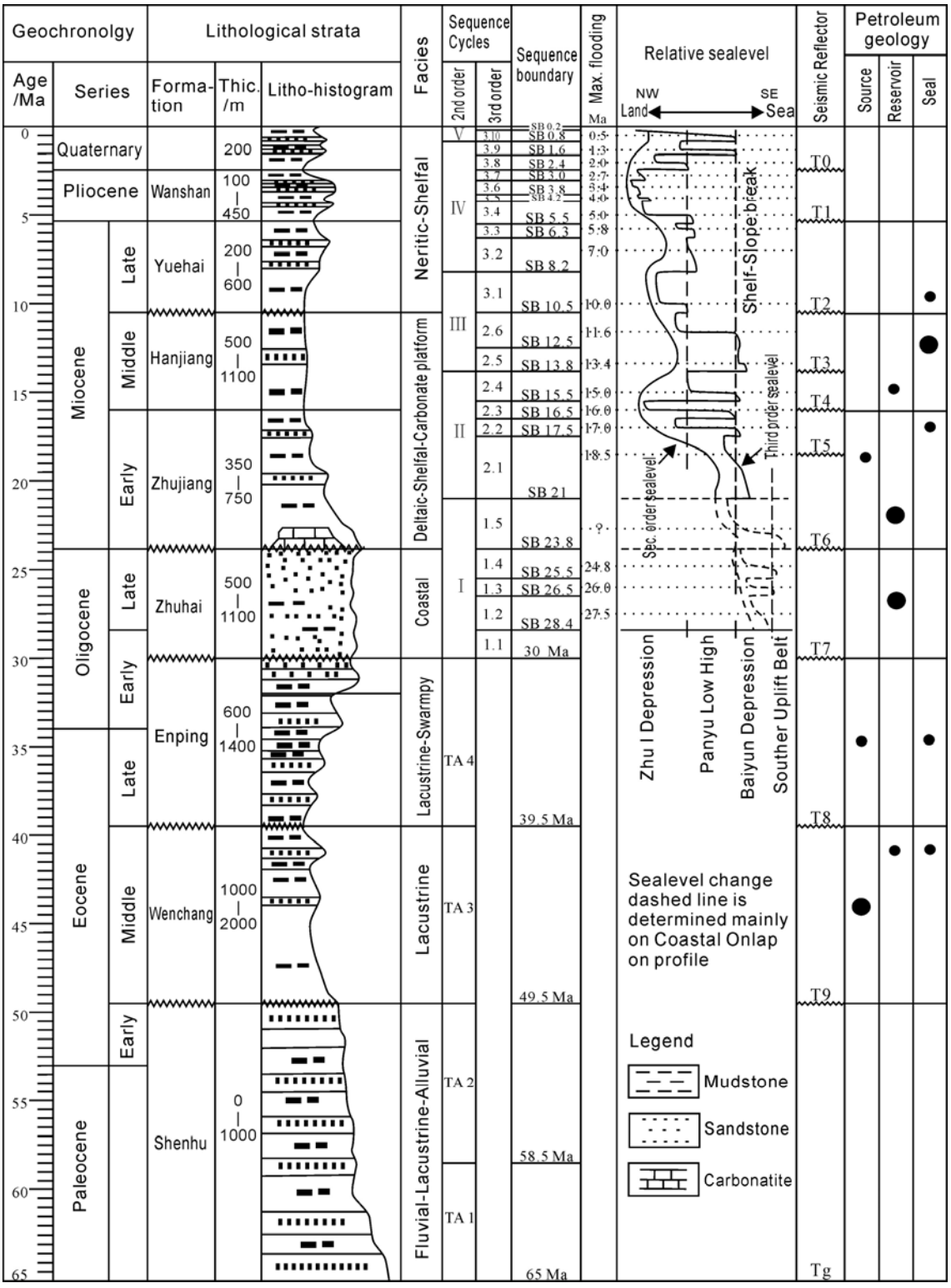

Figure 4.1.3 Stratigraphic column of the Pearl River Mouth Basin. Sequence stratigraphy after Yang et al.(1996) and Pang et al.(2007a), sealevel curve after Qin (2002), and others after Chen et al. (2003).

are small, except the LH11-1 field with proved reserves over 100 Mt (0.73 billion barrels) (Zhu et al., 2008). In recent years, large gas fields have been discovered in the Wenchang Sag of the Zhu-3 depression, and in the Baiyun Sag and its northern edge of the Zhu-2 depression.

4.2 Capacity assessment for Saline formations

Geological conditions for CO_2 storage

The topmost regional seal is the transgressional mudstones in the Middle Miocene Hanjiang Fm. In the Zhu-1 depression the Hanjing Fm contains 400~600 m mudstones, 70%~80% of the formation thickness; while in the Zhu-2 depression to the south these numbers are 700~800 m and 80~90% (Cai, 2005). As the mudstones in the Hanjiang Fm form the uppermost regional seal, in this assessment the strata above the Hanjiang Fm will not be considered. Beneath this regional seal the delta-front sandstones of the Hanjing Fm form good reservoirs, with porosity 28.7% to 37.5%, and permeability 188 mD to 1732 mD (Cai, 2005).

The middle seal-reservoir assemblage is within the Lower Miocene Zhujiang Fm, which is composed of delta front and transgressional mudstones interbedded with delta-front sandstones or carbonates. The mudstones have 57~90% of the formation thickness in most part of the basin. A single mudstone layer of >6 m thickness can form effective seal. The porosity and permeability of the sandstones reservoirs are similar as those in the Hanjiang Fm (Cai, 2005). Reefal carbonates mainly in the Dongsha uplift are important reservoirs with porosity of 9~28% and permeability of 7~1365 mD. The LH11-1 field in the carbonate of the Zhujiang Fm is the largest oil field in the basin. The average porosity and permeability in the LH11-1 field are 23% and 472 mD respectively (Cai, 2005).

The Upper Oligocene Zhuhai Fm has local seals of delta front and lacustrine mudstones. The reservoirs in the formation are transgressional delta front, channel, and sandbar sandstones, with. porosity of 15~20% and permeability of 156-875 mD. Single reservoir thickness up tp 20~37 m (Chen, 2003; Table 4.2.4). The tansgressional sequence in the Zhuhai Fm may have thickness of 145-175 m and porosity of 16~30% (Cai, 2005). A regional unconformity exists beneath the Zhuhai formation, thus the sealing conditions in the bottom should be examined case by case.

The Oligocene Enping Fm and older strata are composed of mainly continental clastic sediments that filled discrete sags. They contain major source rocks for hydrocarbon, but are not favorable for CO_2 storage as their relatively rapid facies changes and large depths.

Data sources

A GIS-based database was built for the Cenozoic formations in the PRMB based on the data compiled from published sources, including those from 31 wells. As available well data are insufficient for depth and isopach mapping, 23 regional seismic profiles (depth converted) and published low-resolution isopach maps (e.g., the three isopach maps from Gong et al., 1997, as well as the isopach maps of the Baiyun Sag from Zhou et al., 2009) have been used to provide additional data points. Resulting isopach maps are in reasonable resolution for assessing the effective capacity (see Fig. 4.1.1 for data point distribution). Water depths are from the Geographic Map of the South China Sea printed by SCSIO in 1983.

Formation volumes

For the assessment of storage capacity the Cenozoic formations of the PRMB are divided into two super sequences: Paleogene (Wenchang, Enping, and Zhuhai Fms), Lower-Middle Miocene (Zhujiang and Hanjiang Fms). The sequence of Upper Miocene to Holocene lies above the uppermost regional seal in the Hanjiang Fm is assessed only for thickness in order to define the upper surface of the sequence bellow. Maps of their surface depths and isopaches were constructed (Figs. 4.2.1 and 4.2.2). Their gross volumes and the volumes below 800 m and above 3500 m from the seafloor, and volumes in the depth range 800~3500 m within the shallow water (<300 m) areas were calculated on a GIS platform (Table 4.2.1).

Table 4.2.1 Areas and volumes of the super sequences in the Pearl River Mouth Basin

Super sequence	Area (km^2)	Depth of top (m)	Thickness (m)	Volume (Gm3)		
				Gross	800-3500 m	Shallow area
Paleogene	197290	0-2600	0-1700	175773	169000	93000
L.-M. Mioc.	174856	0-700	0-2500	235228	203000	141000
U. Mioc. To Q	30185	0	0-700	114490	6240	
Total				525491	378240	234000

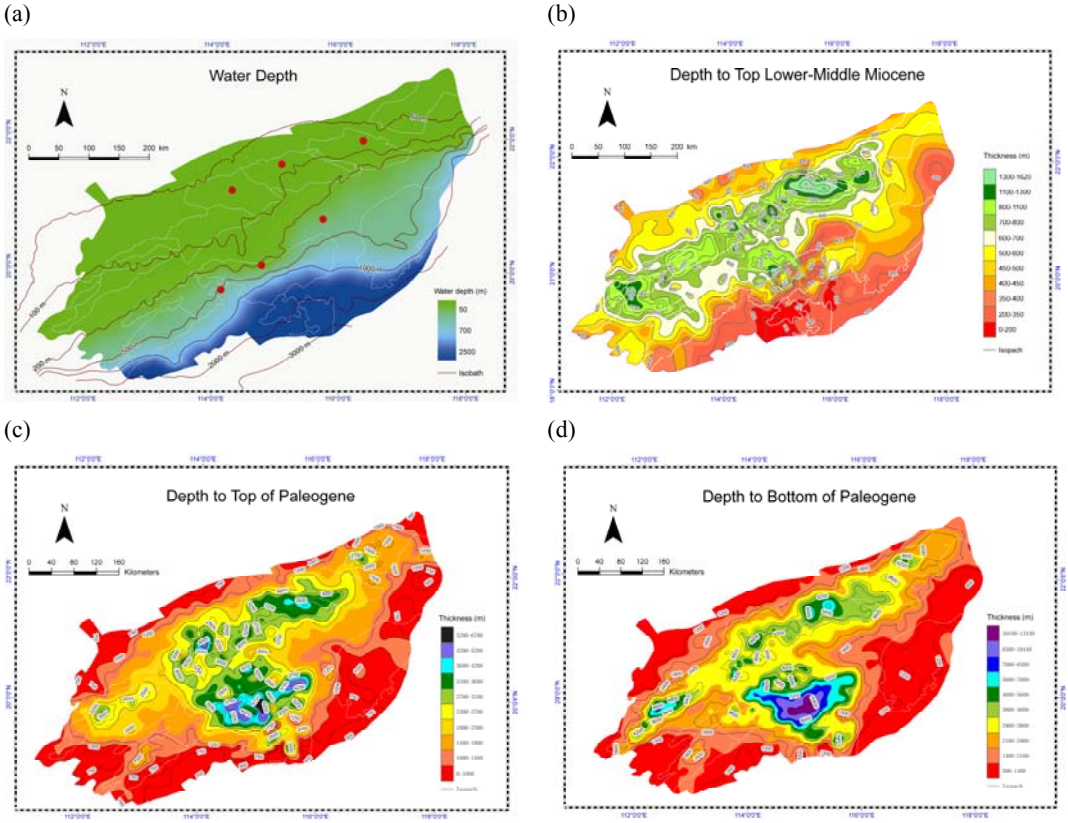

Figure 4.2.1 Depths from seafloor to formation interfaces in the Pearl River Mouth Basin.
(a) Seafloor, red dots are locations of the wells in Table 4.2.2; (b) Top of Lower-Middle Miocene; (c) top of Paleogene; (d) bottom of Paleogene.

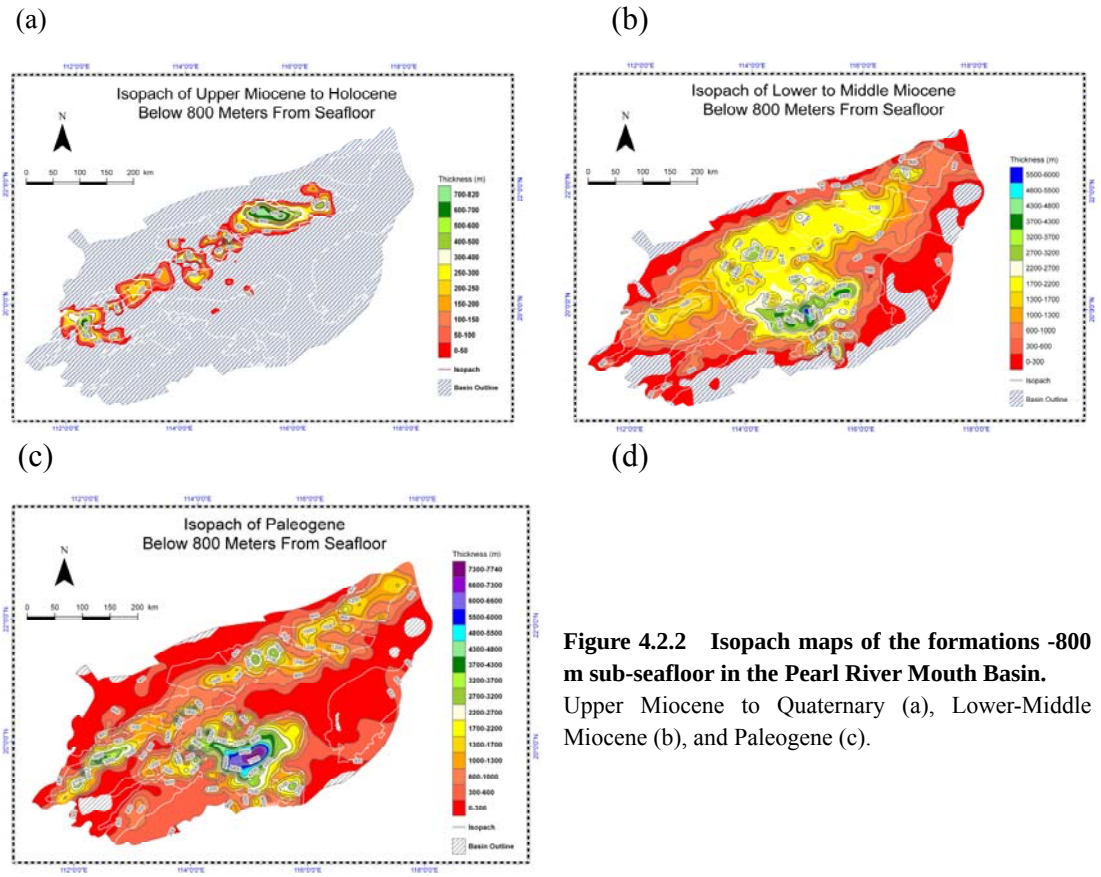

Figure 4.2.2 Isopach maps of the formations -800 m sub-seafloor in the Pearl River Mouth Basin. Upper Miocene to Quaternary (a), Lower-Middle Miocene (b), and Paleogene (c).

Lithological parameters

Published data on net/gross ratio, porosity and permeability of the rocks in the PRMB are sparse. Thus we have to estimate based on several sets of incomplete or indirect data.

Stratigraphic columns from 6 wells in the Zhu-1 and Zhu-2 depressions have been used to measure the net/gross ratio (Table 4.2.3). Simple averages of net/gross ratios in these wells are 0.36, 0.49, and 0.64 for the super layers of Paleogene, Early to Middle Miocene, and Upper Miocene to Holocene, respectively.

Data of oil-tested sandstone segments from 11 wells and of sampled segment from 7 wells of the eastern PRMB (east of longitude 113°E) are published in Tables 5-2, 5-3, and 5-4 of Chen et al. (2003). The average values weighted by segment thickness are listed in Table 4.2.5.

Petroleum systems have been delineated in the eastern PRMB, and their parameters are listed in the Table 8-2 of Chen et al. (2003). Based on these data the parameters of caprocks and reservoirs in the formations of the eastern PRMB are calculated by thickness-weighted averaging (Table 4.2.4).

Table 4.2.2 Statistics for net/gross ratios in 6 wells in the Pearl River Mouth Basin*.

SS-Sandstone, MSS-Muddy Sandstone, CA-Carbonate, MS-Mudstone, SMS-Sandy mudstone, N/G is (SS+MSS+CA)/(MS+SMS).

		HF33 -3-1	%	N/G %	HZ13 -1-1x	%	N/G %	BY7 -1-1	%	N/G %	LH11 -1-2	%	N/G %	XJ33 -2-1A	%	N/G %	PY33 -1-1	%	N/G %	Ave. N/G %
Paleo-gene	SS	0	0.0	0.0	305	22.8	23.8	330	58.1	58.1	85	54.8	54.8	485	25.3	47.0				36.8
	MSS	0	0.0		14	1.0		0	0.0			0.0		410	21.4					
	CA	0	0.0		0	0.0		0	0.0		0	0.0		7	0.4					
	MS	262	23.3		811	60.6		238	41.9		45	29.0		1016	53.0					
	SMS	862	76.7		208	15.5		0	0.0		25	16.1		0	0.0					
	Total	1124	100.0		1338	100.0		568	100.0		155	100.0		1918	100.0					
E-M Mioc	SS	705	54.3	57.0	1471	72.7	81.1	375	25.8	28.5	0	0.0	37.0	1046	36.5	59.4	583	29.6	36.4	49.9
	MSS	7	0.5		171	8.4		40	2.7		305	37.0		653	22.8		134	6.8		
	CA	28	2.2		0	0.0		0	0.0		0	0.0		3	0.1			0.0		
	MS	12	0.9		62	3.1		1040	71.5		520	63.0		1162	40.6		1255	63.6		
	SMS	547	42.1		320	15.8		0	0.0		0	0.0			0.0			0.0		
	Total	1299	100.0		2024	100.0		1455	100.0		825	100.0		2864	100.0		1972	100.0		
L Mioc -Q	SS	832	82.0	98.0	986	74.6	95.6	0	0.0	0.0										64.5
	MSS	20	2.0		0	0.0		0	0.0											
	CA	143	14.1		278	21.0		0	0.0											
	MS	0	0.0		53	4.0		675	100.0											
	SMS	20	2.0		5	0.4		0	0.0											
	Total	1015	100.0		1322	100.0		675	100.0											

* Data are from well log interpretations of CNOOC. Well locations are indicated by red dots in Fig.4.2.1a

Table 4.2.4 Parameters of reservoirs and seals in eastern PRMB based on regional data from Table 8-2 of Chen et al. (2003)

Formation	Region	Reservoirs					Seals			N/G %
		Gross thickness	Sandstone	Max single layer	Porosity	Permeability	Gross thickness	Mudstone	Max single layer	
		(m)	%	(m)	%	(mD)	(m)	%	(m)	
Hanjiang	EP	596.0	51.2	8-22.5	33.1		279.5	46.8	12.0-22.0	
	Range	567-625	43.0-59.5	8-22.5	28.7-37.5		229-330	40.5-53.3	12.0-22.0	31.9
Zhujiang	EP	931.0	49.3	12.5-30	21.5	623.0	468.8	49.1	16.5-21	
	EP-E*	319.0	40.0	10.0-22.0	23.7	750.0	105.0	53.5	20.0-28.0	
	XJ*	1100.0	62.0	71.0	23.0	524.0	616.0	28.0	27.0	
	XJ-E*	470.0	35.0	30.0	24.0	1650.0	1000.0	63.0	105.0	
	HZ-W*	541.0	50.5	43.0	23.3	1536.0	1036.0	66.0	97.0	
	HZ-E	280.0	27.0	9-33	18.8	36.2	624.0	61.0	120.0	
	LF-S	174.0	24.0	32.0	17.0	630.0	500.0	72.0	35-211	
	Range		16-77	9-71		19-1650	70-1408	15-82	20-211	
	W. Ave		47.8		22.3	818.3		57.8		44.8
Zhuhai	XJ	400.0	63.5	35.5	15.0	303.0	440.0	36.0	30.0	
	HZ-W	313.5	86.5	37.0	16.8	875.0	132.0	20.0	10.0	
	HZ-N	147.2	85.0	20.0	18.6		576.0	63.0	4.0	
	LF-S	214.0	66.0	37.0	20.0	316.0	132.0	35.0	7.0-13.0	
	Range		47-96	20-37		156-875	11-576	5-63	4.0-30.0	
	W. Ave		73.7		17.0	430.9		46.4		62.8

* Including Hanjiang Formation.

** "W. Ave." stands for thickness-weighted averages.

The parameters compiled from the above-mentioned sources are compared in Table 4.2.6. The porosities and permeabilities are reasonable consistent, but the net/gross ratio varies significantly. The data in Table 4.2.5 has much higher Net/Gross ratios and can not represent the reservoirs in water zones. The data in Table 4.2.4 are from a regional study and should be more reliable, but they are only for the middle sequence of Lower to Middle Miocene. In this capacity calculation, the net/gross ratios from 6 wells (Table 4.2.3) were used. It should be keep in mind that these parameters were collected from hydrocarbon reservoirs or petroleum systems and thus are not representative for all saline formations in the basin. This is, however, the only feasible practice at the present. As pointed out by USDOE (2008), "Because formation heterogeneity terms are included (in the storage efficiency factor), this estimate could be considered a reasonable maximum storage resource estimate".

Table 4.2.5 Parameters of oil-tested sandstone segments from the wells in eastern PRMB
(thickness-weighted averages based on tables 5-2, 5-3, and 5-4 in Chen et al. 2003)

Formation	Porosity (%)		Permeability(mD)		Net/Gross ratio (%)	# of wells
	Range	Ave.	Range	Ave.		
Zhujiang	13.3~23.9	19.9	20.2~2027.9	916.5	92.6	10
Zhuhai	2.3~22.7	16.8	3.5~299.1	318.0	87.8	11
Enping	0.7~22.0	10.3	0.03~95	7.0	No data	14

Table 4.2.6 Comparison of the reservoir parameters compiled from various data sources.

	Porosity (%)	Permeability (mD)	Net/Gross (%)	Data source
Hanjiang	33.1		31.9	Table 4.2.4
	16.3~29.6	188~1732	10~30	Cai (2005)
Zhujiang	19.9	916.5	92.6	Table 4.2.5
	20.8	624.1	44.8	Table 4.2.4
	16.3~29.6	188~1732	10~43	Cai (2005)
Zhuhai	16.8	318.0	87.8	Table 4.2.5
	17.0	431	62.8	Table 4.2.4
	4.5~16.8	4.4~2434		Cai (2005)
Enping	10.3	7.0		Table 4.2.5

CO_2 density

The density of CO_2 varies with formation temperature and pressure (Bachu, 2003). The PRMB is in general in a normal pressure system. Overpressure is observed only locally in deeply buried (>4600 m) Wenchang and Enping formations (Gong and Li, 2004). Thus in this paper we use the hydrostatic pressure to approximate the formation pressure.

The formation temperature depends on the surface temperature and geothermal gradient. The seafloor temperature of the northern SCS varies with water depth as shown in the inset of Fig. 5. The thermal gradient varies across the PRMB in the range of 26.2~50.6 ºC /km. A contour map of geothermal gradients in the PRMB was compiled based the data of 75 wells (Fig. 5) from Rao

andLi (1991). The gradient is in general lower than 35 ºC /km in the shallow-water Zhu 1 depression, while higher in the deep-water Zhu 2 and shallow-water Zhu 3 depressions. Accordingly we divide the basin into three regions (Fig. 5): the N-PRMB with relatively high seafloor temperature and low thermal gradient, the S-PRMB with relatively low seafloor temperature and high thermal gradient, and the SW-PRMB with both high seafloor temperature and high thermal gradient. Curves of CO_2 density versus formation depth were constructed respectively for each region (Fig. 6) based on Span and Wagner (1996). In Fig.6 selected curves from other publications are also presented for comparison. The increase rate of CO_2 density with depth in the PRMB is much slower than the 35 ºC/km curve of GeoCapacity (2009), and in between the "Typical" and "Hot" curve s of Chadwick et al.(2008).

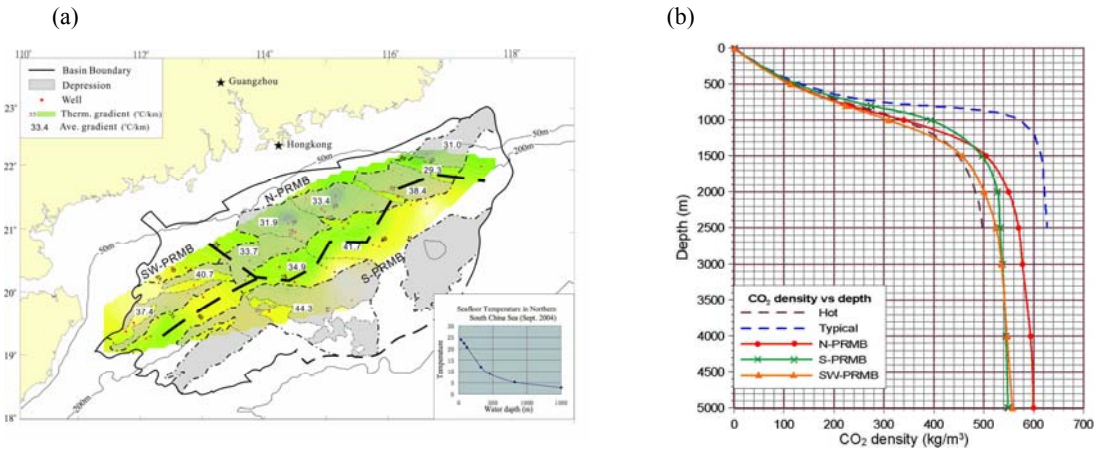

Figure 4.2.4 (a) Contour map of geothermal gradient of the Pearl River Mouth Basin compiled based on drill hole measurements given in Rao and Li (1991) with minor additions. Thick dashed line divides the basin into 3 districts for constructing CO_2 density curves. Numbers show the average gradient (in ◦C/km) for individual sags. Inset is a curve of seafloor temperature in northern South China Sea measured by SCSIO. (b) Curves of CO_2 density versus depth for N-, S-, and SW- Pearl River Mouth Basin. Curves of "Typical" and "Hot" regions from Chadwick et al. (2008) are also shown for comparison.

Capacity calculation

The effective capacity for CO_2 storage in the saline formations in the Pearl River Mouth Basin is estimated under the following assumptions in addition to the general assumptions stated in Chapter 2:

(1) The Middle Miocene Hanjiang Fm forms the upper regional seal, and the delta-front and transgressional mudstone in the Zhujiang Fm form the lower regional seal;

(2) CO_2 reservoirs mainly reside in the sandstones and limestones of the Early Miocene Zhujiang and Zhuhai Fms, and secondarily in Middle Miocene Hanjiang Fm and in Oligocene Enping Fm;

(3) Because to the authors no data are available for the Wenchang Fm., its parameters are assumed to be the same as those of the Enping Fm.

Therefore, only the Paleogene (Wenchang, Enping, and Zhuhai) and Lower-Middle Miocene (Zhujiang and Hanjiang) formations are considered in the capacity calculation. Equation (2.1) is used in the calculation with E = 0.01, 0.026, and 0.04 for a probability level of P15, P50, and P85, respectively. Parameters and results are listed in Table 4.2.7. The effective CO_2 storage capacity in saline formations of the PRMB ranges in 110 Gt CO_2 to 443 Gt CO_2 and in average 289 Gt CO_2,

while the capacity in shallow area of the PRMB ranges in 77 Gt CO_2 to 310 Gt CO_2 and in average 201 Gt CO_2. More than 80% storage capacity resides in Lower to Middle Miocene formations.

Table 4.2.7 Estimates of effective capacity of saline formations in the Pearl River Mouth Basin

Parameter		L.-M. Miocene	Paleogene	Total
Volume 800-3500 m V (Gm3)		203000	169000	
Volume 800-3500 m in shallow area		141000	93000	
Net/Gross ratio R		0.5	0.37	
Average porosity φ		0.2	0.1	
CO_2 density ρ_{CO2} (t/m^3)		As in Fig. 4.2.4b	As in Fig. 4.2.4b	
Effective capacity (GtCO_2), 800-3500 m	***E* = 0.01**	**91**	**19**	**110**
	***E* = 0.026**	**238**	**51**	**289**
	***E* = 0.04**	**365**	**78**	**443**
Effective capacity (GtCO_2), Shallow area	***E* = 0.01**	**64**	**13**	**77**
	***E* = 0.026**	**167**	**34**	**201**
	***E* = 0.04**	**258**	**52**	**310**

4.3 Capacity assessment for oil/gas fields

Up to 2009 there are ~200 wells have been drilled in the PRMB, and ~40 oil/gas fields have been found, with oil production over or near10 million tons since 1996. The estimations of geological resources in the PRMB are 2.2 Gt oil equivalent (MLRC ET AL., 2008). The resources may be underestimated because the PRMB is still in active exploration. For example, the newly estimated resource of the Zhu-1 depression alone reaches 5.9 Gt oil equivalent (Shi et al., 2009), and new gas fields have been discovered in the deepwater Baiyun Sag of the Zhu-2 depression (Pang et al., 2007b).

The capacity of CO_2 in oil/gas fields of the PRMB is estimated using the formulas (2.3) and (2.5). The parameters used are listed in Tables 4.3.1 and 4.3.2, where *OOIP* and *OGIP* are the geological resources in Chinese nomenclature, and the value of storage capacity factor C_e are explained in section of 2.3 in this report.

Assuming that all the oil and gas fields can be used for CO_2 storage after their depletion, our assessment indicates that in the PRMB the oil fields have effective capacity of 0.06~0.2 (average 0.13) Gt CO_2, and the gas fields have effective capacity of 1.1~2.1 (average 1.4) Gt CO_2.

Table 4.3.1 Estimates of the effective CO_2 storage capacity in oil fields of the Pearl River Mouth Basin

Parameter		Value	Data source
OOIP (Mt)		2327	Zhu et al. (2010)
Recovery rate R_f		0. 4	Liu et al. (2009)
Volume factor B_f		1.03	CNOOC
CO_2 density ρCO_2 (t/m3)		0.566	Fig. 4.2.4b
Theoretical CO_2 storage capacity (Mt CO_2)		511	
Effective storage capacity (Mt CO_2)	P85: Ce = 0.12	61	
	P50: Ce = 0.25	128	

	P15: $Ce = 0.4$	205	

Table 4.3.2 Estimation of the effective CO_2 storage capacity of gas fields in the Pearl River Mouth Basin.

Parameter		Value	Reference
OGIP (Gm3)		1961	Zhu et al. (2010)
Recovery rate		0.55	DF1-1 data
Reservoir CO_2 density (ρ_{CO2r})		0.56	Fig. Q5
Gas volume factor (B_g)		0.00385	$=(P_s \times Z_r \times T_r) / (P_r \times Z_s \times T_s)$
Theoretical CO_2 storage capacity		2325 Mt	$=\rho_{CO2r} \times R_f \times OGIP \times B_g$
Effective Storage capacity (Mt CO_2)	P85: $C_e = 0.47$	1093	
	P50: $C_e = 0.6$	1395	
	P15: $C_e = 0.9$	2093	

4.4 Potential of CO_2-EOR and reusing existing infrastructures for CCS

CO_2 injection has proved to be an effective method for tertiary oil recovery. Globally there are nearly 170 CO_2-EOR projects currently in operation, among which all are onshore and mostly in the United States. Offshore CO_2-EOR is more difficult technically and economically. In North Sea, EOR was tested in 19 projects during the period of 1975 to 2005 using water and hydrocarbon gas, but CO_2-EOR was hampered by the lack of reliable large CO_2 supply. There were also concerns about technical and economic feasibility of offshore CO_2-EOR. This situation has changed now, because with the advance of CCS demonstration and commercial deployment the CO_2 supply will no longer be a problem, and with the increased oil price, the economic value of CO_2-EOR may increase also. A recent study predict that CO_2-EOR in the UK continental shelf may have a potential of contribute ~15% oil recovery from the area by 2030 and meanwhile realize large-scaled CO_2 storage (Pershad et al., 2012).

According to our preliminary analysis and discussions with experts in China National Offshore Oil Co., the potential of CO_2-EOR in the PRMB is low unfortunately. Although the crude oil produced from the basin is mostly light oil, and the reservoirs are mostly of good quality suitable for a miscible CO_2 flooding which is favorable for CO_2-EOR, there are a number of negative factors: The oil fields in the basin are of high oil recovery rate (30~>70%, in average 40% (Liu et al., 2010), which is similar to the recovery rate in North Sea. But the oil fields in the PRMB have strong aquifer support so that there has been no need even for the secondary EOR of water flooding. These fields are mostly small, only the LH11-1 field in carbonate reservoirs has proved reserve >100 Mt. These conditions are quite different from those in North Sea and make the potential of CO_2-EOR very limited.

The crude oil production in the PRMB started in 1990 and has kept at the rate about 10 Mt/y for the last 12 years. Although the basin is still in the developing stage with 73% of geological resources (OOIP) yet to be discovered, to date there are several producing fields are close to depletion. The possibility of reusing the infrastructures (platform, well, etc.) of depleted hydrocarbon fields for CO_2 injection exists in the basin, providing opportunities of reducing the cost of CCS implementation. This possibility should be evaluated at least several years before the field depletion and should be taken into account in the regional planning for CCS development.

4.5 Storage prospectivity

The areas favorite for CO_2 storage in the Pearl River Mouth Basin are analyzed qualitatively based the geological conditions, capacity assessments and other economic and environmental factors. Major concerns for the favorability at this preliminary stage are the distribution of reservoirs and seals, the distance from major emission sources (the Pearl River Delta), the depth, and size, and quality of possible reservoirs, and the possibility of CO_2-EOR and of using existing infrastructures.

In general we should prioritize the reservoirs in the Lower and Middle Miocene Zhujiang and Hanjiang Fms and the Upper Oligocene Zhuhai Fm. These formations contain most abundant, thick, and high quality sandstone or carbonate formations, accompanied by well developed mudstone seals.

There may be some sandstone reservoirs in the Lower Oligocene and older sequences, but those continental formations are usually deeper, less understood, and with poorer quality (lower porosity and permeability (Table 4.2.3) and smaller capacity (Table 4.2.7). These make it questionable whether injection and storage would be technically feasible and economic in these formations.

The most promising area for CO_2 storage is the Zhu-1 Depression and the northern Dongsha Uplift (Fig. 4.4.1). Water depth in the area are mostly <200 m. In this area the Lower and Middle Miocene formations are thick and with good reservoir-seal assemblages (Fig. 4.2.2). A number of structural traps in the area have been proved dry, among which the large ones may be good candidates for large-scale CO_2 storage. The producing oil fields of the PRMB reside mostly in this area, among which some are approaching depletion. Most fields are small but distributed as clusters and contain high quality light oil. The CO_2 storage capacity of these oil fields is small (Table 4.3.1), but the capacity may be enlarged by a combined utilization of oil and gas fields and underlying or nearby saline formations. The most important benefit of these fields is the possibility of using their infrastructures for CO_2 injection when the fields are depleted.

The largest oil field in the PRMB is the LH11-1 field. It is a Lower Miocene carbonate oil field with discovered oil reserve of 155 Mt. Oil resides in a coral reef buildup of 87 m height and 59 km^2 trap area. This field is considered less favorable for either CO_2-EOR or CO_2 storage, because it has complex pore structures and high-density and high-viscosity oil, and the field in located relatively far from the coast (220 km from Hong Kong) at relatively deep water (200-380m).

The gas fields so far discovered in the PRMB are relatively large. For example, the newly discovered LW3-1, LH34-2, and LH29-1 gas fields have proved reserve >100 Gm^3 each, and the PY30-1 gas field has proved reserve of 30 Gm^3 and started production in early 2009. The produced gas has been transported to Zhuhai City through underwater pipeline. The gas fields have larger CO_2 storage capacity (Table 4.3.2), however they reside in deepwater areas (> 300 m) where the cost of drilling and infrastructures are much higher. Thus these fields have the potential to be used as the storage sites for CO_2 only in a very long term.

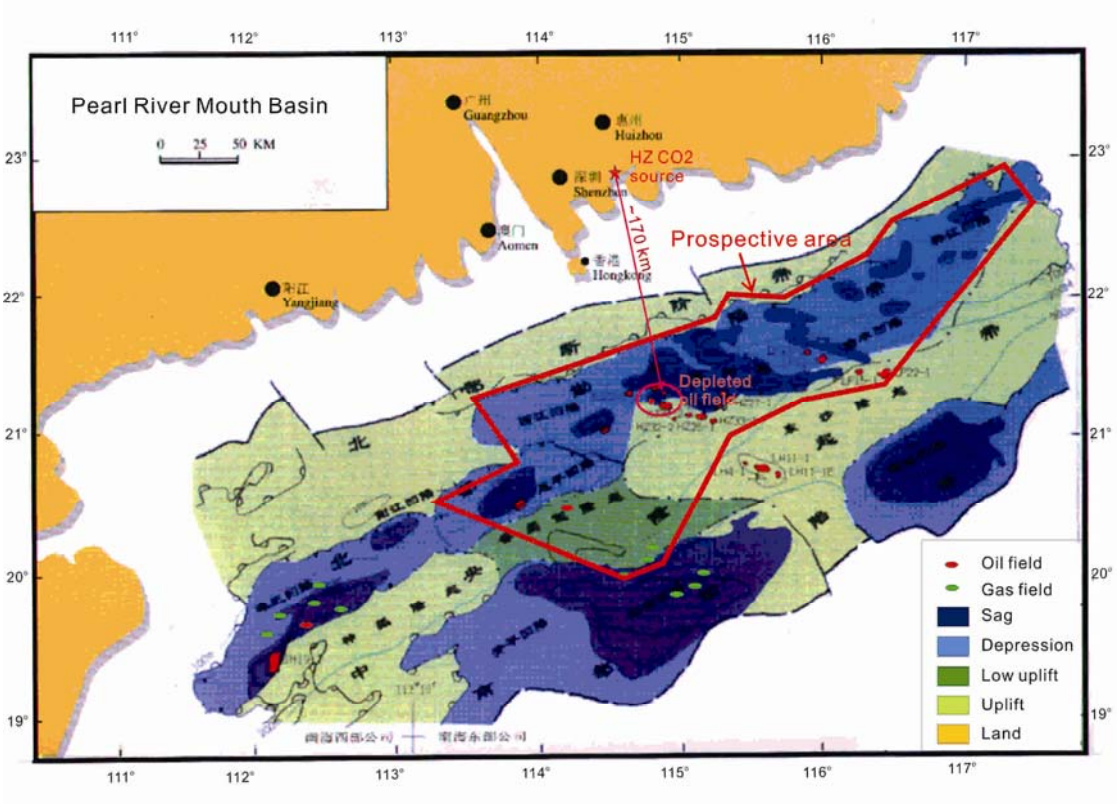

Figure 4.4.1 The prospective area for CO_2 storage in the Pearl River Mouth Basin.

4.6 Conclusions

For the saline formations in the Pearl River Mouth Basin, the estimated effective capacity for CO_2 storage is 110~443 Gt at the probability level of P85~P15, and 289 Gt at the probability level of P50. If only the formations in the shallower water areas (<300 m) are considered, the estimated effective capacity is reduced to 77~310 $GtCO_2$ at the probability level of P85~P15, and 201 $GtCO_2$ at the probability level of P50. According to the estimate of this project (GIEC, 2013), the CO_2 emission from large point sources of thermal power, petrochemical and steel industries was 252 $MtCO_2$ in 2010. Thus the effective capacity in shallower water areas of the PRMB is sufficiently to store >300 years of the CO_2 emission from large point sources in the Guangdong Province on the 2010 level.

The estimated effective storage capacities in oil/gas fields (including the undiscovered oil/gas fields) are small: 0.06~0.2 $GtCO_2$ (average 0.13 $GtCO_2$) in oil fields and 1.1~2.1 $GtCO_2$ (average 1.4 $GtCO_2$) in gas fields. The potential of CO_2-EOR is low because high recovery rate and strong water drive. The value of oil fields is the possibility of using their infrastructure for CO_2 injection after the fields' depletion in order to reduce the cost of offshore CO_2 storage.

The advantages common to all offshore storage of CO_2 are applicable to the PRMB, such as not interfered with population, agriculture, and industry, no damage to groundwater. Schrag (2009) thinks that storing CO_2 in geological formations offshore may be easier, safer, and is probably the best option for large population centers near the coast.

In addition, the advantages of the Pearl River Mouth Basin for CO_2 storage are:

1. The mudstones in Miocene Hanjiang and Zhujiang Fms form excellent regional seal. Frequent sealevel fluctuation in Neogene resulted in multi-layers of local seals. Sandstones and limestones are wide spread in Miocene formations, forming promising reservoirs. Multiple seal-reservoir assemblages have been proved by hydrocarbon exploration.

2. Existing oil/gas fields may be transformed to storage sites after their depletion. After the production for more than 20 years, some fields are close to depletion in the PRMB. Extensive data and infrastructures (platforms, wells, pipelines, etc.) may be suitable for use for CO_2 storage to reduce costs.

3. The shallower area of the basin is proximal to the coast of Guangdong, where major CO_2 point sources are concentrated. The distances between the hubs of source clusters and hubs of sink clusters can be kept within 120 km to 300 km, mostly < 200 km.

As there are little capacity for CO_2 storage onshore Guangdong, the high potential for CO_2 storage in the Pearl River Mouth Basin is even more important to the Guangdong Province.

The disadvantage of the Pearl River Mouth Basin for CO_2 storage, common to all offshore storage sites, is mainly the higher cost of the infrastructures and engineering operations compared with the onshore storage. The high cost may be partially offset by using the infrastructures of depleted offshore oil/gas fields.

Taken into account of geological, economical and source-sink matching conditions, the most prospective area in the Pearl River Mouth Basin is the Zhu-1 depression and the northern Dongsha Uplift.

Chapter 5 CO_2 Storage Capacity of the Beibuwan Basin

5.1 Geography and geology

The Beibuwan Basin (BBWB), 107°20′~111°50′E and 19°40′~21°10′N, is the northwestern corner of the South China Sea. It is a NEE-elongated basin with an area of ~36000 km^2, most offshore within the Beibu Gulf with water depth less than 55 m, but its northern part extends across the Laizhou Peninsula, and its southern part extends to northern Hainan Island (Fig.1.1).

Tectonically the BBWB is a rifted basin intra-continental but close to the continental margin of the northern SCS. It is a composite graben composed of SWW-NEE-running listric half-grabens and intervening uplifts (Fig. 5.1.1).

The basement of the BBWB is made of Paleozoic metamorphic and carbonate rocks. Cenozoic sediments in the basin reach 7 km thick in the gulf area and up to 9 km thick in the northern Hainan Is. The evolution of the basin, similar to other basins in the northern SCS, consists of Paleogene rifting and Neogene post-rifting subsidence. During Paleogene time inland sags filled with lacustrine, deltaic, and fluvial sediments. In Neogene seawater entered the basin, and littoral and neritic clastic and secondarily carbonate sediments deposited (Fig. 5.1.2).

The Paleocene to Lower Eocene Changliu Fm consists of red mudstone, sandstone and conglomerate, with a total thickness of 0-840 m. The Mid- to upper Eocene Liushagang Fm is dominated by dark-grey mudstone and brown oil shale, with minor variegated layers near the bottom. The maximum penetrated total thickness of the Liushagang Fm is up to 1200 m. The Oligocene Weizhou Fm is made of mainly variegated mudstone, with a penetrated thickness of 97-830 m. The Weizhou Fm was subjected to intensive erosion, forming a regional unconformity overlain by the Neogene.

The Neogene consists of 4 formations of marine sediments with a total thickness pf 1200~2100 m in depressions and 300-600 m in uplifts. The major source rocks in the BBWB is the Mid- to Upper Eocene Liushagang Fm deposited in the summit of lake development. Its dark mudstone is of n×10 m to over 1000 m in thickness and contains abundant organic materials (mainly II type kerogen), especially good in the Weixinan and Wushi sags (Zhu et al., 2004).

There are three types of reservoirs in the basin: Lower to Middle Miocene marine sandstones, Eocene and Oligocene fluvial and lacustrine sandstones, and Carboniferous limestones. The Tertiary rhythmic sedimentation resulted in multiple regional seals, such as the thick mudstones in the Eocene, Oligocene, and Mid-Miocene formations (Zhang and Su, 1989; Li and Lv., 2002; Zhu et al., 2004).

The petroleum exploration in the BBWB started since the 60's of the last century. By 2008, 10 oil fields have been found with discovered reserves of 132 Mt crude oil and 7 Gm^3 natural gas. The predicted geological resources of the basin are 970 Mt oil and 85 Gm^3 natural gas (MLRC et al., 2008).

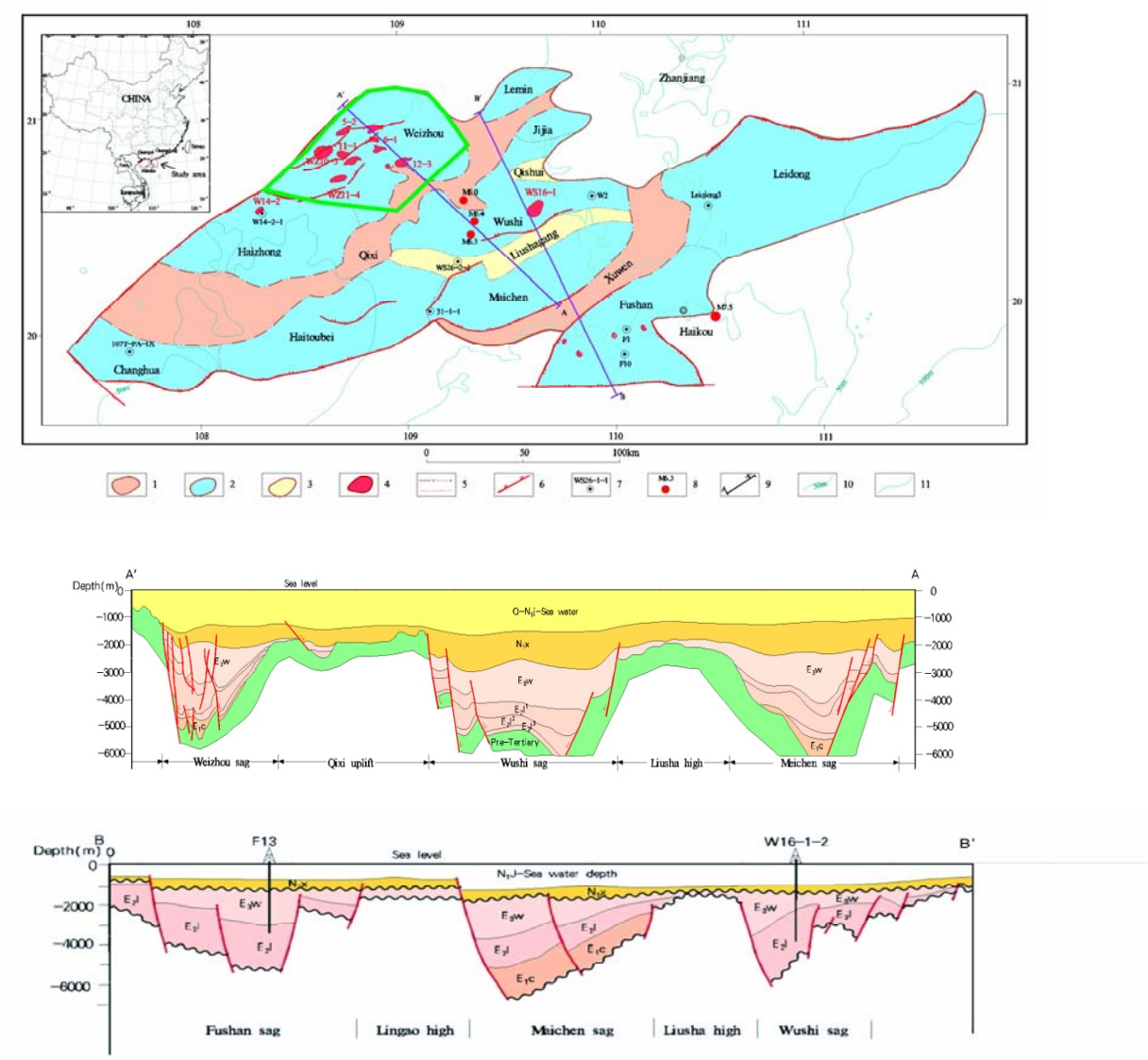

Figure 5.1.1 Simplified structural map and cross sections of the BBWB (Clift et al., 2008; Li and Lv, 2002; Zhu and Mi, 2010). Green polygon delineats the prospective area for CO_2 storage.

1-uplift; 2-sag; 3- high; 4-oilfield; 5- structural unit boundary; 6-fault; 7-well and its name; 8- earthquake and its magnitude 9-section line; 10- sea water depth line; 11-basin boundary

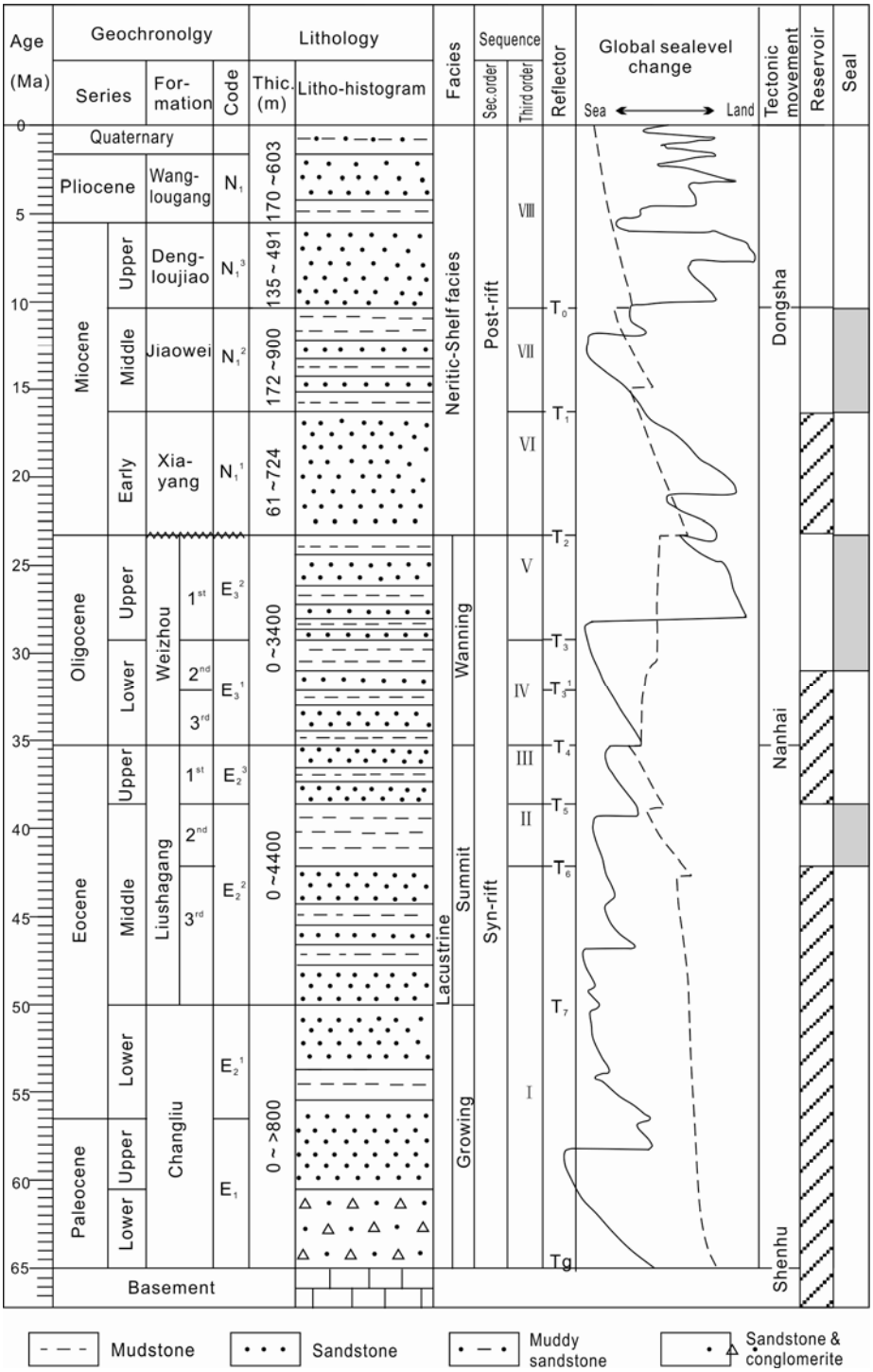

Figure 5.1.2. Stratigraphic column of the Beibuwan Basin.

5.2 Geological conditions for CO_2 storage

Three regional seals developed in the basin. The upper-most regional seal is the thick marine mudstones in the upper part of the Mid-Miocene Jiaowei Fm, which covered the entire basin. The middle seal is the 2nd member of the Oligocene Weizhou Fm consisting of variegated mudstones deposited in wide shallow lakes of the later stage of rifting. The lower regional seal is the 2nd member of the Eocene Liushagang Fm consisting of dark mudstones deposited in discrete deep lakes of the early rifting stage, which are the major hydrocarbon source in the basin with thickness

up to >1000 m (Li and Lv, 2002).

Underneath these regional seals there are three sets of saline formations, which usually have medium to high porosity and permeability favorable for CO_2 storage.

1. The lower set includes saline formations of the sandstones in Eocene-Paleocene Liushagang and Changliu Fms and in fissured limestones in the Paleozoic basement buried hills. In this set the 1st and 3rd members of the Liushagang Fm contain best aquifers. As penetrated by the Wei-1 well, sandstones in the 1st member have single layer thickness >40 m and total thickness 219 m, net/gross ratio is 82.6%, porosity and permeability in average 28% and 500 mD respectively; and those in the 3rd member are >20 m, 94 m, 56.3%, 10%, and 45 mD, respectively (Guo et al., 2009; Sun et al., 2008; Zhai, 1993; Zhang and Su, 1989).
2. The middle set is the saline formations of sandstones and gravel sandstones in the Oligocene Weizhou Fm, which is important reservoir for hydrocarbon. These are high porosity and permeability rocks formed in delta front and delta plain of braided rivers. The single layer thickness of the sandstones is usually >30 m, and the total thickness varies from 50 m to 200 m in depressions. Porosity and permeability in average are 28% and ~500 mD respectively (Guo et al., 2009; Zhang and Su, 1989).
3. The top set is the Mid- to Lower Miocene Jiaowei and Xiayang Fms shallow marine sandstones with thickness between 320~575m showed by Wan-4 and Wei-23 wells (Clift et al., 2008).

Multiple stages of tectonic deformation and sea level oscillations have resulted in abundant structural and stratigraphic traps in the basin. Structure traps in the forms of anticlines and faulted noses or blocks were formed mainly in Paleogene rifting stage. Stratigraphic traps were formed by overlaps or by the Oligocene unconformity and in buried basement hills. Fault-and-lithological composite traps are seen in the Weixinan depression.

Three major periods of fault activities occurred in the basin (Li et al., 2012). During Paleocene and Eocene the rifting formed NE- and NEE-oriented extension faults. In the post-rifting period in Late Oligocene and Early Miocene, NW-oriented strike-slip movement along the Red River Fault system has resulted approximately EW-directed extensional sub faults. The influence of these faults on the CO_2 storage should be examined case by case, but in general the potential of safe storage exists as evidenced by the existence of oil fields. The third stage of faulting occurred in Pliocene to Quaternary. Neotectonic activities are characterized by strong basaltic volcanism, which are mainly in the inland portion of the BBWB such as the Leizhou Peninsular to the east and in the northern Hainan Island to the south. In the Beibu Gulf where the major portion of the BBWB resides, the neotectonic activities are expressed as small active faults and a few volcanic islands occurring in early Quaternary time. Historical and modern earthquakes were recorded, M6 in the center and M>7 at the southeastern corner of the basin (Fig. 4.1.2). The areas having Quarternary volcanics and earthquakes should be avoided in site selection for CO_2 storage.

5.3 Capacity assessment for Saline formations

Data sources

In consideration of the geological conditions and data availability, we divide the Cenozoic sedimentary sequences into two assessment super layers: The upper super layer consists of the Neogene formations underneath the upper-most regional seal of the Mid-Miocene Jiaowei Fm; while the lower super layer consists of Paleogene formations roughly bellow the regional seal within the Oligocene Weizhou Fm. The basement traps are not considered in this study, but should not be left out in future studies because the storage potential is suggested by the existence of oil fields in the Carboniferous limestone in buries hills.

Collected stratigraphic data were compiled into a data base and processed on the MapGIS[3] platform to generate maps (Fig. 5.3.1) and to perform calculations.

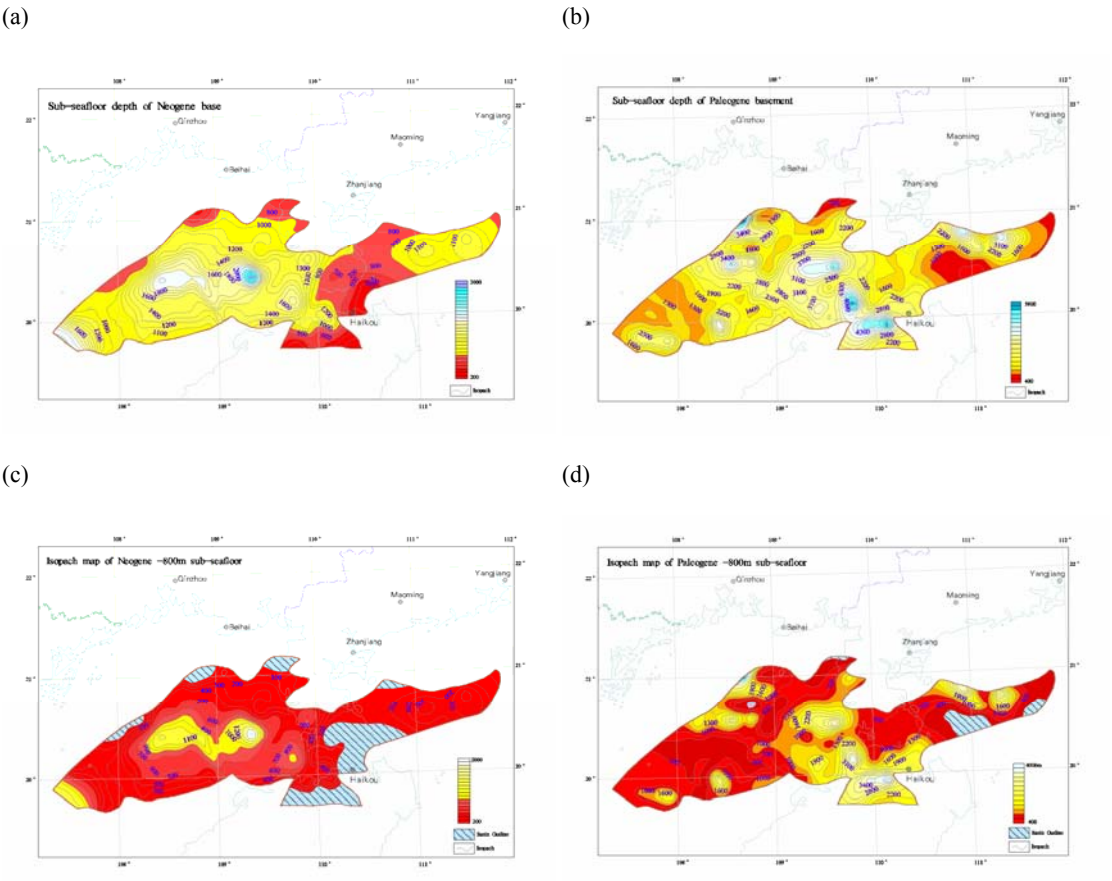

Figure 5.3.1 Contour maps of sub-seafloor formation depth (a, b) and formation thickness between 800 m to 3500 m sub-seafloor (c, d) in the Beibuwan basin.

Parameters

Based on literature data, the parameters of reservoirs in the depressions of the BBWB are summarized in Table 5.3.1, and parameters of formations in the entire basin are estimated and listed in Table 5.3.2.

[3] Trademark of the Zondy Cyber Group, Wuhan, China.

Table 5.3.1 Parameters of Liushagang and Weizhou reservoirs in the Beibuwan Basin*.

Depression	Formation	Porosity (%)	Permeability （mD）	Facies	Lithology	Depth（m）	Thickness (m)	Area (km^2)
Weixinan	3rd member Liushagang	5.16~25.21 Av.9.96	0.3~330 Ave. 44.52	Littoral and shallow lake	Coarse sandstone, Sandy conglomerate	1800~2100	94	3000
	1st member Liushagang	26.65~29.74 Av.28	423~673 Ave. 534	Littoral and shallow lake Fan delta	Silty mudstone and siltstone	1500	219	
	Weizhou	23.32~30 Av.27.5	234.7~689.11 Ave. 511	River delta front, Detaic plain	Sandy conglomerate	1300	85.8	
Maichen	3rd member Liushagang	5.1~11.3 av7.5	0.244~1.78 0.73	Lacustrine	Interbedded mudstone, sandstone, & gravel sandstone	100~2000	215	2600
	Weizhou	15-25	1-760	River delta	gravel sandstone, siltstone, fine sandstone	2000	50	
Haizhong	Liushagang	7.8	0.4~3	River delta, fan delta, lacustrine	Mudstone with minor siltstone	2000~4000	126	2900
	Weizhou	20~24	230~610		Siltstone, sandstone	1000~2000		
Fushan	1st member Liushagang	10~13 av15.6	0.16~500 Ave. 60.3	Fan delta, abyssal to shallow lacustrine	Interbedded sandstone & mudstone	2500~400	100～300	2920
	3rd memb. Liushagang	13~18	1~1600	Fluvial, fan delta, shallow, lake	Siltstone, locally sandy conglomerate			
	Weizhou Liushagang	5.2~33 av19.5	0.04~6930 Ave. 902.7	Fluvial fan and plain	Blocky sandy conglomerate	1000~2500	100~200	
Leidong	Weizhou Liushagang	13~17	44~188	Lacustrine and alluvial plain	Sandstone and conglomerate With mudstone interlayers	1300	1200	7500
Wushi	Weizhou Liushagang	15～25	1～760	Fluvial, shallow to bathyal lacustrine	Sandstone with mudstone interlayers	3000	1500	2800

***** Data compiled from Zhang and Su (1989); uo et al. (2009); He et al.(2008).

Table 5.3.2 Parameters of the stratigraphic formations in the Beibuwan Basin.

Formation	Porosity(%)	Permeability(mD)	N/G %	Data source
Neogene (average -800 m subseafloor,)	>20	~300	66	Zhang (1989) He et al.,(2008) Wang et al.(1992)
Jiaowei	>20	~300	55	
Xiayang	>20	~300	77	
Paleogene (average -800 m subseafloor)	3.34~23.2 av.23.0	1~6930 av.354	41	Guo et al.(2009) Zhang (1989) He et al.,(2008) Wang et al.(1992) Liu et al.(2009) Sun et al.(2008)
Weizhou Fm	5.2~30 av.27.2	1~6930 av.604	39	
Liushagang Fm	17.6~23.2 av.18.9	1~1600 av.104	36	
1st member	18-22 av.18.8	1-600 183.6		
2nd member	18-22 av.18.3	1-200 av.50		
3rd member	17.6-23.2 av. 19.7	137.6-435.5 av.178.6	50	
Changliu Fm	3.34~12.69 av.7.7	0.11~17.28 av.3.85	81	

CO_2 density

Based on well testing data, the geothermal gradient is 32.7℃/km in average for the BBWB (38.6℃/km for the Weixinan depression, 33.5℃/km for the Haizhong depression, 35.0℃/km for the Wushi depression, and 32.5℃/km for the Maichen-North Haitou depression). The heat flow varies in 50~80 mW/m^2 and in average 61.7 mW/m^2. A thermal event occurred at ~6 Ma which increased the heat flow in the basin significantly (Kang et al., 1995).

The CO_2 density varies with temperature and pressure at depth. The density-depth curve was calculated for four depressions in the BBWB and for the entire basin using hydrostatic pressure of reservoir formation and average seabed temperature of 25℃. Curves of CO_2 density versus formation depth were d using the online calculator[4] for Weixinan, Wushi, Haizhong and Maichen sag, and also for BBWB (Fig.5.3.2). Selected curves for typical geothermal gradient such as "cold" (25℃/km) and "warm" (50℃/km) basins (Bachu, 2003) are also presented for comparison. The increase rate of CO_2 density with depth in the BBWB is in between the "cold" and "warm" basins curves.

Calculation of the effective storage capacity of saline formations

The definition and formulation of the effective CO_2 storage capacity is given in Chapter 2 of this report. The calculations were performed for the two super layers, Neogene and Paleogene, which lie under the regional seals in the Mid-Miocene Jiaowei Fm and the Upper Oligocene Weizhou Fm respectively.

The parameters used in calculations are listed in Table 5.3.3. The parameter V is the formation volume calculated via GIS. The net/gross ratio R and porosity φ are the average values based on the data in Table 5.3.3. The storage efficiency factor E = 0.01, 0.026, and 0.04 respectively at P15, P50, and P85 probability level following IEA (2009).

[4] http://www.peacesoftware.de/einigewerte/co2_e.html

(a)

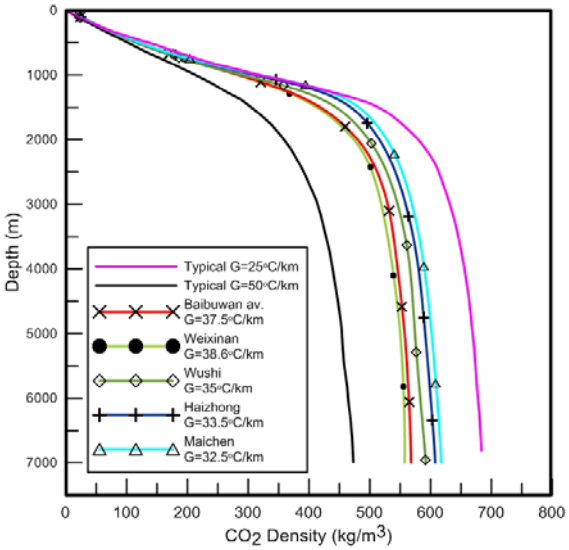

(b)

Depth (m)	CO_2 density (kg/m^3)
800~1000	245.8
1000~1200	317.6
1200~1400	374.7
1400~1600	417.8
1600~1800	435.9
1800~2000	448.5
2000~2200	471.4
2200~2400	489.5
2400~2600	502.7
2600~2800	513.8
2800~3000	522.1
3000~3200	528.4
3200~3400	533.9
3400~3500	537.3

Figure 5.3.2. (a) Curves of CO_2 density vs. depth, and (b) the data table for the average curve for the Beibuwan basin. Curves of "cold" and "warm" regions from Bachu (2003) are also shown for comparison.

The differences between the density-depth curves for four depressions in the BBWB are not large, thus we used the curve for the entire basin in the calculation. For porosity and net/gross ratio of Neogene and Paleogene we use the average values in Table 5.3.2.

The estimated effective storage capacity of the BBWB is 52.6 Gt_{CO2} in average, and 20.2 ~80.9 Gt_{CO2} at the P15 ~ P85 probability level (Table 5.3.3).

Table 5.3.3 Parameter and estimation of the effective CO_2 storage capacity in the saline formations of the Baibuwan Basin

Parameter		Neogene	Palaeogene	Total	Data source
Volume below 800m V ($\times 10^9 m^3$)		13 900	34 000	48 000	This paper
Net/gross ratio R (%)		66	41		Table 5.3.2
Average porosity φ(%)		20	23		Table 5.3.2
CO_2 density ρ(kg/m^3)		From Fig. 5.3.2			
Effective capacity 800~3500m ($GtCO_2$)	E=0.01	5.9	14.3	20.2	
	E=0.026	15.5	37.1	52.6	
	E=0.04	23.8	57.1	80.9	

5.4 Calculation of the effective storage capacity in oil/gas fields

According to the 2008 assessment, the BBWB has the geological resources of 734 Mt oil and 60 Gm^3 gas, and discovered reserves of 132 Mt oil and 7 Gm^3 gas. The gas resource in the BBWB is low and thus being ignored in our calculation. Recent study gave the average oil recovery factor of ~24% for the BBWB (Liu etal., 2010).

Using the Eq.(2.3) the storage capacity factors explained in Chapter 2, and the parameters in Table 5.4.1, the effective CO_2 storage capacity in oil fields (including undiscovered fields) of the

BBWB is estimated as 10.5 ~ 35 Mt CO_2 and in average 22 Mt CO_2.

Table 5.5. Estimation of the effective CO_2 storage capacity for oil fields in the Beibuwan Basin.

Parameter		Value	Data source
OOIP (Mt)		734	Zhu et al.(2010)
Recovery rate R_f		0.24	Liu et al.(2010)
Volume factor B_f		1.03	Zhou et al.(2011) for PRMB
CO_2 density ρ_{CO2} (t/m^3)		0.460	Fig.5.3.2 at 2000m
Effective storage capacity ($MtCO_2$)	C_e = 0.12 C_e = 0.25 C_e = 0.4	10.5 22 35	

5.5 Prospective areas for CO_2 storage

In consideration of geological, geographical, social, and economic conditions, the most favorable area for CO_2 storage in the Beibuwan Basin is the Weixinan Sag (the green polygon in Fig. 5.1.1), which is located in the northwestern Beibu Gulf, with area of 3000 km^2 and water depth of ~30 m. The sag is only 30 km from the Weizhou Island, 40~100 km from the Beihai city in the Guangxi province and 140~200 km from the Zhanjing city of the Guangdong province.

The Weixinan Sag is a half graben bounded to the NW by a growth fault and filled with up to 8000 m Paleogene and up to 1200 m Neogene sediments. The Mid-Miocene Jiaowei Fm and the upper member of the Lower Miocene Xiayang Fm are dominated by mudstones, forming excellent upper regional seal. The lower member of the Xiayang Fm is made of coarse, medium-grained, and gravel sandstones intercalated with mudstones and of a total thickness of 200~700 m, forming high-quality reservoirs. The upper and middle members of the Oligocene Weizhou Fm consist of lacustrine mudstone intercalated with thin layers of sandstone. Especially the 500 m thick 2nd member contains 70% mudstone and is called as a "stable mudstone member", forming excellent lower regional seal. Below this regional seal the 3rd member of the Weizhou Fm consists of fluvial-laustrine-deltaic bulk sandstones interbedded with siltstone and mudstone. The sandstones have large single-layer thickness, stable lateral continuity, intermediate depth, and excellent physical properties, forming high-quality reservoirs.

The Weixinan Sag has been a major target area for hydrocarbon exploration for half century and still active to date with new discoveries. Eight oilfields have been found in the sag, among which five are producing and one is depleted. These are mainly small sized oilfields with OOIP ranges in 1.7 Mt to 3.4 Mt. The fields are grouped in clusters and characterized by light crude oil (Zhou, 2009; Zhu and Mi, 2010). The effective CO_2 storage capacity in the Weixinan Sag is 2~8 Gt CO_2 (ave. 5 Gt CO_2) in saline formations, which is several orders of magnitude greater than storage capacity in oil fields: 6~21 Mt CO_2 in range and 13 Mt CO_2 in average. Existing data and facilities of the oil fields are potentially useful for CO_2 geological storage.

Neotectonic activities (volcanism, earthquakes, active faults) are intensive in the onshore portions of the BBWB (in the Leizhou Peninsular and the northern Hainan Island) and should be avoided in the selection of storage site. In the Weixinan Sag, well integrity is an important issue to be carefully examined and treated to ensure the storage safety.

Chapter 6 CO_2 Storage Capacity of the Qiongdongnan Basin

6.1 Geography and geology

The Qiongdongnan basin (QDNB) occupies the offshore area between the Hainan Island and the Xisha islands, with water depth 20~200 m in the north and >2000 m in the southeast, and a total area of 88000 km^2, among which the area of shallow water (depth <300m) is 21000 km^2 (Fig.1.1).

The QDNB experienced three tectonic evolutionary stages: rifting, post-rifting and tectonic reactive stage. The rifting stage began from Eocene to Early Miocene and formed discrete rifts. In post-rifting stage from Early to Middle Miocene, the basin was filled with deltaic and shallow marine clastic and carbonate deposits, which contain important reservoirs. In the last stage since Late Miocene, the basin was filled with neritic, bathyal, and abyssal deposits and formed the basin-wide caprocks (He et al, 2002).

The QDNB consists of three depression belts separated by two uplift belts, which are further divided into 10 sags and 9 uplifts. The sags are mostly composed of half grabens bounded by generally NEE-striking normal faults (Fig. 6.1.1). Subordinary faults developed and controlled the formation of structural traps.

Cenozoic strata in the basin have a total thickness up to 12 km. Frequent sea level variations resulted in rhythmic Paleogene and Neogene strata in the QDNB. The upper parts of the Yinggehai, Meishan, and Shanya, and Lingshui Fms contain more than 40% marine mudstones, forming regional seals in the basin. Three types of reservoirs developed: fan delta and delta front, channel and gravity flow, reef and platform carbonates (Fig. 6.1.2) Sandstones reservoirs have been found mostly in Upper Oligocene to Miocene Lingshui, Sanya and Huangliu Fm (Liu et al, 2006). Gravity flow accumulated in Miocene Huangliu and Pliocene Yinggehai Fms are the second most important type of reservoirs. These include slope, basin floor, turbidite channel and mass transport complex and display good porosity and permeability. The central canyon in the Qiongdongnan basin as a special sedimentary system is filled with Miocene to Quarternary turbidites, slumps and mass transport complex (Fu et al, 2009). The third type of reservoirs is associated with platform limestones and reef complexes, mostly in the Lower Miocene Sanya Fm, and also seen in the Paleozoic basement (Li et al, 2007).

The hydrocarbon exploration in the QDNB started in the 1960s. The Yacheng 13-1 gas field discovered in 1983 is the largest gas field offshore China to date, with the discovered reserves of 98×10^9 m^3 natural gas and 4.3×10^6 t condensate from Upper Oligocene Lingshui formation tidal flat to lagoon sandstones. This field has been in production since 1996 (Zhu and Mi, 2010). Gas and oil shows have been found in the Yacheng and Songtao uplifts, Baodao, southern Songtao sags (Huang, 1999), and recently in the deepwater Lingshui sag. According to the 2008 assessment (MLRC et al., 2008), the QDNB has the total resources of 426×10^6 t oil and 1890×10^9 m^3 gas, and discovered reserves of only 4×10^6 t oil and 104×10^9 m^3 gas.

The Neogene and Quaternary neotectonics has been weak in the QDNB. No M>5 earthquake

has occurred (Fig. 4.1.2),

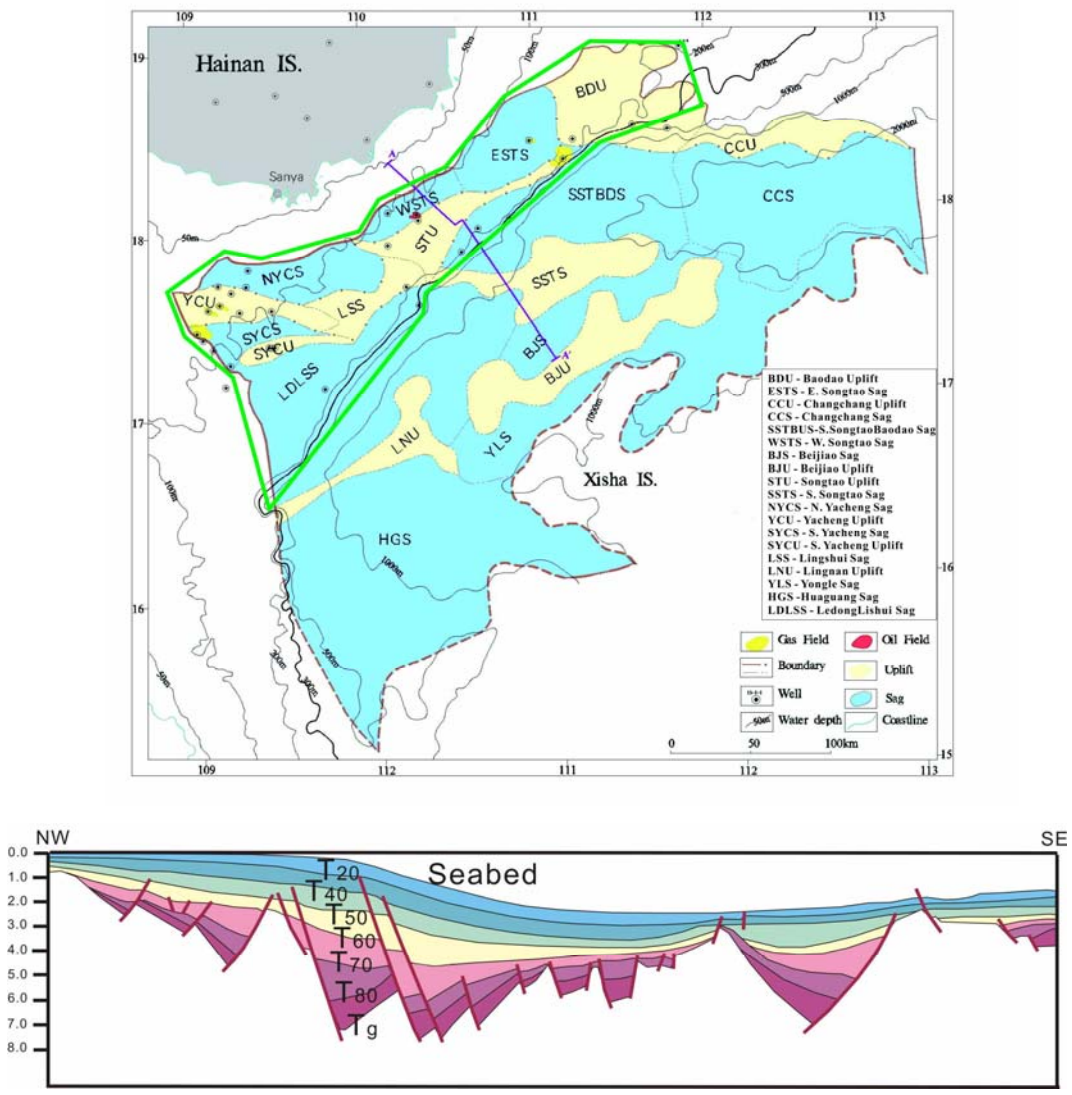

Figure 6.1.1 Simplified geological map and cross section of the Qiongdongnan Basin. Green polygon delineats the prospective area for CO_2 storage.

6.2 Geological conditions for CO_2 storage

Marine mudstones layers form four regional seals in the upper parts of the Yinggehai, Meishan, Shanya, and Lingshui Fms which covered almost the entire basin except the northern slope and the central uplift. Together with underlying sandstones and limestones they form four seal-reservoir assemblages for CO_2 storage (Fig. 6.1.2),

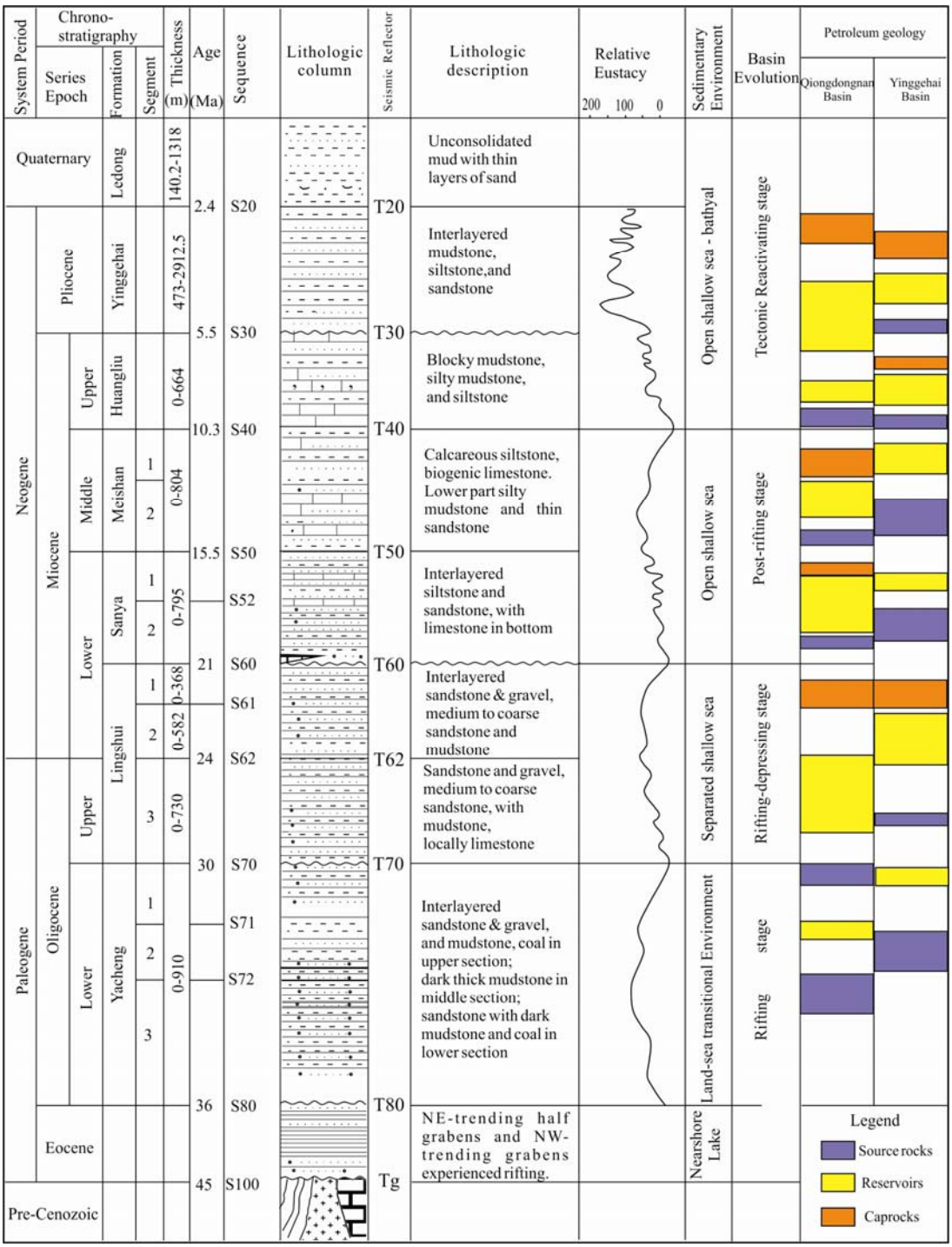

Figure 6.1.2 Stratigraphic column for theQiongdongnan and Yinggehai basins.

The upper assemblage consists of the regional seal in the upper Yinggehai Fm and the reservoirs in the Upper Miocene Huangliu Fm and the Pliocene Yinggehai Fm. The marine mudstones in upper Yinggehai Fm formed the topmost regional seal. It is an excellent seal, for example, the YC8-2-1 well in the northern Yacheng sag penetrated 820 m mudstone which is 73.8% of the total thickness of the Yinggehai Fm (Wang and He, 2003). Reservoirs are gravity flow accumulations (slope, basin floor, turbidic channel and mass transport complex) with high porosity and permeability in the Huangliu and Yinggehai Fms, and neritic sandstone layers in the Huangliu Fm.

The second assemblage consists of the regional seal in the upper Meishan Fm and the reservoirs in the Lower to Middle Miocene Meishan Fm. In the upper Meishan Fm thick mudstones have 41-51 % of the total formation thickness (Li & Lv, 2002). It is a good regional seal without destruction by faults. The reservoirs include marine sandstones and limestones.

The third assemblage consists of the seal in the upper sector and the reservoirs in the Lower sector of the Sanya Fm. Previous study suggested that mudstones of the Sanya Fm were mainly distributed in the northeast and southwest of the Qiongdongnan basin (Wang and He, 2003). Seven sandstone layers of basin floor and turbidite channels in the Lower Miocene Sanya Fm have been penetrated by Well LD30-1-1A in the Ledong and Lingshui Sags (Fig. 6.1.1). Single layer ranges from 18.6 m to 87 m in thickness and has porosity of 20% and permeability of 11.72 mD. (Fu et al, 2009). In the YA13-1 gas field the Sanya Fm contains high quality reservoir of feldspar sandstone and feldspar-quarts sandstone with porosity 16%~20% and permeability >2.5 D (Zhu and Mi, 2010). Platform limestone and reef complexes in the Sanya Fm have porosity and permeability up to 24% and >3 D respectively (Table 6.2.1).

The fourth assemblage consists of the regional seal in the second member of the Lingshui Fm and the reservoirs in lower Lingshui Fm. The second member of the Lingshui Fm formed local seals at rifted sags but was eroded in structural highs. The delta front fan sandstones accounts for 50-87% of the 3rd member of Lingshui Fm and are the principal reservoir in the YA13-1 gas field, with porosity of 14%~20% and permeability 810 mD (Zhu and Mi, 2010). The YA13-1 reservoir, however, is capped by the high quality seal in Meishan Fm because the second member of the Lingshui Fm is absent in the structural high. The lower assemblage is the most important one for hydrocarbon because the lower Lingshui Fm and the Yacheng Fm below contain good source rocks. But this assembledge may not be the first choice for CO_2 storage because of its greater depths and smaller volume (see Table 6.3.1).

6.3 GIS and parameter estimations

The Cenozoic strata are divided into three super-layers for the assessment (Fig. 6.1.2): 1) The upper layer: Upper Miocene to Pliocene Huangliu and Yinggehai Fms under the regional seal in the upper Yinggehai Fm; 2) the middle layer: the Lower to Middle Miocene Sanya and Meishan Fms under the regional seal in the upper Maishan Fm; and 3) the lower layer: the Upper Oligocene Lingshui Fm under the regional seal in the upper Lingshui Fm.

Contour maps of the bottom depths and sub-800 m thickness of these super layers are compiled (Figs. 6.3.1 and 6.3.2), and their volumes are calculated on the MapGis platform (Table 6.3.1). Because the depth data for the top Yinggehai Fm (the T2 reflector) are not available, the Quaternary deposits above the top-most regional seal could not be excluded from our calculation.

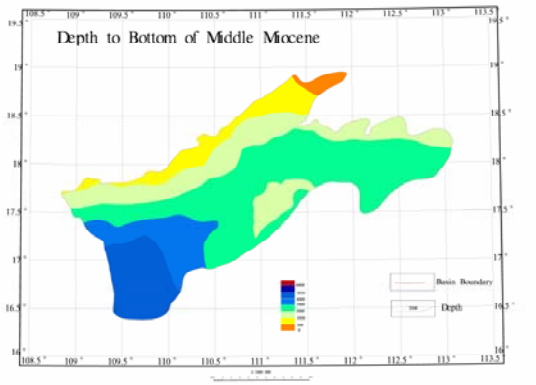

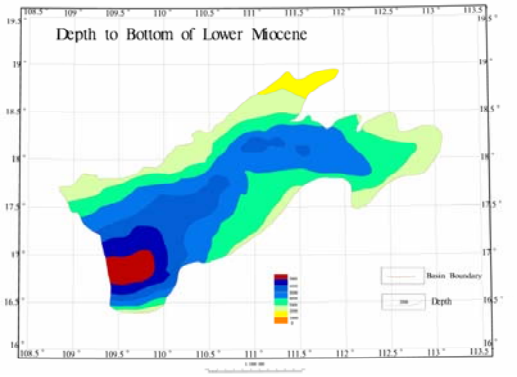

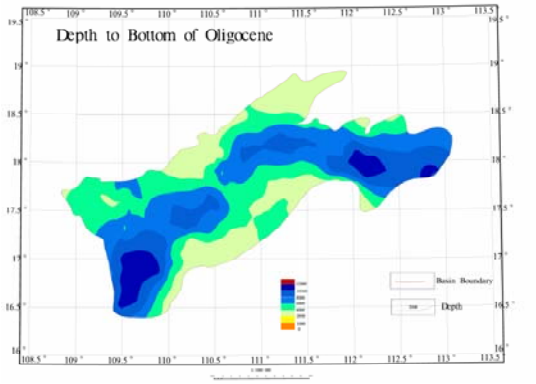

Figure 6.3.1 Contour maps of the sub-seafloor formation depths in the Qiongdongnan basin.

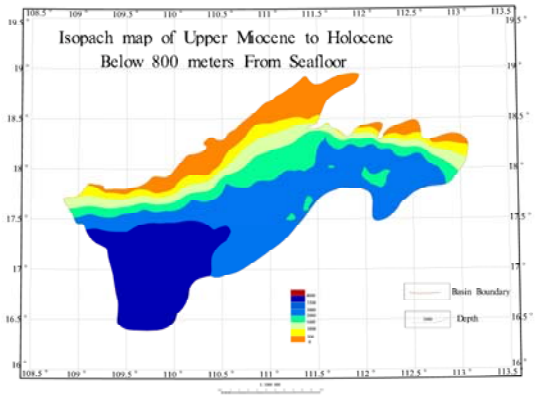

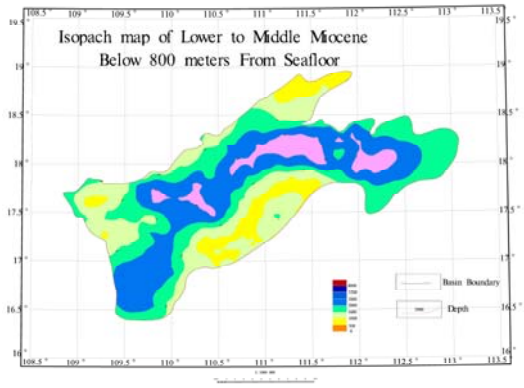

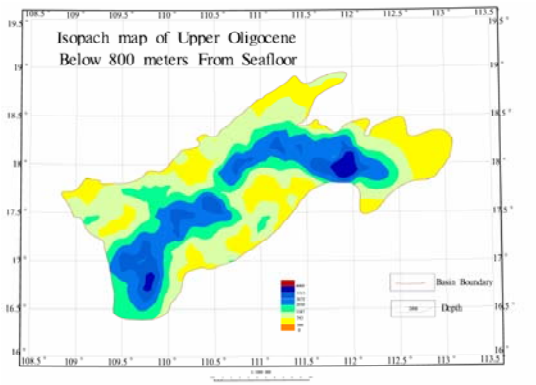

Figure 6.3.2 Contour maps of formation thickness between 800 m to 3500 m sub-seafloor in the Qiongdongnan basin.

Thus the volume for the upper layer is over-estimated. But the overestimation in the effective volume of the super layer should not be very large, as the Quaternary thickness varies in 140-1318 m and only the portion below 800m sub-seafloor is considered for CO_2 storage.

The lithological parameters are listed in Table 6.3.2 and 6.3.3.

To estimate the CO_2 density at formation depths, we divide the QDNB into three regions roughly by the bathymetry contours of ~100 m and ~1000 m, the shallowest N-QDNB to the north, the M-QDNB in the center, and the deepest SE-QDNB in the southeast. The geothermal gradient of the basin is relatively high (35-42.5℃/km) and increases SE-wards in the M- and SE- regions (Table 6.3.4). The CO_2 density at various depths (the midpoint of each 200 m depth range) are calculated by the online calculator of the Peace Software[5], with temperatures calculated based on seafloor temperature (Zhou et al., 2011) and thermal gradient, and pressure is assumed as the normal hydrostatic pressure. The SE-QDNB is left out from the estimation because its water depth is too large for CO_2 storage. The curves of CO_2 density vs. depth for the other two regions are shown in Fig.6.3.3.

Table 6.3.1 Area and volumes of the formations in the Qiongdongnan Basin

Formation	Bottom reflector	Area(km^2)	Bottom depth (m)	Thickness (m)	Volume (km^3)	
					Gross	-800m
Quaternary	T20	38372	140-1318	140-1318	20903	14512
Yinggehai	T30		300-3200	473-2912		
Huangliu	T40		500-4900	0-664		
Meishan	T50	46425	500-5000	0-1000	52624	47785
Sanya	T60		1000-8000	200-2000		
Lingshui	T70	46503	1600-10450	100-4600	46711	45843
Total					120238	108140

Table 6.3.2 Lithological parameters of the formations in the Qiongdongnan Basin.

Formation	Avg Porosity (%)[1]	Avg Permeability（mD）[1]	Net/Gross Ratio[2]
Yinggehai			0.13
Huangliu	15	11.7	
Meishan	18	2.3	0.26
Sanya	16	1000	
Lingshui			0.28
Yacheng			

[1] From Wang & He (2003). [2] Thickness-weighted average based on data from 3 wells.

[5] http://www.peacesoftware.de/einigewerte/co2_e.html

Table 6.3.3 Parameters of sandstones in the Qiongdongnan Basin (data from Wang and He, 2003)

	Well	Lithology and sedimentary facies	Porosity (%)			Permeability（mD）		
			Max	Min	Avg	Max	Min	Avg
Yinggehai Fm.	YC8-2-1	Sandstones	30.4	20.4	25.6			
	YC13-1-4	Sandstones	31.14	34	27.1			
	Ying9	Sandstones	23.8					
	YC35-1-1	Turbidite channel sandstones	14.8	5.9	13.2	2.58	0.03	1.52
Huangliu Fm.	YC13-1-1	Carbonate platform	21.14	2.52	6.9	2.58	0.01	0.21
	YC13-1-2	Carbonate platform	11.4	6.6	9.2	2.9	0.02	0.18
	YC13-1-4	Turbidite fan sandstones	20	9	13.75			
			12	7.5	9.75			
			19.5	15	17.83			
	YC35-1-2	Turbidite channel sandstones	14	11.8	12.9	64.5	41.9	53.2
			19	17	17.9	26.5	12.1	16.9
			18	10.5	16.6	11.9	0.64	8.6
			17.1	3.4	14.29	6.54	0.02	2.46
			13.1	2.3	8.85	9.08	0.01	0.95
Meishan Fm.	YC7-4-1	Shallow-water platform sandstones	7.52	2.68	6.37	1.67	0.01	3.07
	Ying9	Shallow-water platform sandstones	35.1	34.3	34.7			
	YC35-1-2	Sandstones	15.1	15.1	15.1	90.9		
	LS2-1-1	Delta front sandstones	25.7	18.7	22.2			
	BD19-2-1	Sandstones	17	12.8	14.33			
		Sandstones	21.2	15.5	18.35			
	ST36-1-1	Delta front sandstones	21.6	17.25	18.62	6.25	0.11	0.84
Sanya Fm.	YC8-2-1		27	19	22.92			
	YC14-1-1		23	21	22			
	YC7-4-1	Coastal sandstones	27		22			
	Ying9		23.8	5.8	14.76			
	YC13-1-4	Channel sandstones	16	12				
	YC13-1-A8	Channel sandstones	19.1	9.2	15.57	7733	267	2445.8
	YC13-1-8	Channel sandstones	17.6	6.9	12.81	3173	0.36	533.4
	YC21-1-1	Channel sandstones	19.3	7.6	13.5			
	YC21-1/2/3	Carbonate platform limestones	24	0.5	2.4			
	YC35-1-2	Delta front sandstones	12		12	49.3		
	LS2-1-1	Coastal sandstones	32	19.2	24.06			
	BD19-2-1	Delta front sandstones	19.5					

Table 6.3.4 Geothermal parameters of the Qiongdongnan basin.

Region	Maximum sed. thickn.[1] (m)		Geothermal gradient [1] (℃/km)	Seafloor temperature[2] (℃)
	Neogene	Paleogene		
N-QDNB	3300	4000	35-42.5	22
M-QDNB	4000	6600	42.5-45.5	8
SE-QDNB	4000	3000	42.5	3

[1] Huang (1999). [2] Zhou et al., 2011.

6.4 Capacity estimation for saline formations

The parameters and estimates of the effective CO_2 storage capacity in saline formations of the QDNB and its shallow (<300 m) portion are listed in Table 6.4.1. The mean value of the effective CO_2 storage capacity in saline formations of the QDNB is 41 $GtCO_2$, with lower and upper bands of estimates in 15 $GtCO_2$ and 63 $GtCO_2$ respectively. The effective capacity resides in shallower water areas is in average 11.4 $GtCO_2$, with lower and upper bands (at P85 and P15 probability levels, respectively) of estimates in 3.5 $GtCO_2$ and 17.3 $GtCO_2$ respectively.

Table 6.4.1. parameters and estimates of the effective CO_2 storage capacity in saline formations of the Qiongdongnan basin.

Formation		Yinggehai & Huangliu	Meishan & Sanya	Lingshui	Total
The Qiongdongnan Basin					
Volume below 800m $V(\times 10^9\ m^3)$		46 710	43 135	4051	93 895
Net/gross ratio R(%)		13	26	28	
Average porosity φ(%)		18.75	16	11.5	
Effective storage capacity ($GtCO_2$) 800~3500m sub-seafloor	E=0.01	5.5	9.6	0.7	14.8
	E=0.026	14.3	24.9	1.9	41.1
	E=0.04	22.0	38.4	2.9	63.3
The shallow portion of the Qiongdongnan Basin with water depth <300 m					
Volume below 800m $V(\times 10^9\ m^3)$		12822	11840	1112	25774
Net/gross ratio R(%)		13	26	28	
Average porosity φ(%)		18.75	16	11.5	
Effective storage capacity ($GtCO_2$) 800~3500m sub-seafloor	E=0.01	1.5	1.2	0.8	3.5
	E=0.026	4.9	3.9	2.6	11.4
	E=0.04	7.5	5.9	3.9	17.3

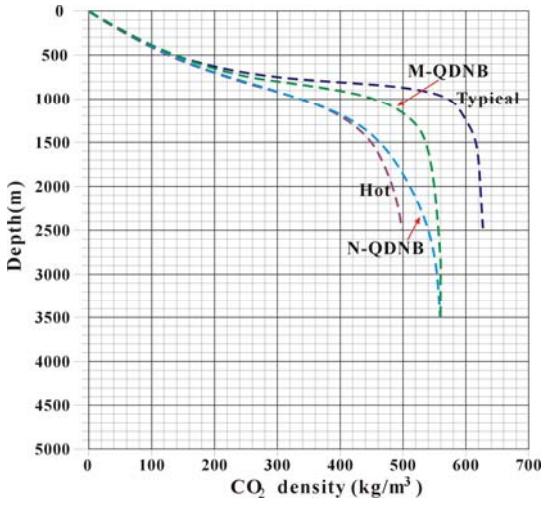

Figure 6.3.3 Curves of CO_2 density vs. depth in the north and middle regions of the Qiongdongnan basin.

6.5 Capacity estimation for oil/gas fields

According to the 2008 assessment, the QDNB has the geological resources of 272 Mt oil and 1114 Gm^3 gas, and discovered reserves of only 4 Mt oil and 104 Gm^3 gas.

The effective CO_2 storage capacities in oil and gas fields of the QDNB are estimated using the equations and storage factors described in Chapter 2. Parameters and results of the estimation are listed in Tables 6.5.1 and 6.5.3. It should be noted that these estimates include the capacity in deep-water areas.

The YA13-1 gas field has been in production since 1996 and is the largest gas field offshore China and the only producing field in the QDNB to date. This field has gas geological reserve of 97.85×10^9 m^3, from which 37.1×10^9 m^3 gas and 1.1×10^6 m^3 condensate was produced by the end of 2007 (Zhu and Mi, 2010), accounts for ~38% of the geological reserve. Reservoir is the fan delta sandstones mainly in the 3rd member of the Upper Oligocene Lingshui Fm but also in the 2nd member of the Lingshui Fm and in the lower Sanya Fm, at depths of 3752~3961 m, 54.2 km^2 in trap area and 77-163 m in thickness, and overlain unconformably by the mudstone seal in the Mid Miocene Meishan Fm (Li and Lv, 2002; Zhu and Mi, 2010). This field has thermal gradient of 40 ºC/km and a normal pressure system. Estimated using the Eq.(2.5) with parameters listed in Table 6.5.2, the effective CO_2 storage capacity in the YA13-1 gas field ranges in 48~93 Mt and in average 62 Mt. This storage capacity might not be available for many years, as by the end of 2007 the gas produced from the YA13-1 field is less than half of the discovered reserve (Zhu and Mi, 2010). However, in the YA13-1 field some blocks or horizons contain 7-10% CO_2. The possibility of CO_2-EGR should be investigated.

The parameters for the YA13-1 field are applied to the entire QDNB based on the 2008 assessment of 1114 Gm^3 gas geological reserves. The expected effective CO_2 storage capacity in the gas fields (including the undiscovered fields) of the QDNB ranges in 620~1190 Mt and in average 790 Mt (Table 6.5.3). Most of this would appear to be in undiscovered fields.

Table 6.5.1 Effective CO_2 storage capacity for oil fields in the Qiongdongnan Basin.

Parameter		Value	Data source
OOIP (Mt)		272	Zhu et al.(2010)
Oil density (t/m3)		0.9	Zhou et al.(2011) for PRMB
Recovery rate Rf		0. 4	Liu et al.(2010)
Volume factor Bf		1.03	Zhou et al.(2011) for PRMB
CO2 density ρCO2 (t/m3)		0.503	Fig.B5 at 2000m
Effective storage capacity (Mt CO_2)	Ce = 0.12	7	
	Ce = 0.25	15	
	Ce = 0.4	24	

Table 6.5.2 Estimation of the effective CO_2 storage capacity for the YA13-1 gas field.

Parameter	Value	Reference
OGIP	98 Gm^3	Zhu et al. (2010)
Recovery rate	55 %	DF1-1 data
Compression factor:		
Surface (Z_s)	0.987	LD22-1 data
Reservoir (Z_r)	0.938	LD22-1 data
Reservoir pressure (P_r)	38.2 MPa	Hydrostatic pressure at 3900 m depth
Reservoir temperature (T_r)	449 K	At 3900 m depth
Surface temperature (P_s)	293 K	Chinese standard
Surface pressure (T_s)	0.101 MPa	Chinese standard
Gas volume factor (B_g)	0.00385	$=(P_s \times Z_r \times T_r) / (P_r \times Z_s \times T_s)$
Reservoir CO_2 density (ρ_{CO2r})	0.56	Fig. Q5
Theoretical CO_2 storage capacity	116 Mt	$=\rho_{CO2r} \times R_f \times OGIP \times B_g$
Effective Storage capacity (Mt_{CO2})		
$C_e = 0.47$	55	
$C_e = 0.6$	70	
$C_e = 0.9$	104	

Table 6.5.3 Effective CO_2 storage capacity in gas field of the Qiongdongnan Basin.

Parameter	Value	Reference
OGIP	1114 Gm^3	Zhu et al. (2010)
Recovery rate	55 %	DF1-1 data
Reservoir CO_2 density (ρ_{CO2r})	0.56	Fig. Q5
Gas volume factor (B_g)	0.00385	$=(P_s \times Z_r \times T_r) / (P_r \times Z_s \times T_s)$
Theoretical CO_2 storage capacity	1320 Mt	$=\rho_{CO2r} \times R_f \times OGIP \times B_g$
Effective Storage capacity (Mt_{CO2})		
$C_e = 0.47$	620	
$C_e = 0.6$	790	
$C_e = 0.9$	1190	

6.6 Prospective areas for CO_2 geological storage

Concerning with geological and geographical conditions, the shallow portion (<300m water depth) is the most suitable structural zone for CO_2 geological storage in the QDNB (Fig. 6.1.1). This area is favorable because it is the area nearby the Hainan Island (40~100 km to the coast) and at shallow water depth (<50 m to 300 m), and also is the area of good seal-reservoir combinations and traps and has been the major target for hydrocarbon exploration in the past years. Accumulated wealth of data may facilitate the site characterization for CO_2 storage. The estimated effective storage capacity in the area is 3.5~17.3 $GtCO_2$ with average of 11.4 $GtCO_2$ (Table 6.4.1).

Within this area the Yacheng Uplift in the west is the most prosperous. It is an overlapping half anticline above a buried basement high The YA13-1 gas field was discovered in the uplift. The field started production since 1996, with annual production of 3.4 Gm^3, among which 2.9 Gm^3 is piped to Hong Kong, and 0.5 Gm^3 piped to Hainan. Estimated CO_2 storage capacity in the YA13-1 field is 60~114 $MtCO_2$ with expectation of 76 $MtCO_2$. A number of structural traps nearby the YA13-1 field were found of no economic significance, and the saline formations in these traps may be used to enlarge the capacity for CO_2 storage.

Disadvantages of the shallow portion of the QDNB for CO_2 storage are that the industrial development is rather weak in the adjacent Hainan Island, and this situation will continue in the future as the island is defined as an "Island for international tourism" by Chinese government in 2009.

If the favorite area in the QDNB is to be used for CO_2 storage, the CO_2 could be supplied from the following sources: 1) The CO_2 produced from gas fields in the QDNB and in the adjacent Yinggehai basin. The YA13-1 gas field contains ~8% CO_2 (Li and Lv, 2002), and many gas fields in the adjacent Yinggehai Basin contain >60% CO_2. The feasibility of CO_2.-EGR in the YA13-1 gas field needs to be investigated. 2) The CO_2 from major point sources in Hong Kong or in Guangdong. The feasibility of using the gas field for CO_2 storage after its depletion and of using the gas pipeline now transporting gas from YA13-1 to Hong Kong to transport CO_2 back to the storage site in the basin should be explored.

Chapter 7 CO_2 Storage Capacity of the Yinggehai Basin

7.1 Geography and geology

The Yinggehai basin (YGHB) is the only NW-SE-striking basin in the northern South China Sea. It lies NW of the Beibu Gulf with water depth <100 m mostly. The basin is the second largest sedimentary basin in northern South China Sea after the Pearl River Mouth Basin, with an area of 100,000 km^2 (Fig.1.1).

The YGHB was formed by a combination of rifting and transtension along the offshore extension of the Red River fault system (Gong & Li, 1997). It has a relatively simple structure as a semi-symmetrical graben, composed of the Central Sag, the Lingao Uplift, and the surrounding slopes (Fig.7.1.1).

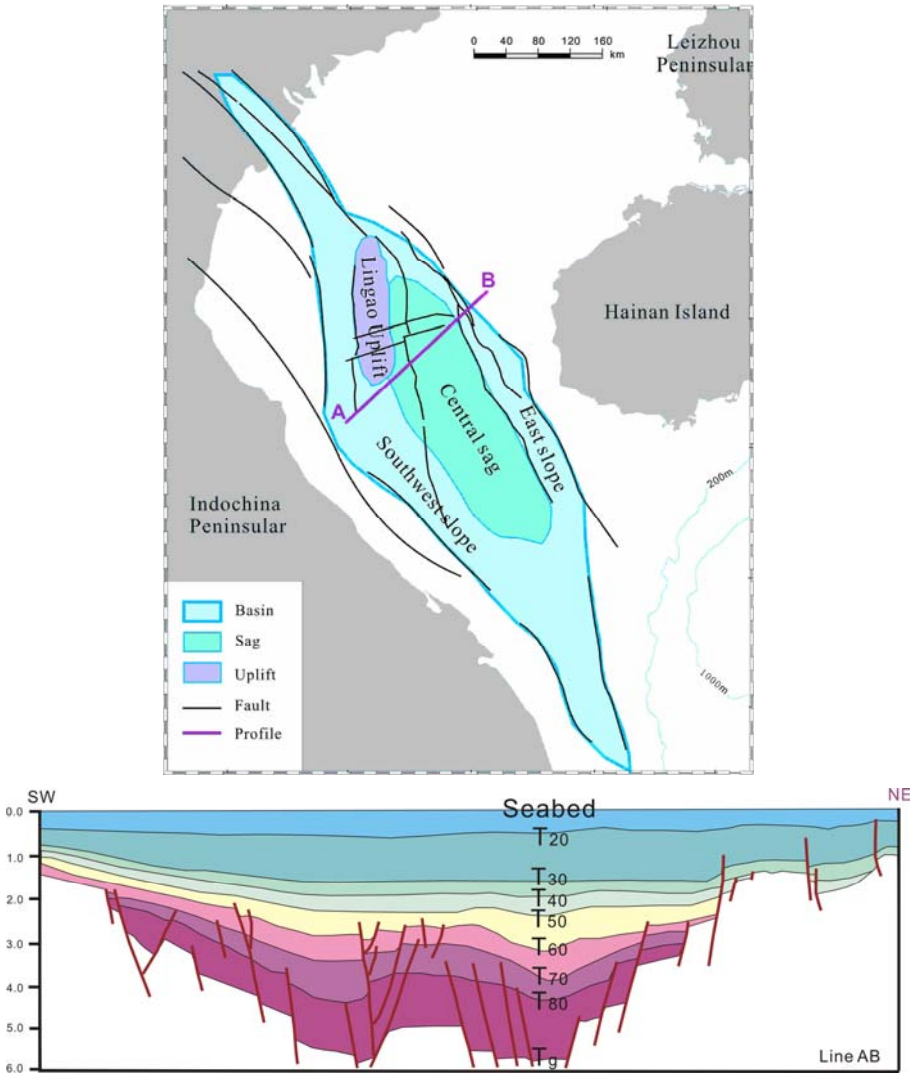

Figure7.1.1. Simplified geological map and cross section of the Yinggehai Basin.

The Cenozoic thickness in the YGHB is up to 17 km, the thickest in the northern South China Sea. The YGHB uses the same stratigraphic system and nomenclature as that for the QDNB (see Fig. 6.1.2). Its Paleogene consists of fluvial, lacustrine, and land-sea transitional sediments, while Neogene are of mainly deltaic, littoral, and neritic sediments.

Due to the abundant sediment supply from the Red River system, in the YGHB developed basin-wide thick reservoirs. Sandstones deposited in fan delta, fluvial delta, neritic environment formed good reservoirs in the Eocene Lingshui Fm, so do the sandstones deposited in turbidity current, neritic, and bathyal environment in Neogene Sanya, Huangliu and Yinggehai Fms (Gong and Li, 1997).

Potential source rocks in the YGHB reside in the Yacheng, Sanya, and Meishan Fms (Chen, 1990; Zhang et al, 1993; Hao et al, 1995; Gong and Li, 1997; Hao et al, 1998). The thick mudstones in the Oligocene Yacheng Fm were deposited during the rift stage, which is the major source of the YA13-1 gas field in the adjacent Qiongdongnan Basin (Hao et al., 1998). The Miocene Sanya and Meishan Fms are shale-dominated units deposited in marine environments during the regional subsidence.

Generally, the petroleum system in the YGHB is divided into two groups: (1) source rocks in Shanya and Meishan Fms accompanying with sandstone reservoirs in the upper Meishan, middle Yinggehai and Huangliu Fms sealed by mudstones of upper Yinggehai and Huangliu Fms; (2) source rocks in the lower Yinggehai and Huangliu Fms covered by middle sandstone reservoirs and upper mudstone seals (Xu and Wan, 2008).

In the central sag of the basin diapir structures developed, which served not only as the major hydrocarbon migration pathways but also as the best places for gas accumulations (He et al, 1994; Zhang et al, 2004). The diapirism occurred since Late Miocene and continued to Quarternary, and is related to the high sedimentation rate in the center of the basin (Gong, 2004).

Because of the large sediment thickness and high geothermal gradient (35~47 °C/km), the hydrocarbons in the YGHB are over mature. Until now, commercial gas fields have been found over diapir structures in the central sag, such as DF1-1, LD5-1, LD22-1 and LD8-1 (Zhu et al, 2004). The new assessment (MLRC et al., 2008) suggests ~1307 Gm^3 gas geological reserve in the YGHB, but only and 156 Gm^3 gas reserve is discovered. Many gas fields in the basin contain variable amount of CO_2, for example, 1% to >50% CO_2 in the gas produced from the largest gas field DF1-1. High concentration CO_2 is thought to be originated from thermal decomposition of carbonates at depths (Wang and Huang, 2008).

7.2 Geological conditions for CO_2 storage

During the Cenozoic era the YGHB experiences four periods of major marine transgression, which produced four layers of excellent regional seals. The uppermost seal is in the Quaternary mud existed where its thickness exceeds 1000 m. Although it capped several lower Quaternary gas layers, it would not be considered in our assessment because the relatively shallow depth and poor seal quality. The second seal is the thick mudstones in the Yinggehai and Huangliu Fms. These widespread marine mudstones are of good quality and large thickness (173~2048 m), forming the best regional seal in the basin. The third seal is the calcareous mudstone in the Maishan Fm, equivalent to the regional seal which caps the YA13-1 gas field in the adjacent Qiongdongnan basin. The forth regional seal is the mudstones in the 1st members of the Sanya Fm. These are

neritic to abyssal mudstones with a total thickness ~200 m which is 40~50 % of the formation thickness (Zhang and Huang, 1993; Gong and Li, 1997).

Potential reservoirs in the YGHB include deltaic, channel, neritic, turbidites sandstones found mostly in Lingshui, Sanya, Huangliu and Yinggehai Fms. For example, the DF1-1 gas fields at water depth of 63~70 m is a NS-elongated diapir dome, with area of 350 km^2 and closure height of 255 m. Gas reservoirs are mostly in the Pliocene Yinggehai Fm, with thickness of 5~40m, depth of 1157~1525m, porosity of 21~25%, and permeability of 4~275 mD (Li & Lv, 2002). The well LD30-1-1(A) in the Central Sag penetrated 4 layers of sandstones deposited in the gravity flow channel, with total thickness of 361m. Single layer ranges from 18.6m to 87m in thickness and has porosity of 20% and permeability of 11.72md (Gong and Li, 1997). Littoral sandstones in the Yinggehai Fm show good porosity and permeability.

Overpressure is an important factor to be considered. The high subsidence rate (500-1400 m/Ma) and thick sediments caused rapid loading and under compaction in the basin. These, in combination of hydrocarbon generation and thermal expansion of pore fluids, generated diapirs in the center of the basin as well as strong overpressure over a large part of the basin (Gong and Li, 1997; Zhang and Li, 2000). The overpressured system in the central sag of the YGHB is, with the pressure coefficient up to 2.1, developed in the section from Sanya Fm to Lower Yinggehai Fm starting at depth usually greater than 3000 m and may be shallower to 1800 m. Overpressure is not favorable for CO_2 storage because it increases the difficulty of drilling and increases the required injection pressure.

7.3 GIS and parameter estimations

The sedimentary sequences in the YGHB (Fig. 6.1.2) are divided into three super layers in our assessment: The upper layer consists of Pliocene Yinggehai Fm and the Upper Miocene Huangliu Fm, under the regional seal in the Upper Yinggehai Fm; the middle layer of Middle Miocene Meishan Fm and the Lower Miocene Sanya Fm, under the regional seal in the Meishan Fm; and the lower layer of lower Miocene to Oligocene Lingshui and Yacheng Fms, under the regional seal in the upper Sanya Fm. Thickness and interface depths of these layers are input into the MapGis system, and isobath maps of the layers at depths of 800m~3500m sub-seafloor are compiled (Fig. 7.3.1).

(a) (b)

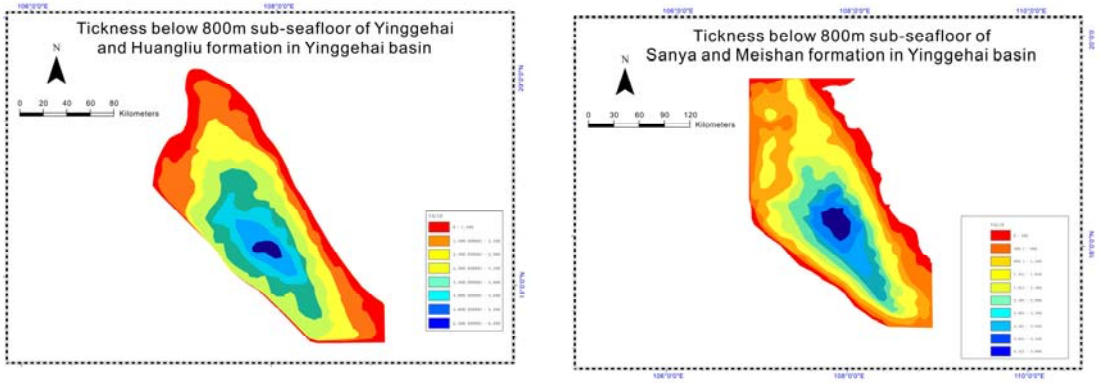

Figure 7.3.1 Isopach maps of the supper layers in the Yinggehai Basin.

The YGHB is a hot basin with geothermal gradient >40℃/km in general (Gong and Li, 1997) and seafloor temperature of 10~25 °C variable with water depth (Table 7.3.1 and Fig.7.3.2b). The basin is divided by its geothermal characteristics into Central, SW, and SE regions as shown by dashed purple lines in Fig. 7.1.1, and curves of CO_2 density vs. depth for these regions are calculated according to Span & Wagner (1996) and presented in Fig. 7.3.2a. Lithological parameters collected from literatures for the YGHB are listed in Tables 7.3.2 and 7.3.3.

Table 7.3.1 Geothermal gradient in Yinggehai basin.

Region*	**Thermal gradient** (℃/km)	**Seafloor Temp.**
Entire basin	42.07	
Central	43.22	20 ℃
SW	42.56	15 ℃
ES	36.28	10 ℃

* For division of regions see the purple dashed lines in the Fig. 7.1.1.

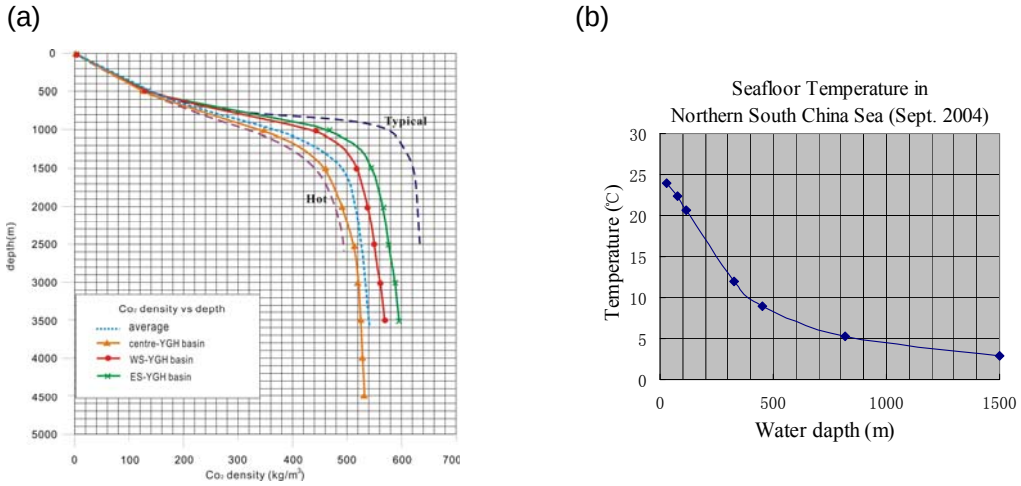

Figure 7.3.2 Curves of CO_2 density vs. depth for the Yinggehai basin（a）, and seafloor temperature of the northern South China Sea (b) .
For division of regions in (a) see the purple dashed lines in the Fig.Y1. The figure (b) is from Zhou et al. (2011).

Table 7.3.2 Parameters of sandstones in the Yinggehai Basin

Well	Formation	Sedimentary facies	Lithology	Porosity (%)	Permeability（mD）	Reference
LG20-1-1	Yinggehai	delta	sandstone	13-15		(1)
LT1-1-1	Yinggehai	coastal	sandstone	25	600	(1)
HK30-3-1A	Yinggehai	coastal	sandstone	21.5		(1)
LD15-1-1	Yinggehai	neritic	Fine sandstone	30	800	(1)
LD30-1-1	Yinggehai	turbidite fan	Fine sandstone	22	12	(2)
DF1-1	Huangliu	neritic	Sandstone	21~25	4~274	(2)
	Meishan & Sanya	neritic	sandstone	20~25		(2)
	Meishan & Sanya	neritic	carbonate	20		(2)
	3rd member of Lingshui	littoral	sandstone	14		(2)

(1) Gong and Li (1997); (2) Li and Lv, (2002).

Table 7.3.3 Average parameters of formations in the Yinggehai Basin

Formation	Area (km^2)	Bottom depth (m)	Thickness (m)	Porosity (%)	Net/Gross ratio
Ledong	20149	200-1500	200-1500		
Yinggehai		500-3800	600-3500	15	0.24
Huangliu		600-5400	100-800	14.7	
Meishan	18380	800-6000	300-2100	13.2	0.15
Sanya		4500-9000	320-2900	11	

7.4 Capacity estimation for saline formations

The assessment of the effective CO_2 storage capacity in saline formations was performed for the entire YGHB according to the methodology specified in Chapter 2. The storage efficiency factor E was chosen according to the average values in IEAGHG (2009) with no differentiation made for overpressure zones because we do not have pertaining data.

The parameters and estimates are listed in Table 7.4.1. The mean value of the effective CO_2 storage capacity in saline formations of the YGHB is 160 $GtCO_2$, with lower and upper bands of estimates in 62 $GtCO_2$ and 248 $GtCO_2$ respectively.

Table 7.4.1 Parameters and estimates of the effective CO_2 storage capacity in saline formations of the Yinggehai basin (800~3500 m sub-seafloor).

Formation		Huangliu & Yinggehai Fms	Sanya & Meishan Fms	Total
Volume below 800m $V(\times 10^9\ m^3)$		188 855	50 339	239 194
Net/gross ratio R(%)		40.43	55.25	
Average porosity φ(%)		12.48	12.24	
Effective capacity	E=0.01	44.9	17.1	62.0
800~3500m	E=0.026	116.6	44.5	161.1
sub-seafloor ($GtCO_2$)	E=0.04	179.4	68.5	247.9

7.5 Capacity estimation for oil/gas fields

In the YGHB only gas fields have been found to date. According to the 2008 assessment, the YGHB has the total resources of 1300 Gm^3 gas, in which 156 Gm^3 are discovered reserves. The DF1-1 gas field is the largest producing field in the basin. Capacity assessment was performed for the DF1-1 field and for the entire basin according to the methodology described in Chapter 2.

The DF1-1 gas field has the geological reserve of 87 Gm^3 and discovered reserve of 41 Gm^3, and started production in 2003 (Zhu et al., 2010). This field has reservoir depth of 1200~1600 m, thermal gradient of 46.7 ℃/km, and a normal pressure system. Using the Eq.(2.4) with parameters listed in Table 7.51, the effective CO_2 storage capacity in the DF1-1 gas field ranges in 87~166 $MtCO_2$ and in average 111 $MtCO_2$.

If the parameters for the DF1-1 field are applied to the entire YGHB based on the 2008 assessment of 1300 Gm^3 gas resources, the expected effective CO_2 storage capacity in the YGHB ranges in 1300~2486 $MtCO_2$ and in average 1660 $MtCO_2$ (Table 7.5.2).

Table 7.4.1. Estimation of the effective CO_2 storage capacity for the DF1-1 gas field.

Parameter	Value	Reference
OGIP	87 Gm^3	Zhu et al. (2010)
Recovery rate	0.55	
Compression factor:		
Surface (Z_s)	0.999	
Reservoir (Z_r)	0.932	
Reservoir pressure (P_r)	13.7 MPa	Hydrostatic pressure at 1600 m depth
Reservoir temperature (T_r)	358.4 K	At 1600 m depth
Surface temperature (P_s)	293 K	Chinese standard
Surface pressure (T_s)	0.101 MPa	Chinese standard
Reservoir CO_2 density (ρ_{CO2r})	0.46	Fig. 7.2.2a
Gas volume factor (B_g)	0.0084	$=(P_s \times Z_r \times T_r) / (P_r \times Z_s \times T_s)$
Theoretical CO_2 storage capacity	185 Mt	$=\rho_{CO2r} \times R_f \times OGIP \times B_g$
Effective storage capacity (Mt CO_2)		
$C_e = 0.47$	87	
$C_e = 0.6$	111	
$C_e = 0.9$	166	

Table 7.5.2. Estimation of the effective CO_2 storage capacity in the gas fields of the Yinggehai Basin.

Parameter	Value	Reference
OGIP	1300 Gm^3	
Recovery rate	0.55	
Reservoir CO_2 density (ρ_{CO2r})	0.46	Fig. 7.2.2a
Gas volume factor (B_g)	0.0084	$=(P_s \times Z_r \times T_r) / (P_r \times Z_s \times T_s)$
Theoretical CO_2 storage capacity	2760 Mt	$=\rho_{CO2r} \times R_f \times OGIP \times B_g$
Effective storage capacity (Mt CO_2)		
$C_e = 0.47$	1298	
$C_e = 0.6$	1658	
$C_e = 0.9$	2486	

7.6 Favorable areas for CO_2 geological storage

At this preliminary stage, major concerns for assessing the storage prospectivity are the distribution of reservoirs and seals, the distance from major emission sources, the depth and size of possible reservoirs, the distribution of overpressure and high thermal gradient, and the possibility of CO_2 extraction from gas fields.

The Yinggehai basin is characterized by high thermal gradients and widespread overpressure at depths. A diapir structure zone developed in the center of the Central depression. All the gas fields discovered so far in the basin are found in the diapir zone. The hydrocarbon gas in this zone often contains high CO_2. For example, the gas produced from its east block of the DF1-1 field contains 55~71 % CO_2; and the gas fields LD8-1 and LD15-1 contain >60% CO_2 (Li et al., 2002). The existence of high-CO_2 gas fields indicates the existence of favorable geological conditions for CO_2 trapping. Thus the diaper zone in the YGHB has the geological conditions favorable for CO_2 storage, but the high-degree of fracturing and shallow occurrence of overpressure should be avoided carefully in site selection.

Gas produced from the DF1-1 field is now transported through pipelines to the Hainan Island, and a fraction of CO_2 separated from the gas is used to produce urea. Remaining CO_2 (~100 KtCO_2 per year) may be used for CO_2 storage.

The eastern flank and the SE region of the YGHB (see Fig.7.1.1) have favorite geographic location vary close to the Hainan Island. But this region may not be prospective for CO_2 storage, because the sealing condition may not be favorable, as shown by abundant gas seeps. In this area the Yinggehai and Huangliu formations are thick and with good reservoir properties. The geothermal gradient is lower than that in the Central Sag. Although hydrocarbon exploration has been extensive in this region, no major discovery so far. The reasons for the failure are yet to be resolved but the sealing property has been questioned.

Chapter 8 Overall Evaluation and Source-Sink Match

8.1 Conclusions on the CO_2 storage potential for Guangdong Province

In this study we have reviewed storage potential and capacity for all the main basins onshore and offshore Guangdong Province. Following the definitions of CSLF(2007), we estimated the total storage capacity for each basin at the level of "effective" storage capacities, which is a subset of the theoretical storage capacity multiplied by the storage efficiency factor *E* (for saline formation) or *Ce* (for oil and gas field) which reflects a number of geological and engineering limitations. We provided regional estimates of the total potential storage capacity in saline formations and in oil and gas fields for each basin. Subtotals of estimated capacity are presented by major geological intervals, and for shallower water (<300 m) areas. Major conclusions on the CO_2 storage potential of Guangdong are as follows:

(1) The CO_2 storage potential inland Guangdong is very small and should not considered practical in consideration of the dense population.

(2) The CO_2 storage potential is very large offshore in the northern South China Sea (Table 8.1.1). The conservative (at P85 probability level) estimate of the effective CO_2 storage capacity is 205 $GtCO_2$ in saline formations, including 0.142 $GtCO_2$ in oil fields and 1 $GtCO_2$ in gas fields. If only the shallow areas (water depth <300m) are considered for CO_2 storage, the conservative effective storage capacity is 163 $GtCO_2$ in saline formations, which are more than 600 times of the CO_2 emission (252 $MtCO_2$ in 2010) from large point sources in Guangdong. Thus the storage capacity in the shallow areas of the northern South China Sea is large enough to support the CCS development in Guangdong.

(3) The CO_2 storage potential is predominantly in saline aquifer formations. This type of storage is in use in some other areas of the world but is at an early stage of research, demonstration and development. This type of storage is likely to be important for future large scale CCS. The storage capacity of oil and gas fields is relatively small and will principally be available after the end of hydrocarbon production. Opportunities for CO_2 utilization and EOR appear limited in the region. These may provide some early opportunities for storage in oil and gas fields with cost benefits from re-use of infrastructure and oil/gas field data; in addition these may allow combination with storage in underlying or adjacent saline formations.

(4) In consideration of geological and geographical conditions, the high graded area for CO_2 storage is the Zhu-1 Depression and the northern Dongsha Uplift in the Pearl River Mouth Basin (Fig. 4.1.1). This ~400 km^2 area has shallow water depth (mostly <200 m), thick Lower and Middle Miocene formations with good reservoir-seal assemblages, large amount oil fields and dry structures. The conservative estimation of the effective CO_2 storage capacity in the area is 77 $GtCO_2$ at P85 probability level, more than 300 times of the CO_2 emission from the large point sources in Guangdong in 2010. The producing oil fields of the PRMB reside mostly in this area, among which some are already depleted and some are approaching depletion. The oil fields in the area are all small, and the potential of CO_2-EOR in the area (and in the entire Pearl River Mouth

Basin) is low because the oil fields have high recovery rate (>40%) and strong water drive. However there is the possibility for reusing the infrastructure of these fields for CO_2 injection after the fields' depletion. This might reduce significantly the cost of offshore CO_2 storage. The major disadvantage is the small storage capacity in these oil fields. The storage capacity should be enlarged by utilization ambient saline formations. The evaluation of feasibility of using offshore oil/gas production facilities for CO_2 storage is an urgent task, as this should be done far ahead of the field depletion.

Table 8.1.1 The effective CO_2 storage capacity[1] (in $GtCO_2$) of saline formations and oil/gas fields[2] of the northern South China Sea.

The effective CO_2 storage capacity (in $GtCO_2$) of saline formations (Range[3] is calculated with *E*=0.01 ~ 0.04, and mean with *E*=0.026 following IEAGHG(2009))						
		BBWB	QDNB	YGHB	PRMB	Total
Entire basin	Range	20.2~80.9	12.8~63.3	62.0~247.9	110~443	205~835
	Mean	52.6	41.1	161.1	289	544
Shallow water area (<300 m)	Range	20.2~80.9	3.5~17.4	62.0~247.9	77~310	163~656
	Mean	52.6	11.3	161.1	201	373
The effective CO_2 storage capacity (in $GtCO_2$) of oil and gas fields (For oil fields "Range" is calculated with *Ce*=0.12 ~ 0.4, and "Mean" with *Ce*=0.25, while for gas fields "Range" is calculated with *Ce*=0.47 ~ 0.9, and "Mean" with *Ce*=0.6, as explained in Section 2.3 of this report)						
		BBWB	QDNB	YGHB	PRMB	Total
Oil fields	Range	0.011~0.035	0.070~0.024	-	0.061~0.205	0.142~0.264
	Mean	0.022	0.015	-	0.128	0.165
Gas fields	Range	-	0.620~1.190	1.300~2.490	1.093~2.093	3.013~5.773
	Mean	-	0.790	1.660	1.395	3.845
Oil and Gas fields	Range					3.149~6.016
	Mean					3.997
YA13-1 gas field	Range		0.055~0.104			
	Mean		0.070			
DF1-1 gas field	Range			0.087~0.166		
	Mean			0.111		

[1] The effective storage capacity is a subset of the theoretical (maximum) storage capacity multiplied by the storage efficiency factor *E* or *Ce* which reflects a number of geological and engineering limitations (CSLF, 2007).
[2] Undiscovered oil and gas fields are included.
[3] In this table, "Range" corresponds to the probability levels of P85~P15; "Mean" the probability level of P50.

(5) The second priority area for CO_2 storage is the Weixinan Sag in the Beibuwan Basin. This 3000 km^2 area has up to >9000 m thick Cenozoic sediments with good reservoir-seal

assemblages. Through the half century explorations eight small oilfields were founded in the sag, among which five are producing and one is depleted. The estimated effective CO_2 storage capacity in the area is 2~8 $GtCO_2$ (ave. 5 $GtCO_2$) in saline formations. A specific advantage of the area is its shallow water depth (~30 m) and short distance from the coast of the Guangxi Province and the Leizhou Peninsular of the Guangdong Province. Thus this area may be a potential storage area for the CO_2 emitted from the industry in western Guangdong and in Guangxi. The disadvantage of this area is the relatively strong neotectonic activities including volcanism and earthquakes, but the M6.0 earthquakes occurred to the east of this area (Fig. 4.1.2). Well integrity is another issue to be carefully examined and treated to ensure the storage safety.

(6) The Qingdongnan Basin and Yinggehai Basin have large effective CO_2 storage capacity, but they are relatively distant from the inland large emission sources inland China. A common feature of these basins is that they have large gas fields which often have high CO_2 content. For example the YA13-1 gas field in the Qingdongnan Basin has geological reserve of 97.85×10^9 m^3 gas in which the CO_2 content is about 8%. The DF1-1 gas field in the Ynggehai Basin has geological reserve of 87×10^9 m^3 gas in which the CO_2 content is about 55~71%. Currently the CO_2 produced from these fields are mostly emitted to the air except a small portion used for fertilizer production. CCS project with CO_2 sourced from these fields might be considered in the future.

8.2 Source-sink match and early opportunity

In the Guangdong province, most large point sources (LPSs) of CO_2 emissions are distributed along the coast, especially concentrated in the Pearl River Delta (Fig. 8.2.1). These LPSs may be matched with the potential storage sites in the Pearl River Mouth Basin (PRMB) offshore.

There might be various schemes of source-sink matching for Guangdong. We put forward a conceptual scheme of source hubs matching sink hubs within the straight-line distances of 120 km to 200 km as shown in Fig. 8.2.1. The source hubs would be built along the coast with CO_2 treatment facilities, while the sink hubs could be built utilizing the existing facilities of depleted oil/gas fields or upon large dry structures. A regional planning is needed for the pipeline routes from a cluster of emission sources to a source hub and from a sink hub to a cluster of sinks, as well as a grand pipeline linking the source hub to the sink hub. In this scheme a most efficient and economic transportation of CO_2 may be achieved.

An early opportunity for a full-chain CCS demonstration (the HZ project) has been identified, which consists of a low-cost capture from the high purity CO_2 from a planned refinery and a low-cost storage using the infrastructures of a near-depleted oil field in the PRMB. The source-sink distance is ~170 km, as shown by the solid blue line in Fig. 8.2.1. A planned oil refinery on the coast of the Huizhou city will emit a total of 2.6 Mt/yr high purity CO_2 from H_2 production. The near-depleted oil field is in Lower Miocene marine sandstone at depths of 2820 m to 3000 m in a dome structure. Preliminary injection modeling indicates that the CO_2 storage capacity of the field is very small, but the ambient saline formations may be used and then the capacity is sufficient to support the suggested storage rate of 3000 tCO_2/d (1 MtCO_2/a). A study on the technical and economical feasibility of the HZ project is needed urgently, because these have to be done several years before the depletion of the oil field.

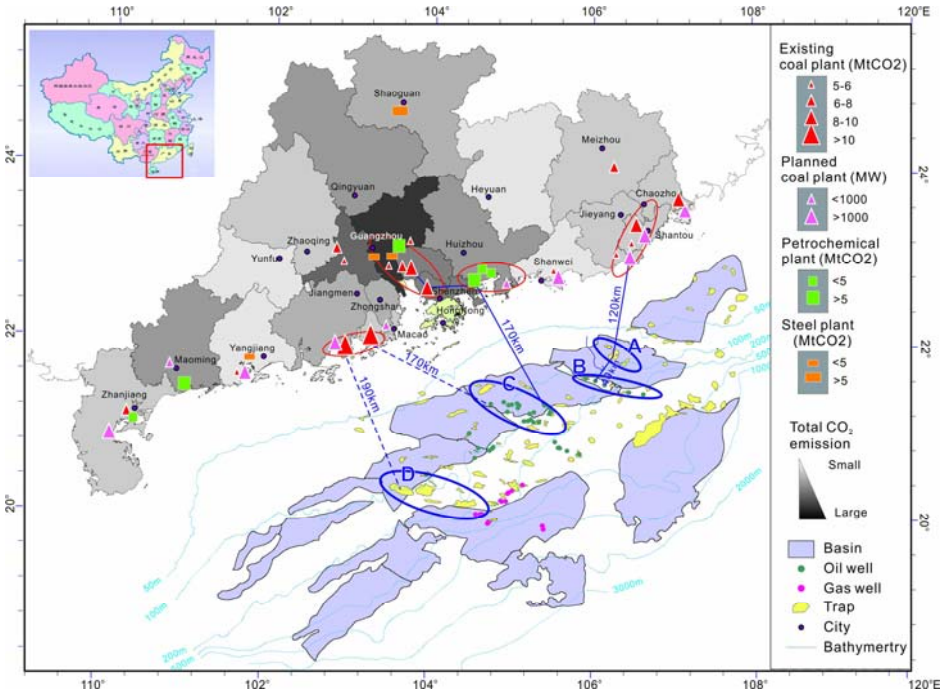

Figure 8.2.1 Proposed scheme of CO_2 source-sink match for the Guangdong province.
Grey scale shows the relative intensity of CO_2 emission by counties. Red and blue circles indicate source and sink clusters respectively. Blue lines connect potential source hubs and sink hubs, with distance indicated. Inset shows the map location in China.

8.3 CCS strategic considerations

In the aspect of CO_2 storage, Guangdong is superior over other province in southeast China. All these provinces have little potential for onshore CO_2 storage, but only Guangdong is adjacent to the Pearl River Mouth Basin, which has not only large storage capacity but also producing oil fields. When the fields are depleted, their infrastructure might be used for CO_2 injection, and the cost for CO_2 storage might be reduced significantly.

In the aspect of CO_2 capture, Guangdong might be benefited by her strong petrochemical industry whose hydrogen production by-produces high-purity CO_2 and enables a low-cost capture. In 2010 the CO_2 emission from petrochemical is 8% of industrial total, and will be 16.3% in 2020, the number one exceeding the emission of cement and pottery.

Taken into account of the status of Guangdong as the leading provincial economy in China and the only low-carbon pilot province in southeast China, Guangdong should have the ambition and capability to lead the CCS development in southeast China.

From these strategic considerations, the HZ demonstration project would be a good start. The key of the project is to ensure the possibility and to develop the techniques for offshore CO_2 storage using the existing infrastructure of depleted oil field. When this breakthrough is made, a large-scaled CCS employment would be foreseeable in the Guangdong province, and this will have a significant impact to the low-carbon development in southeast China and in the world.

Acknowledgement

The authors of this report thank the Strategic Programme Fund of the UK Foreign & Commonwealth Office and the Global CCS Institute for funding the GDCCSR project. We are grateful to the British Consulate General in Guangzhou, especially Wayne Ives, Qiao Feng, Adee, Phyla and their colleagues for managing the project, and to the Guangdong Provincial Development and Reform Commission for supporting the GDCCSR project. Special thanks are due to Bill Senior and Andrew Minchener, whose advices have improved the quality of this work. We are also benefited from discussions with CNOOC experts.

References

Bachu, S., 2003. Screening and ranking of sedimentary basins for sequestration of CO2 in geological media. Environmental Geology 44, 277-289.

Cai, Q., 2005. Oil and Gas Geology in China Seas. Ocean Press, Beijing.

Chen, C., Shi, H., Xu, S., Chen, X., 2003. Formation Conditions of Tertiary Oil/Gas Reservoirs in Pearl River Mouth Basin (East). Science Press, Beijing.

Chen, W. H., 1990, Natural gas resource prediction in major sedimentary basins in the north continental shelf of the South China Sea (in Chinese): CNOOC Research Report, 238 p.

Chen, Y.-l., Zhang, Z.-g., Jiang, Z.-l., Li, W.-b., Li, W.-y., Ma, H., 2008. Structure evolution and petroleum geology of the Sanshui Basin. J. Taiyuan Univ. Technology 39, 144-147.

Clift, P., Lee, G.H., Duc, N.A., Barckhausen, U., Long, H.V., Zhen, S., 2008. Seismic reflection evidence for a Dangerous Grounds miniplate: No extrusion origin for the South China Sea. Tectonics 27, TC3008.

CSLF, 2007. Estimation of CO2 Storage Capacity in Geological Media - Phase 2 . Carbon Sequestration Leadership Forum, p. 43.

CSLF, 2008. Comparison between Methodologies Recommended for Estimation of CO2 Storage Capacity in Geological Media - Phase 3. Carbon Sequestration Leadership Forum, p. 21.

Dong Weiliang. Ananalysis of the natural gas exploration areas in Ying-Qiong basin in western South China Sea. Narural gas industry, 1999, 19(1): 7-11 (in Chinese with English abstract).

Dong, Y.-x., Xiao, L., Zhou, H.-m., Zeng, G.-c., Wang, F.-z., Wang, X.-d., Xiang, H., Zhao, T.-p., Liu, X.-m., 2006. Special distribution and petrological characteristics of the bimodal volcanic rocks from Sanshui Basin, Guangdong province: Implication for basin dynamics. Geotectonica et Metallogenia 30, 82-92.

Fu, Yanhui, Lu, Fuliang, Yuan, Shengqiang, et al., 2009. Characteristics of seismic facies in the deepwater turbidite channel system on the slope of the Qiongdongnan basin. Journal of tropical oceanography, 28(4): 87-92 (in Chinese with English abstract).

GCCSI, 2013. The global Status of CCS: Update January 2013. Global CCS Institute, Canberra, pp. 12.

Gong Zaisheng. Neotectonic movement and hydrocarbon accumulation in petroliferous basins, offshore China. Oil & Gas Geology, 2004, 25(2): 133-138 (in Chinese with English abstract).

Gong Zaisheng, Li Sitian, Continental Margin Basin Analysis and Hydrocarbon Accumulation of the Northern South China Sea (in Chinese), Beijing: Science Press, 1997.

Gong, Z., Li, S., 2004. Dynamic Research of Oil and Gas Accumulation in Northern Marginal Basins of South China Sea. Science in China Press, Beijing.

Guo, F., wang, S., Sun, J., Lu, J., Wang, X., 2009. Analysis on the conditions of petroleum accumulation in Weixinan sag, Beibuwan basin. Marin Geology ＆ Quaternary Geology 29, 93-98.

Hao Fang, Li Sitian, Dong Weiliang et al. Abnormal organic matter maturation in the Yinggehai basin, offshore South China Sea: Implications for hydrocarbon expulsion and fluid migration from overpressured systems, Journal of Petroleum Geology, 1998, 21: 427-444.

Hao, F., Y. C. Sun, S. T. Li, and Q. M. Zhang, 1995, Overpressure retardation of organic-matter maturation and hydrocarbon generation: a case study from the Yinggehai and Qiongdongnan basins, offshore South China Sea: AAPG Bulletin, v. 79, p. 551-562.

Hao, H., Zhang, X., Chen, Z., Jiang, T., Tang, S., 2009. Mesozoic in the Chaoshan Depression and its petroleum Geology. China Offshore Oil and Gas (Geology) 21, 151-156.

He,,iaxiong, Li,qiang, Chen,Weihuang, et al. Oil/gas mechanism type and gas exploratory direction in southeast Hainan basin. Offshore Oil, 2002, 22(1): 47-56 (in Chinese with English abstract).

He, Jiaxiong, Liu,Hailing, Yao,Yongjian, et al., 2008. Petroleum Geology and Resource Perspective of the Marginal Basins in Northern South China Sea. Petroleum Industry Press, Beijing.

He, Jiaxiong, Zan, Lisheng, Chen, Longcao, et al., 1994. The formation and evolution of mud diapir and its relationship with hydrocarbon accumulation mechanism in Yinggehai basin. Acta Sedimentologica Sinica, 12(3): 120-129.

Hou, M.-c., Chen, H.-d., Tian, J.-c., Wan, L., 2007a. The lithofacies—paleogeographic character and evolution of the Sanshui basin during Cretaceous in Guangdong，China. J. Chengdu Univ. Technology (Science＆Technology Edition) 34, 238-244.

Hou, M.-c., Chen, H.-d., Tian, J.-c., Wan, L., 2007b. Sedimentary facies and palaeogeography of the Sanshui Basin，Guangdong during the Pelaeogene. Sedimentary Geology and Tethyan Geology 27, 37-44.

Huang, Baojia, 1999. Gas potential and its favorable exploration areas in Qiongdongnan basin. Narural gas industry, 19(1): 34-39 (in Chinese with English abstract).

IEAGHG, 2009. Development of storage coefficients for carbon dioxide storage in deep saline formations, pp. 118.

Kang, X., Li, S., Li, Y., Hu, Z., 1995. Characteristics of present and paleo-geothermal field and geothermal evolution of the Beibuwan Basin. Transaction of the Changchun University of Geosciences 25, 5.

Li, C., Zhang, G., Liang, J., Zhao, Z., Xu, J., 2012. Characteristics of fault structure and its control on hydrocarbons in Beibuwan Basin. Acta Petrolei Sinica 33, 195-203.

Li, G., Lv, M., 2002. Atlas of China'a Petroliferous Basins, 2nd ed. Petroleum Industry Press, Beijing.

Li, Xuxuan, Liu, Baoming, Zhao, Junqing, 2007. Paleogene sequence configuration, depositional filling pattern and hydrocarbon-generation potential in Qiongdongnan basin. China offshore oil and gas, 19(4): 217-223 (in Chinese with English abstract).

Liang, H., Li, P., 1992. Cenozoic magmatism in the Pearl River Mouth Basin. Guangdong

Petroleum 16, 81-103.

Liu, C., Che, C., Zhu, J., Yang, H., Fan, B., 2010. Recovery Factors of Oil Resources in China. Natural Resources Research 19, 23-31.

Liu, Jun, Wang, Hua, Jiang, Hua, et al. , 2006. Prospects for deepwater oil and gas exploration in Qiongdongnan basin. Xinjiang petroleum geology, 27(5): 545-548 (in Chinese with English abstract).

Liu, Z., Zhao, Z., Li, J., 2009. The sedimentary facies analysis and its significance in Haizhong sag, Beibuwan basin, the South China Sea. Offshore oil 3, 14-18.

MLRC, NDRC, MFC, 2008. Report on The New Round Assessment of National Oil and Gas Resources, Beijing, p. 124.

Pang, X., Chen, C., Peng, D., Zhou, D., Chen, H., 2007a. The Pear River Deep-water Fan System & Petroleum in South China Sea. Science Press, Beijing.

Pang, X., Chen, C., Peng, D., Zhu, M., Shu, Y., He, M., Shen, J., Liu, B., 2007b. Sequence stratigraphy of Pearl River Deep-water Fan System in the South China Sea. Earth Frontiers 20, 220-229.

Pershad, H., Durusut, E., Crerar, A., Black, D., Mackay, E., Olden, P., 2012. Economic impacts of CO_2-enhanced oil recovery for Scotland: Final report. Element Energy Limited Dundas Consultants Heriot Watt University, p. 111.

Qin, G., 2002. Late Cenosoic Sequence Stratigraphy and Sealevel Changes in Pearl River Mouth Basin, South China Sea. China Offshore Oil and Gas (Geology) 16, 1-18 (in Chinese).

Schrag, D.P., 2009. Storage of Carbon Dioxide in Offshore Sediments. Science 325, 1658.

Shi, H., Zhu, J., Jiang, Z., Shu, Y., Xie, T., Wu, J., 2009. Hydrocarbon resources reassessment in Zhu I depression，Pearl River M outh basin. China Offshore Oil and Gas 21, 9-14.

Span, P., Wagner, W., 1996. A new equation of state for carbon dioxide covering the fluid region from the triple-point temperature to 1100 K at pressures up to 800 MPa. Journal of Chemical Reference Data 25, 1509-1596.

Sun, J., Xu, X., Xi, M., 2008. Analysis of oil accumulation conditions in Haizhong depression, Beibuwan basin. Offshore Oil, 36-39.

Tang, Z.-y., 1994. Cretaceous-Eocene rift vlley type volcanism in Sanshui Basin, Guangdong. Guangdong Geology 9, 49-57 (in Chinese).

Tao Weixiang, He Shibin, Zhao zhigang, et al. Reservoir distribution in deepwater area of the Qiongdongnan basin. Petroleum geology & experiment, 2006, 28(6): 554-559 (in Chinese with English abstract).

Team12, 1981. Explanation for Geological Maps of Major Cretaceous-Tertiary Basins in Guangdong Province. Ministry of Geology, p. 57.

Team12, 1982. Structure and oil/gas resources in Sanshui Basin. Ministry of Geology, p. 60.

Team735, 1975. Report on Geological Reconnoissance in Sanshui Basin, Guangdong Province. Guangdong Geological Bureau, p. 71.

Team735, 1976. Report on 1975 Petroleum Geology Reconnoissance in Pearl River Delta, Guangdong Province. Guangdong Geological Bureau, p. 24.

USDOE, 2008a. Methodology for Development of Geologic Storage Estimates for Carbon Dioxide, Appendix B, 2 ed. Carbon Sequestration Program, p. 18.

USDOE, 2008b. Stationary Source and Geologic Storage Estimates for Carbon Dioxide by State/Province，Appendix C. Carbon Sequestration Program, p. 10.

Wan Zhifeng, Xia Bin, He Jiaxiong et al. The comparative study of hydrocarbon accumulation conditions in Yinggehai and Qiongdongnan basins, Northern south china sea. Narural gas geoscience, 2007, 18(5): 648-652 (in Chinese with English abstract).

Wang, J., 1996. Geothermics in China. Seismological Press, Beijing.

Wang, Zhenfeng, He, Jiaxiong, 2003. Miocene hydrocarbon's transferring and collecting condition and reservoir combination analysis in Qiongdongnan basin. Narural gas geoscience, 14(2): 107-115 (in Chinese with English abstract).

Wang, Z., Huang, B., 2008. Dongfang 1-1 gas field in the mud diapir belt of the Yinggehai Basin, South China Sea. Marine and Petroleum Geology 25: 445-455.

Xu, Yan, Wan, Zhifeng, 2008. The relationship between the diapiric structural and natural gas accumulation in the Yinggehai basin. Marine geology letter, 24(2): 1-5.

Yan, J., Jin, Z., 1997. The features of the Sanshui Relict Basin and its conditions of petroleum geology，Guangdong Province. Acta Sedimentologica Sinica 15, 141-146.

Yang Hongjun. Hydrocarbon carrier system types and accumulation models in Qiongdongnan basin. China offshore oil and gas, 2008, 20(2): 87-91 (in Chinese with English abstract).

Yang, S., Huang, L., Li, X., Lv, Q., 1996. Special sequential stratigraphic pattern in the Pearl River Mouth Basin and its significance to exploration. China Offshore Oil and Gas (Geology) 10, 137-143.

Yuan S Q, Wu S G, Thomas L, et al. Fine-grained Pleistocene deepwater turbidite channel system on the slope of Qiongdongnan basin, northern South China Sea. Marine and Petroleum Geology, 2009, 26: 1441-1451.

Zhai, G., 1993. Petroleum geology of China: Vol.16. Petroleum Industry Pres, Beijing.

Zhang Minqiang, Li Sitian. Active hydrothermal fluid flow and pool-forming studies in the Yinggehai basin, in Natural Gas Geology Studies and Application (in Chinese) (eds. Song Yan, Wei Guoqi), Beijing: Petroleum Industry Press, 2000, 177-187.

Zhang Minqiang, Zhong Zhihong, Xia Bin, et al. Genetic mechanisms of mud-fluid diapir in Yinggehai Basin and hydrocarbon accumulation. Geotectonica et Metallogenia, 2004, 28(2): 118-125.

Zhang, Q., Su, H., 1989. Petroleum geology of the Beibu Gulf Basin. Marin Geology & Quaternary Geology 9, 73-82.

Zhang, Q. X., L. Li, and B. J. Huang, 1993, Discrimination of hydrocarbon source rocks in the gas field Ya13-1 using GC-MS data, in Q. M. Zhang, ed., A collection on the petroleum geology of the Yinggehai Basin, South China Sea (in Chinese): Beijing, Seismic Press, p. 37-43.

Zhang, X.-q., 1999. Geology of Cretaceous-Tertiary sedimentary basins in Guangdong. Guangdong Geology 14, 53-57.

Zhang, X.-q., Zhou, X.-p., Chen, X.-y., 1993. Atlas of Cretaceous to Tertiary Strata Classification and Correlation in the Sanshui Basin of South China. Marine Press, Beijing.

Zhou, D., Sun, Z., Liao, J., Zhao, Z., He, M., Wu, X., Pang, X., 2009. Filling History and Post-Breakup Acceleration of Sedimentation in Baiyun Sag, Deepwater Northern South China Sea. Journal of Earth Science 20, 160-171.

Zhou, D., Zhao, Z., Liao, J., Sun, Z., 2011. A preliminary assessment on CO2 storage capacity in the Pearl River Mouth Basin offshore Guangdong, China. International Journal of Greenhouse Gas Control, 308-317.

Zhou, S., 2009. The development practice of typical oil fields offshore China. Petroleum industry

Press, Beijing.
Zhu, W., Mi, L., 2010. Atlas of oil and gas basins, China sea. Petroleum Industry Press Beijing.
Zhu, W., Mi, l., Gao, L., Gao, Y., 2008. A review of China offshore hydrocarbon exploration in 2007. China Offshore Oil and Gas 20: 1-8.
Zhu Weilin, Wang Zhenfeng, Huang Baojia. Dynamics of gas accumulation in Yinggehai basin. Journal of China University of Geosciences, 2004, 29(5), 563-568.